

**COMPUTATIONAL STUDY OF
PINCER IRIIDIUM/RHODIUM CATALYTIC SYSTEMS**

by

CHANGJIAN GUAN

A dissertation submitted to the
Graduate School-New Brunswick

Rutgers, The State University of New Jersey

In partial fulfillment of the requirements for the degree of

Doctor of Philosophy

Graduate Program in Chemistry and Chemical Biology

Written under the direction of

Alan S. Goldman

And approved by

New Brunswick, New Jersey

January 2017

ABSTRACT OF THE DISSERTATION

Computational Study of Pincer Iridium/Rhodium Catalytic Systems

By **CHANGJIAN GUAN**

Dissertation Director:

Alan S. Goldman

Nowadays, catalysis is of critical importance in chemical and pharmaceutical industry, and understanding the underlying mechanism of small molecule activation boosts development in the fields of organometallics and catalysis. In this Dissertation, we discuss DFT studies of several catalytic systems explored in our research lab. Headlines in the works are: (1) For pincer PCP iridium complexes catalyzed olefin hydroaryloxylation reaction, an organometallic mechanism via olefin insertion into an iridium–alkoxide bond, followed by rate-determining C–H reductive elimination, is proposed against a hidden Brønsted acid pathway common to previously developed transition-metal-based catalysts. (2) For a newly prepared carbazolidate-based pincer PNP iridium complexes catalyzed olefin hydrogenation reaction, C₂H₄ and H₂ assisted pathways are discovered. Especially, the more efficient H₂ assisted pathway is found undergoing an Ir(III)/Ir(V)/Ir(III) cycle, in contrast to the Ir(III)/Ir(V)/Ir(III) cycle proceeded by isoelectronic (PCP)Ir systems. (3) For carbazolidate-based pincer PNP rhodium complexes catalyzed hydrogenation /dehydrogenation reactions, the forming/

opening of a β -H agostic intermediate is found to be the rate determining step. (4) For the olefin insertion reaction and alkane hydrogenolysis reaction on (Phebox)Ir acetate complexes, Na^+ is found to catalyze the reactions through bonding to the terminal acetate O atom on key intermediates and rate determining states, thus stabilizing these states.

Acknowledgement

First, I wish to express my sincere thanks to my advisor, Alan Goldman, who is the best advisor I could ever imagine. During my five and a half years' study at Rutgers, Alan not only helped me out through all difficulties and obstacles but also demonstrated scientific rigor, innovative thinking, and responsibility. I am fortunate to have been his student no matter where and which field I am in my future life.

I am also deeply grateful to Professor Karsten Krogh-Jespersen, who educated me in computational chemistry, which makes up most parts of this thesis. Karsten has the power to teach me chemistry and to make me laugh at the same time with his humorous language and body language. In addition to academic study, he used his own story to tell me how to live a good life.

I would like to thank Professor Fuat Celik and Dr. Yury Kissin for their valuable time and support serving on my thesis committee.

I would like to thank current and previous Goldman group colleagues, working with whom has been a great pleasure. I would like to thank my collaborators, David Wang, Michael Haibach, Chen Cheng, David B ézier, Tian Zhou, and Yang Gao, who contributed much to this thesis.

Finally, I wish to thank my family and friends for their everlasting support. During my life time, I changed a couple of times the way I wish to live my life; their love, however, never changed.

Dedication

To my family

Table of Contents

Abstract of the Dissertation	ii
Acknowledgement	iv
Dedication	v
Table of Contents	vi
Chapter 1 Introduction	1
Chapter 2 Computational Study of PCP Pincer Iridium Complexes Catalyzed Olefin Hydroaryloxylation	3
Introduction	4
Results and Discussion	9
Conclusions	22
References	23
Computational Details	26
Computational Section References	33
Chapter 3 Computational Study of PNP Pincer Iridium Complexes Catalyzed Alkene Hydrogenation	35
Introduction	36
Results and Discussion	43
Conclusions	56
References	60
Computational Details	64
Computational Section References	70
Chapter 4 Computational Study of PNP Pincer Rhodium Complexes Catalyzed Hydrogenation and Dehydrogenation	71
Introduction	72
Results and Discussion	78
Conclusions	86
References	88
Computational Details	92
Computational Section References	93

Chapter 5	Computational Study of Alkane Dehydrogenation Reaction Co-Catalyzed by Pincer Iridium Complexes and Lewis Acids	94
	Introduction	94
	Results and Discussion	100
	Conclusions	110
	References	111
	Computational Details	114
	Computational Section References	119
Chapter 6	Computational Study of Biphenylene C-C Bond Addition to Pincer-Iridium Complexes	120
	Introduction	121
	Results and Discussion	124
	Conclusions	140
	References	142
	Computational Details	144
	Computational Section References	145

Chapter 1

Introduction

This thesis covers computational mechanism studies of functionalization of small molecules, especially alkanes and alkenes through organometallic chemistry and catalysis. Themes of the research are arranged in order of the activated substrates and catalysts explored.

In the first theme, we discuss the mechanism study of an organometallic operating olefin hydroaryloxylation catalysis recently discovered in our lab. In contrast to previously reported systems operating through a hidden Brønsted acid pathway, our system displays full regio- and chemoselectivities. DFT calculations propose an olefin insertion into an iridium–alkoxide bond, followed by rate-determining C–H reductive elimination pathway, which is in good agreement with experiment facts. This study offers a new approach to the atom-economical synthesis of industrially important ethers and, potentially, a wide range of other oxygenates.

The second theme stems from a newly synthesized carbazolide-based PNP pincer ligand, which was designed to favor oxidative addition of C-H bonds onto late metal complex fragments. As it turns out, while this ligand does form complexes favoring C-H addition as expected, this may be beneficial or detrimental to hydrogenation/dehydrogenation reaction depending on the metal center. In the iridium case, it makes C-H reductive elimination too hard, but opens up the possibility for hydrogenation through a less common Ir(III)/Ir(V)/Ir(III) cycle. In the rhodium case, it enables hydrogenation/

dehydrogenation via routine pathway. This theme is separated into two chapters, one for iridium complexes and the other for rhodium complexes.

In the third theme, we discuss that Na^+ plays the role of a Lewis acid and catalyzes olefin insertion and alkane hydrogenolysis reactions on (Phebox)Ir acetate complexes. Such catalyzed reactions are orders of magnitudes faster than uncatalyzed counterparts. DFT calculations capture the effect of the Na^+ cation and indicate that it operates by promoting κ^2 - κ^1 dechelation of acetate anion, which opens the coordination site needed to allow the observed reaction to proceed.

In the last theme, we explore addition of the strained C-C bond of biphenylene onto pincer iridium complexes. Two similar pincer complexes, $(^{\text{tBu}}\text{PCP})\text{Ir}$ and $(^{\text{iPr}}\text{PCP})\text{Ir}$, both activate the C-C bond but the kinetic barrier are quite different. While the sterically crowded $(^{\text{tBu}}\text{PCP})\text{Ir}$ forms C-C addition product after heating at high temperature, $(^{\text{iPr}}\text{PCP})\text{Ir}$ undergoes the same reaction at room temperature. The large difference in the apparent barriers to C-C addition is notable in view of the fact that the addition products are not particularly crowded, since the planar biphenyl unit adopts an orientation perpendicular to the plane of the $^{\text{R}}\text{PCP}$ ligands. Based on DFT calculations, the large difference in the barriers to C-C addition can be explained in terms of a “tilted” transition state, which results in very short, unfavorable, non-bonding contacts with the t-butyl groups in the case of the $^{\text{tBu}}\text{PCP}$ ligand.

Chapter 2

Computational Study of Catalyzed Olefin Hydroaryloxylation

Majority of this chapter is reproduced with permission from

Olefin Hydroaryloxylation Catalyzed by Pincer-Iridium Complexes

Michael C. Haibach, Changjian Guan, David Y. Wang, Bo Li, Nicholas Lease, Andrew

M. Steffens, Karsten Krogh-Jespersen and Alan S. Goldman

J. Am. Chem. Soc., **2013**, 135, 15062–15070

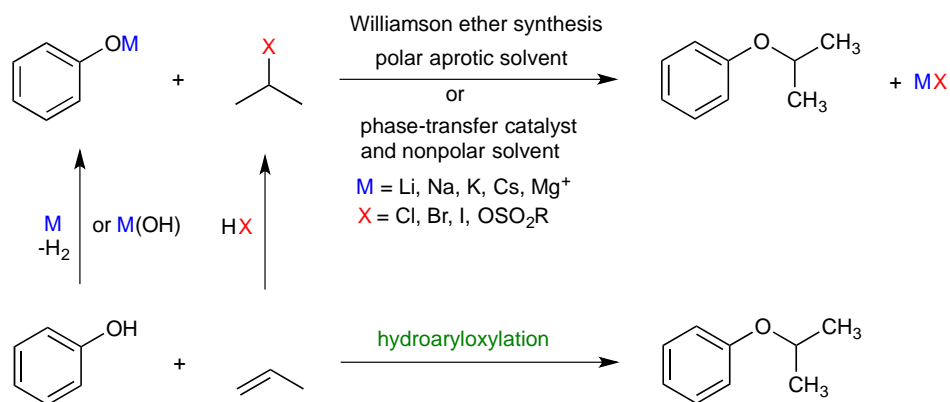
Copyright © 2013 American Chemical Society

Introduction

The addition of H-X bonds across olefinic double bonds catalyzed by transition metal complexes represents a reaction class of great importance in organic chemical synthesis.¹⁻³ Recent years have seen significant developments in catalytic hydroamination;⁴⁻⁶ however, progress toward the development of transition metal complexes for catalytic addition of O-H bonds to olefins has been much more limited.^{1-3,6,7} Such additions of alcohol O-H bonds, especially intermolecular, remain a particularly important and attractive challenge.

Alkyl aryl ethers are an important class of commodity chemicals, with applications ranging from solvents, to fragrances, to pharmaceutical building blocks.⁸ They are currently synthesized primarily via the very classical⁹ Williamson ether synthesis, whereby an alkali salt of the appropriate phenol (preformed or generated *in situ*) is coupled with an alkyl halide or alkyl sulfonate ester, typically in a polar aprotic solvent (Scheme 1).

Scheme 1. Alternative syntheses of alkyl aryl ethers (shown for the addition of phenol to propene)



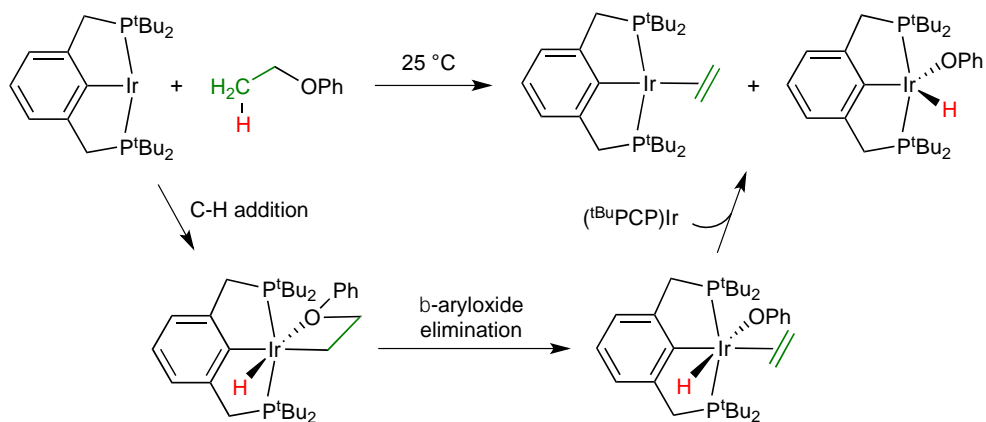
In some cases, phase transfer catalysis can be used to avoid the requirement of a polar aprotic solvent. The use of alkyl alcohols in place of alkyl halides typically requires a gas-phase reaction or dehydrating agent. For the industrially preferred route, one equivalent of alkali halide or alkali sulfonate waste is generated per equivalent of product produced, in addition to the waste associated with preparation of the alkali phenoxide and the alkyl halide, which is typically prepared from the corresponding olefin.

Despite these drawbacks, the Williamson ether synthesis is widely used for both industrial and small-scale applications, rather than the atom economical olefin hydroaryloxylation route shown in Scheme 1. This is due at least in part to the fact that, until quite recently, the known catalysts for olefin hydroaryloxylation were all strong Brønsted or Lewis acids such as H_2SO_4 or $\text{BF}_3 \cdot \text{OEt}_2$. While this class of catalysts is highly active, its use suffers from competing Friedel-Crafts alkylations and very poor chemoselectivity. For example, the reaction of propene with phenol catalyzed by $\text{BF}_3 \cdot \text{OEt}_2$ affords comparable amounts of both *C* and *O*-isopropylphenol, even at $0\text{ }^\circ\text{C}$.¹⁰

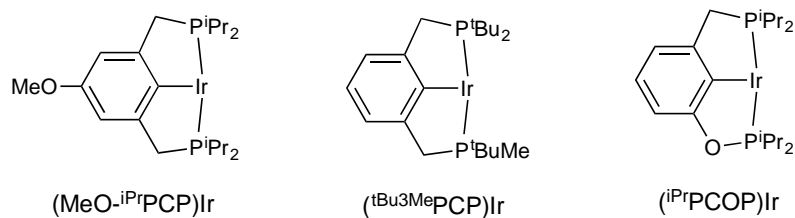
Beginning with He's report in 2005,¹¹ significant attention has been focused on transition metal precatalysts for hydroaryloxylation, such as $(\text{PPh}_3)\text{Au}(\text{OTf})$. Despite early evidence that triflic acid was the catalytically active species,^{12,13} researchers continued to identify numerous transition metal "precatalysts" that were later shown by Hintermann to be Brønsted acid delivery systems (with $\text{Ag}(\text{OTf})$ in chlorinated solvents serving as the most common source).^{14,15} Many recent and classic examples employing Lewis acid catalysts, particularly lanthanide triflates, are also proposed to operate via Yamamoto's Lewis-assisted Brønsted acid¹⁶ mode of activation.^{12,14,15} Indeed, to our knowledge, at the outset of this work there were no well-defined examples of intermolecular addition of alcohol O-H bonds across the double bond of simple olefins directly catalyzed by a transition metal complex.^{7,14,17} In this communication, we report the first such catalysts, specifically for the reaction of phenols, and support for a likely mechanism based on experimental and computational evidence.¹⁸ These catalysts offer selectivity much greater than, and in some cases orthogonal to, that of previously reported acid catalysts.

Our group previously reported that precursors of the fragment $(^{\text{iBu}}\text{PCP})\text{Ir} (^{\text{R}}\text{PCP} = \kappa^3\text{-C}_6\text{H}_3\text{-2,6-(CH}_2\text{PR}_2)_2)$ could cleave aryl- sp^3 C-O bonds stoichiometrically via an initial C-H oxidative addition step.^{19,20} In the case of ethyl phenyl ether, for example, this led to dehydroaryloxylation and formation of the iridium adducts of ethylene and phenol (Scheme 2). The potential ability of such species to undergo kinetically facile olefin loss and phenol elimination suggested the possibility of a catalytic cycle; in the thermodynamically favorable reverse direction such a cycle would constitute olefin hydroaryloxylation.

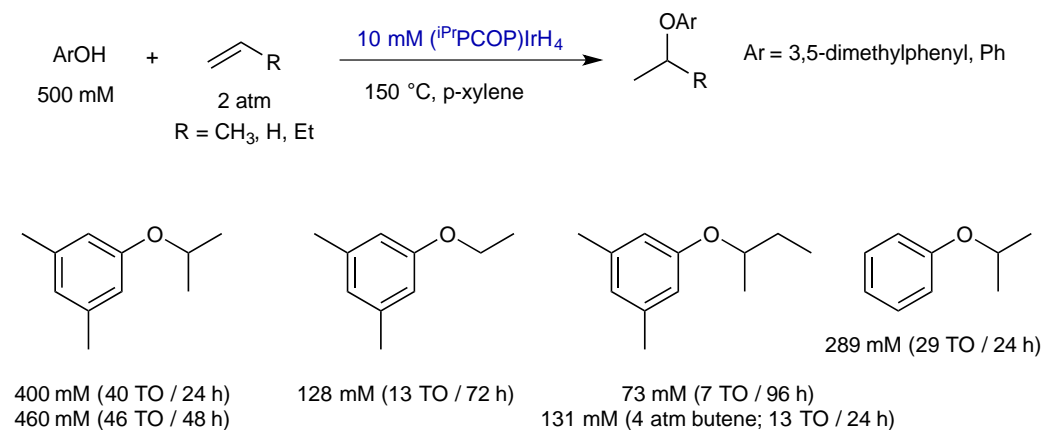
Scheme 2. Stoichiometric dehydroaryloxylation of ethyl phenyl ether by (^tBuPCP)Ir



Even though (^tBuPCP)Ir does not effectively catalyze the hydroaryloxylation reaction at 100 - 150 °C, a group of sterically less congested catalysts, (^tBu³MePCP)Ir,²² (MeO-ⁱPrPCP)Ir,²³ and (ⁱPrPCOP)Ir were identified to be active catalysts.



Scheme 3. Hydroaryloxylation of olefins catalyzed by (*i*PrPCOP)IrH₄

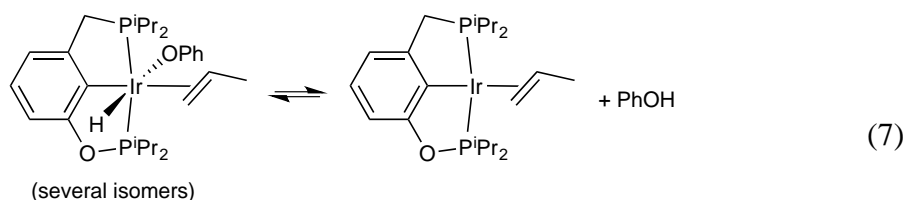


In reaction between 3,5-dimethylphenol and propene catalyzed by (*i*PrPCOP)IrH₄²⁸, isopropyl aryl ether is the only major product, without detectable *n*-propyl aryl ether or other alkylphenols, indicating that the reaction is fully regio- and chemoselective. The same hydroaryloxylation reaction also works if ethylene or 1-butene is used instead of propene, and unsubstituted phenol is used instead of 3,5-dimethylphenol. An interesting fact is that although propene reacts significantly faster with 3,5-dimethylphenol than does ethylene in independent experiments, ethylene reacts preferentially vs. propene with selectivity larger than 3:1 in an internal competition experiment (eq 4). Above facts strongly suggest an organometallic mechanism instead of “hidden Brønsted acid” mechanism, and are consistent with DFT calculation of the energy diagram of the catalytic cycle.

The apparently high regioselectivity for formation of *i*-PrOAr vs. *n*-PrOAr (Scheme 3) and the high chemoselectivity for hydroaryloxylation of propene vs. isobutene (eq 2) might be attributed, *a priori*, to thermodynamic rather than kinetic factors. In such a case the rate of the respective hydroaryloxylation might be comparable

to or even more rapid than the reaction to give *i*-PrOAr, but the respective dehydroaryloxylation back-reactions could be even faster. In a competition reaction between *i*-PrOAr and *n*-PrOAr in catalytic condition, *i*-PrOAr, however, shows much higher activity and therefore suggests a kinetic reason for the regioselectivity.

In process of identifying catalytic resting state, it is revealed that complexes of the composition $(iPrPCOP)Ir(\eta^2\text{-propene})(OPh)(H)$ coexist with $(iPrPCOP)Ir(\eta^2\text{-propene})$ complex at 25 °C in a solution with free propene and phenol of concentrations similar to those applied in typical reaction. When this solution is heated to 120 °C,³¹ however, a temperature at which there is catalytic activity, the only species observable in solution is $(iPrPCOP)Ir(\eta^2\text{-propene})$. Thus the apparent equilibrium of $(iPrPCOP)Ir(\eta^2\text{-propene})(OPh)(H)$ isomers with $(iPrPCOP)Ir(\eta^2\text{-propene})$ plus free phenol (eq 7) is driven toward the side with free phenol at higher temperature, and $(iPrPCOP)Ir(\eta^2\text{-propene})$ is the resting state under catalytic conditions.



Results and Discussion

Computational (DFT²¹) studies have been conducted which shed light on the mechanism and selectivity of the hydroaryloxylation reactions. We employed the widely

used M06 and M06-L density functionals. Both functionals predicted regio- and chemoselectivity in full agreement with our experimental results. Since the M06-L functional provided slightly better quantitative agreement, we will primarily discuss M06-L energies and present those values in the figures shown here; energies obtained with the M06 functional are given in Tables in the Supporting Information. We have focused on the reaction of phenol with propene by our most effective catalyst, (ⁱPrPCOP)Ir. Although the calculations assume idealized gas-phase conditions, free energies have been calculated at conditions (T, P) that are closer to those of the actual catalytic experiments than are standard conditions (T = 298.15 K, P = 1.0 atm). Specifically, we use T = 150 °C = 423.15 K, and, in order to approximate the concentrations of reagents in solution, partial pressures of 34.7 atm were assumed, which correspond to concentrations of 1 mol/liter at 150 °C.

Experimentally, as noted above, (ⁱPrPCOP)Ir(η^2 -propene) (**1a**) was found to be the only major species in solution at the standard reaction conditions. Using the M06 functional and the above noted thermodynamic conditions (T = 150 °C, P = 34.7 atm), (ⁱPrPCOP)Ir(η^2 -propene) was indeed computed to be the lowest energy species, 1.7 kcal/mol lower in free energy than (ⁱPrPCOP)Ir(H)(OPh) (**3**) (Table S4) and 3.9 kcal/mol below (ⁱPrPCOP)Ir(H)(η^2 -propene)(OPh) (**4**) (the lowest energy conformer, with propene coordinated trans to the pincer aryl group; Table S5). The corresponding M06-L values for (ⁱPrPCOP)Ir(H)(OPh) and (ⁱPrPCOP)Ir(H)(η^2 -propene)(OPh), relative to **1a**, are -2.3 kcal/mol and -0.1 kcal/mol at 150 °C, respectively (Table S1). In both cases, we judge the differences to be within the error margins of the calculations when comparing species that are significantly different (e.g. an Ir(I) complex and an Ir(III) complex, π - vs. σ -

coordination, 4-coordination vs. 5- or 6-coordination). Accordingly, we will only consider energies relative to the experimentally observed resting state, the olefin π -complex **1a**.

Under typical reaction conditions, (ⁱPrPCOP)Ir(η^2 -propene) (**1a**) is calculated to be the major resting state (the kinetically accessible species of lowest free energy) in the (ⁱPrPCOP)Ir/phenol/propene system using the M06 functional. However, at 25 °C the free energy of (ⁱPrPCOP)Ir(H)(η^2 -propene)(OPh) is calculated to be -0.6 kcal/mol below the four-coordinate propene adduct, whereas (ⁱPrPCOP)Ir(H)(OPh) remains higher in energy than **1a** by 2.0 kcal/mol. The corresponding M06-L values for (ⁱPrPCOP)Ir(H)(OPh) and (ⁱPrPCOP)Ir(H)(η^2 -propene)(OPh), relative to **1a**, are -2.1 kcal/mol and -4.5 kcal/mol at 25 °C. These results are consistent (at least within the limits of precision of the calculations) with the observation that a mixture of (ⁱPrPCOP)Ir(η^2 -propene), (ⁱPrPCOP)Ir(H)(OPh), and (ⁱPrPCOP)Ir(H)(η^2 -propene)(OPh) appear to be present in a typical reaction solution at 25 °C, whereas only (ⁱPrPCOP)Ir(η^2 -propene) is observed at 120 °C.

The results of the selectivity experiments discussed above argue strongly against a Brønsted-acid catalyzed pathway, or any pathway involving a carbocationic or carbocation-like intermediate, and instead favor a genuinely “organometallic-catalyzed” mechanism. Generally speaking, “organometallic” mechanisms for hydrofunctionalization (addition of species H-X across multiple bonds) may proceed via insertion of olefin into a M-H bond followed by alkyl-X elimination (Figure 1a); known examples include X = SiR₃, BR₂, and CN¹. Such mechanisms can favor formation of anti-Markovnikov products (e.g. CH₂X-CH₂R from CH₂=CHR plus HX). It is generally

assumed that such selectivity is attributable to the preference of transition metals for less substituted alkyl ligands³²⁻³⁵ (e.g. primary vs. secondary) reflected in the TS preceding or perhaps following the intermediate species $L_nM(\text{alkyl})X$.

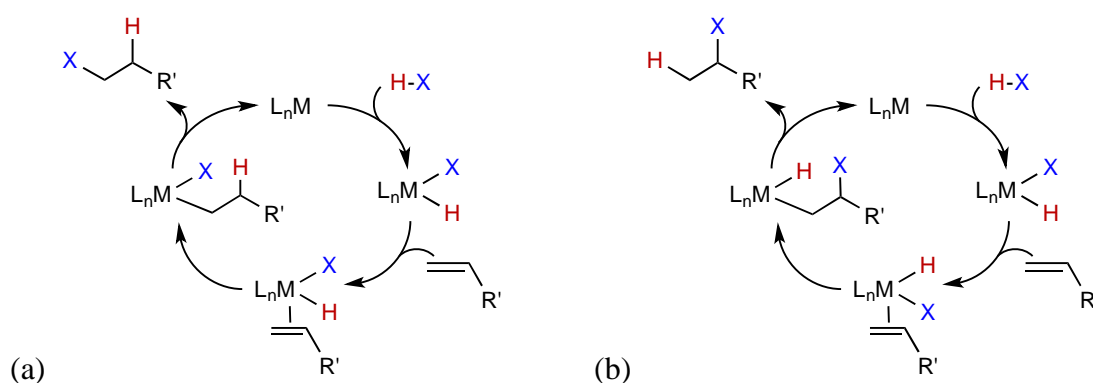


Figure 1. Typical “organometallic” pathways (proceeding via H-X addition, olefin insertion, and C-X or C-H elimination) for generic hydrofunctionalization of an olefin (addition of H-X). Cycle (a) is shown giving anti-Markovnikov product and cycle (b) is shown giving the Markovnikov product. This represents the regioselectivity commonly expected of each pathway, but neither mechanism is necessarily limited to either type of regioselectivity.

In the case of the present system, the free energy calculated for the TS for the key step of C-X elimination as per Figure 1a ($L_nM = (i\text{Pr}^{\text{PCOP}})\text{Ir}$; $X = \text{OPh}$; alkyl = *i*-Pr) is 47.3 kcal/mol above that of the calculated resting state, $(i\text{Pr}^{\text{PCOP}})\text{Ir}(\text{propene})$ (M06-L; Table S1). This value is substantially greater than the overall barrier indicated by experiment, $\Delta G^\ddagger \sim 32$ kcal/mol (based on ca. 1.2 turnovers per hour). The pathway of Figure 1a is thus calculated not to be viable in this case, regardless of the energies of any other intermediates and transition states in that pathway. This result is consistent with and

closely related to our previous work in which it was found that the barrier to direct C-O bond oxidative addition to (^tBuPCP)Ir is prohibitively high.^{19,20}

Interestingly, although the pathway of Fig. 1a is precluded by the high barrier to C-O bond elimination, the initial steps appear to be quite favorable. Addition of ArOD (0.5 M) and (perprotio) propene (1 atm) to a *p*-xylene-d₁₀ solution of (ⁱPrPCOP)IrH₄, to give the mixture of species indicated in eq 6 (and isotopologues thereof), results in rapid H/D exchange between propene and ArOD (50% conversion to ArOH within 15 minutes at room temperature as revealed in the ¹H NMR spectrum). This is most easily explained in terms of reversible insertion of propene into the Ir-H/D bond of (ⁱPrPCOP)Ir(η²-propene)(OPh)(H/D). The thermodynamics of this insertion are calculated to be quite allowable for such an exchange mechanism (ΔG = +7.3 kcal/mol and +8.6 kcal/mol for 1,2- and 2,1-Ir-H addition, respectively), although we were unable to locate the TS's for these insertions.

Rather than the mechanism indicated in Figure 1a, the calculations are instead consistent with the hypothesis that led to this work, namely, that the mechanism indicated in Scheme 2 could be implemented catalytically in the reverse direction (as shown explicitly in Figure 1b). The mechanism of Figure 1b proceeds via olefin insertion into the M-X (Ir-O) bond, rather than insertion into the M-H bond as in Figure 1a, and is followed by C-H rather than C-X (C-O) elimination. There are relatively few well characterized examples of insertion of olefins into transition metal-oxygen bonds, but the reaction is certainly not without precedent.³⁶⁻⁴⁰

Figure 2 shows results of calculations of the catalytic cycle (as per Figure 1b) for the (ⁱPrPCOP)Ir-catalyzed reaction of propene and phenol to give *i*-PrOPh and *n*-PrOPh

(all free energies are expressed relative to the free three-coordinate pincer iridium complex and free propene and phenol). 1,2-Addition of the Ir-OPh bond of (*i*^{Pr}PCOP)IrH(OPh)(η^2 -propene) (**4a**) across the double bond of coordinated propene is calculated to have a barrier of only ca. 16 kcal/mol, with a transition state (TS; **TS-4a-5a**) that is 21.5 kcal/mol above the propene complex resting state (**1a**). This is in agreement with a theoretical study³⁹ by Hartwig on olefin insertion into the Rh-X bond (X = CH₃, NH₂, OH) of (PMe₃)₂RhX, in which it was calculated that the barrier to 1,2 insertion of coordinated propene into a Rh-O bond was 19.3 kcal/mol. Moreover, also in accord with Hartwig's results,³⁹ in the present system the metal-oxygen bond remains largely intact during and even after the insertion step. The Ir-O bond distances in *trans*-(*i*^{Pr}PCOP)IrH(OPh)(propene) (**4a**), **TS-4a-5a**, and the insertion product **5a**, are 2.30 Å, 2.33 Å and 2.42 Å, respectively (Figure 3); thus, the Ir-O bond appears to transition smoothly from formally covalent to dative.³⁹ A conformer of **5a** in which there is no significant Ir-O interaction ($d_{\text{Ir-O}} = 4.4 \text{ \AA}$) is a local minimum with a free energy 7.0 kcal/mol above the lowest free energy conformer of **5a**; this value presumably represents the approximate strength of the dative interaction.

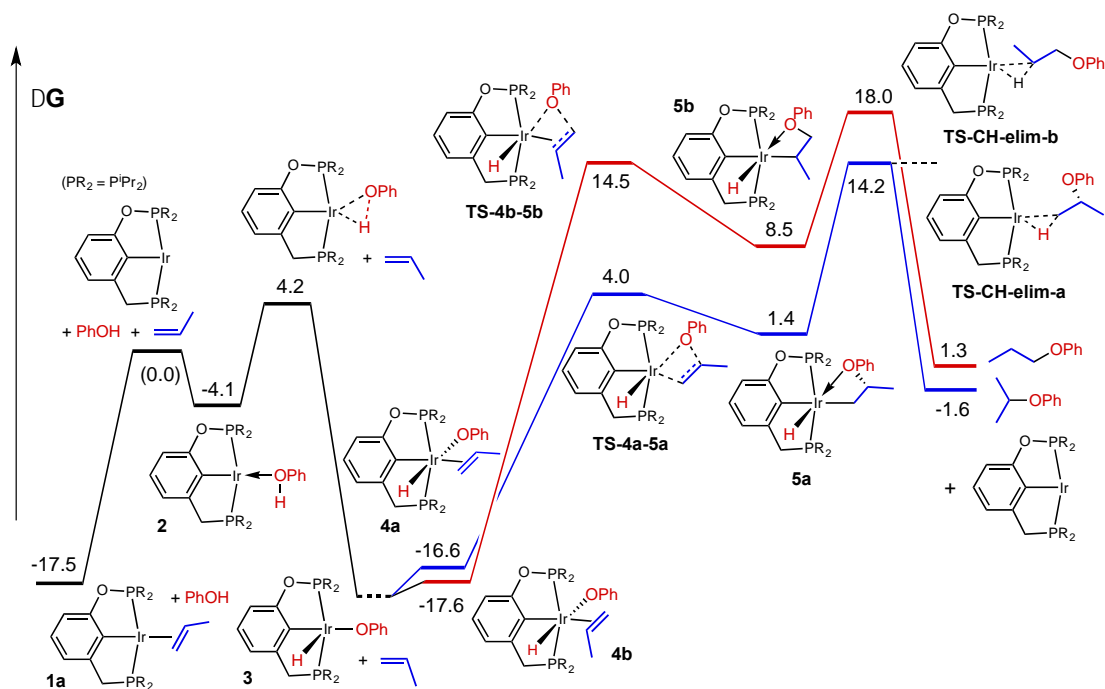


Figure 2. Free energy diagram (M06-L; values of ΔG in kcal/mol) for the proposed 1,2-Ir-O addition pathway for hydrophenoxylation of propene by $(iPrPCOP)Ir$ to give i -PrOAr (observed product; blue lines) and n -PrOAr (not observed; red lines).

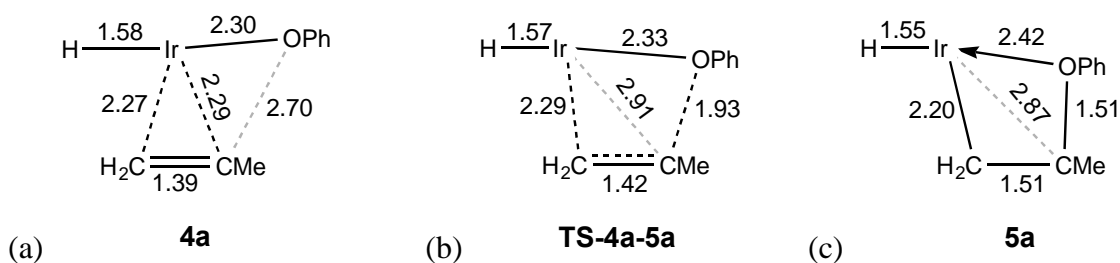


Figure 3. Calculated distances (\AA) for the H-Ir-C-C(propene)-O(phenoxide) unit for the 1,2-Ir-O insertion step. (a) $trans$ - $(iPrPCOP)IrH(OPh)(propene)$ (**4a**) (b) TS for propene insertion (**TS-4a-5a**) (c) insertion product $(iPrPCOP)IrH[CH_2CH(CH_3)OPh]$ (**5a**)

The product of the 1,2-Ir-Oph addition to propene,

(ⁱPrPCOP)Ir[CH₂CH(OPh)CH₃](H) (**5a**), is 18.9 kcal/mol above the propene resting state **1a** (Figure 2). The TS for C-H elimination from this species (**TS-CH-elim-a**), to give *i*-PrOPh, is calculated to have a free energy 31.7 kcal/mol above the resting state (i.e. 14.2 kcal/mol above the reference); this TS leads to a C-H sigma-bond complex (not shown in Fig. 2) that is 22.9 kcal/mol above the resting state (i.e. 5.4 kcal/mol above the reference). We have been unable to locate a proper TS for dissociation of this sigma-bond complex. However, it seems likely (although not certain) that loss of the sigma-C-H-bound ether product (which may proceed dissociatively or via displacement by solvent, phenol, or propene) is fast relative to the back-reaction, C-H addition. In that case, the C-H elimination is the rate-determining step for formation of *i*-PrOPh, with an overall calculated barrier height of 31.7 kcal/mol (**TS-CH-elim-a**), in complete (and presumably fortuitously excellent) agreement with the approximate experimental barrier, $\Delta G^\ddagger \sim 32$ kcal/mol.

Figure 2 also shows a pathway that proceeds via a 2,1-Ir-O addition which would lead to *n*-PrOPh; this represents the mechanism shown in Figure 1b but with the reverse regioselectivity. The 2,1-Ir-O addition has a calculated barrier substantially higher than the 1,2 Ir-O addition; **TS-4b-5b** is 32.0 kcal/mol above the resting state vs. 21.5 kcal/mol for **TS-4a-5a**. The energy of the resulting phenoxy-substituted secondary alkyl hydride, **5b**, is 7.1 kcal/mol above that of the primary alkyl hydride, **5a**, derived from the 1,2-addition (26.0 kcal/mol above the resting state vs. 18.9 kcal/mol). This is also in agreement with Hartwig's study in which it was found that 1,2 addition of the M-O bond was much more favorable than 2,1 addition (with the difference being much greater than that found for M-C addition).³⁹ But, while these 1,2 Ir-O addition energies are higher than

the corresponding values for the 2,1-Ir-O addition, they are not so high as to necessarily preclude formation of the *n*-propyl ether at a rate comparable to that observed for formation of *i*-PrOAr.

The calculations illustrated in Fig. 2 predict that the subsequent C-H elimination, not insertion into the Ir-OAr bond, is both rate- and product-determining. The TS for the C-H elimination, **TS-CH-elim-b**, is of higher energy for the secondary alkyl hydride than for the primary, **TS-CH-elim-a**, by a substantial margin of 3.8 kcal/mol. This difference would correspond to a factor greater than 90 in the rates for formation of *i*-PrOAr ($\Delta G_{\text{calc}}^{\ddagger} = 31.7$ kcal/mol) vs. *n*-PrOAr ($\Delta G_{\text{calc}}^{\ddagger} = 35.5$ kcal/mol) at 150 °C. The calculations thus fully account for the observed rate of formation of *i*-PrOAr and for the absence of *n*-PrOAr. Moreover, the same energy diagram illustrates that the barrier to the back reaction (dehydroaryloxylation) is calculated to be slightly higher for the reaction of *i*-PrOPh than for *n*-PrOPh (by 0.9 kcal/mol). This is also in excellent agreement with experimental observations noted above.

The free energy difference between the two rate-determining C-H elimination TS's, which may determine the very high regioselectivity for formation of *i*-PrOAr vs. *n*-PrOAr, can perhaps be most simply explained by considering the reaction proceeding in the *reverse* direction. The difference of 3.8 kcal/mol can then be viewed as resulting from a combination of two simple factors: (i) The energy of free *i*-PrOAr is lower than that of free *n*-PrOAr (2.9 kcal/mol calculated difference, 3.35 ± 0.43 kcal/mol experimental³⁰). (ii) The barrier for the oxidative cleavage of primary C-H bonds is generally less than for secondary C-H bonds;³⁴ in this case addition of the primary C-H bond of *i*-PrOPh is

calculated to be 0.9 kcal/mol lower than that for the secondary C-H (C2) bond of *n*-PrOPh.

Overall, the calculated results presented above, obtained with the use of the M06-L functional, strongly indicate that C-H elimination is the rate-determining step in the cycle. The calculations are in excellent agreement with experimental results, including the absolute rate and the selectivities for formation of *i*-PrOAr vs. *n*-PrOAr (very high) and for dehydroaryloxylation of *i*-PrOAr vs. *n*-PrOAr (ca. 6-fold). Calculations using the M06 functional lead to essentially the same predictions, including the rate-determining nature of C-H elimination. However, whereas the use of M06-L leads to barrier heights for C-H elimination that are much higher than for insertion (by 10.2 kcal/mol and 3.5 kcal/mol for 1,2-addition and 2,1 addition, respectively), the differences are much less pronounced using M06 (3.5 kcal/mol and 0.7 kcal/mol for 1,2-addition and 2,1 addition, respectively; see Tables S4-5 and Fig. S4). Thus, while DFT calculations obtained using either functional indicate that C-H elimination is rate-determining for hydroaryloxylation (and C-H addition rate-determining for dehydroaryloxylation), future studies to test this important conclusion seem warranted.

It should be noted that two geometrically distinct variants of either the 1,2- or 2,1-Ir-O addition pathways have been calculated. For each pathway there is the variant in which the olefin is initially coordinated trans to the PCP aryl of (ⁱPrPCOP)Ir(OPh)(H) (shown in Fig. 2), and another in which olefin coordinates cis to the PCP aryl, while the phenoxy group is coordinated trans (shown in Figure 4 for 1,2-addition leading to *i*-PrOPh). The olefin-trans variant has a lower-energy TS for insertion of olefin into the Ir-O bond in for both 1,2- and 2,1-additions. Each variant gives rise to a different isomer of

(ⁱPrPCOP)Ir(phenoxypropyl)(H) upon Ir-O addition (**5a** vs. **5c** in the case of the 1,2-addition shown in Fig. 4). In both cases the olefin-trans insertion TS is higher energy than the olefin-cis TS (**TS-4c-5c** vs. **TS-4a-5a** in the case of 1,2-addition). However, the intermediates resulting from Ir-O addition can probably interchange readily (the barrier to decoordination of the phenoxy group, as noted above, is only 7 kcal/mol). Thus, even if the olefin-cis insertion were more facile than the olefin-trans, since the insertion step is not rate-determining the distinction between these pathways would not necessarily be significant.

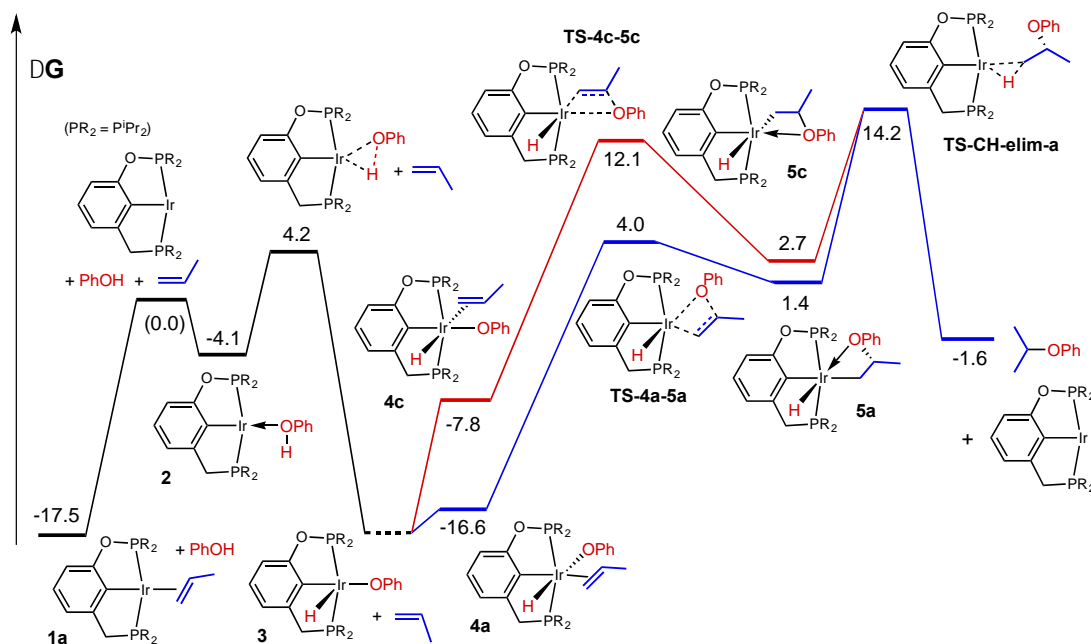


Figure 4. Free energy diagram (M06-L; values of ΔG in kcal/mol) for the proposed 1,2-Ir-O addition pathway for hydrophenoxylation of propene by $(i\text{PrPCOP})\text{Ir}$ to give *i*-PrOAr proceeding via “olefin-trans” (blue) and “olefin-cis” (red) pathways.

Finally, Figure 5 illustrates the results of calculations for the addition of PhOH to ethylene proceeding via the mechanism of Figure 1b, along with the calculated values for the addition to propene in the presence of ethylene, thereby modeling the competition experiment of eq 4. The overall barrier for PhOH addition to ethylene (which is not affected by the presence of propene) is calculated to be 35.6 kcal/mol (the difference between the free energy of **TS-CH-elim-d** and the free energy of $(i\text{PrPCOP})\text{Ir}(\text{ethene})$, **1c**). The overall barrier for hydroaryloxylation of propene, *in the presence of ethylene* (which results in an ethylene bound resting state), is calculated to be 37.7 kcal/mol (the free energy of **TS-CH-elim-a** minus the free energy of the resting state ethene complex **1c**) as compared with 31.7 kcal/mol above the propene-bound resting state. Thus, these

calculations successfully capture both the greater reactivity of ethylene in competition experiments *and* the greater reactivity of propene in independent runs, providing additional support for the proposed mechanism of Fig. 1b. Interestingly, the TS for ethene insertion **TS-4d-5d** is slightly higher than that for propene insertion, **TS-4a-5a**. If that is in fact the case (although the small difference of 0.9 kcal/mol is arguably not meaningful), and if insertion into the Ir-O bond, not C-H elimination, were rate-determining, then the competition experiment of eq 4 would have yielded more *i*-PrOAr than EtOAr, in contrast with the experimental result.

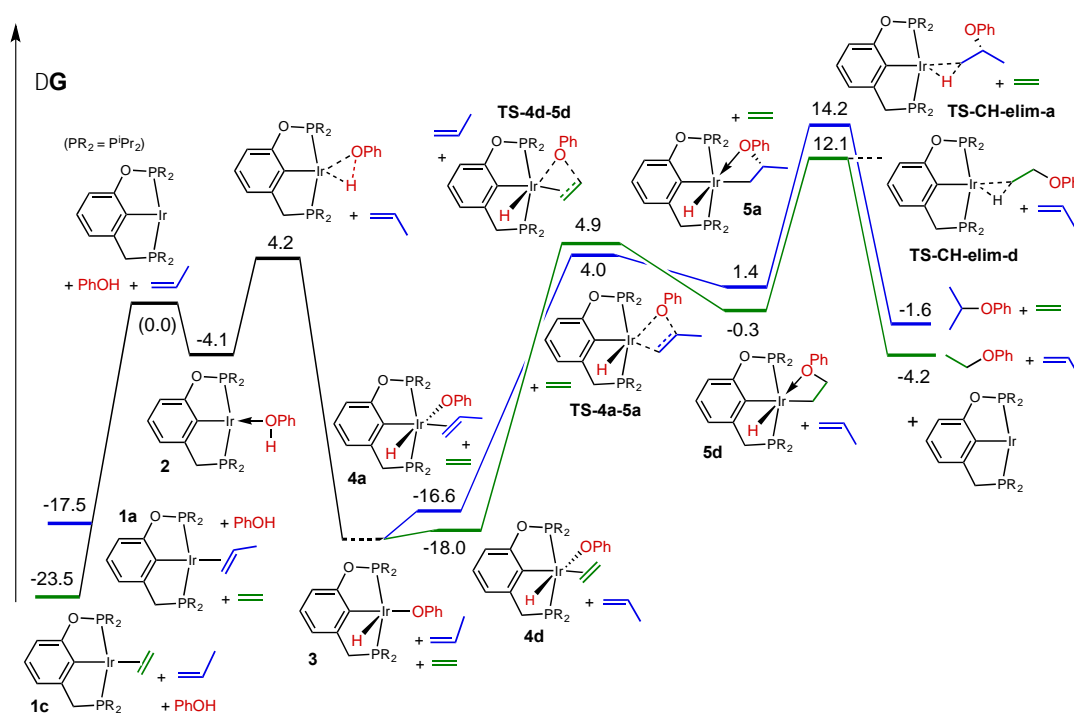


Figure 5. Free energy diagram (values in kcal/mol) for proposed pathway for hydrophenoxylation of ethylene (green lines) and propene (blue lines) by $(i^{\text{Pr}}\text{PCOP})\text{Ir}$. From a common resting state (as in a competition experiment) the barrier to the reaction

of ethylene is lower, but in individual experiments, the overall barrier is lower for the reaction of propene.

Conclusions

DFT studies are conducted on iridium pincer complexes catalyzed olefin hydroaryloxylation systems with simple olefins and phenols. Results from the DFT calculations are consistent with experiments and supports a mechanism proceeding via insertion of olefin into the iridium-aryloxy Ir-O bond. DFT calculations explained the experimentally observed high regioselectivity by showing that this is determined by the energy of the respective TS's for C-H bond elimination, which derives in part from the same factors that control selectivity for C-H bond addition.

The nature of the sterically congested and geometrically well-defined pincer-metal unit, and the formation of secondary alkyl ethers, suggest an entry into the development of olefin hydroaryloxylation catalysis that may display unusual selectivity or enantioselectivity. More generally, the discovery of these well-defined non-acid catalysts suggests the possibility of catalytic intermolecular O-H addition across multiple bonds with a scope broader than phenols and simple olefins. Finally, we find that the catalysts are also effective for the reverse, C-O bond cleavage reaction, dehydroaryloxylation.

References

- (1) Hartwig, J. F. In *Organotransition Metal Chemistry*; University Science Books: Sausalito, CA, 2010, p 667-699.
- (2) Yadav, J. S.; Antony, A.; Rao, T. S.; Subba Reddy, B. V. *J. Organomet. Chem.* **2011**, *696*, 16-36.
- (3) Ananikov, V. P.; Beletskaya, I. P. In *Hydrofunctionalization*; Ananikov, V. P., Tanaka, M., Eds.; Springer Berlin Heidelberg: 2013; Vol. 43, p 1-19.
- (4) Muller, T. E.; Hultsch, K. C.; Yus, M.; Foubelo, F.; Tada, M. *Chem. Rev.* **2008**, *108*, 3795-3892.
- (5) Julian, L. D.; Hartwig, J. F. *J. Am. Chem. Soc.* **2010**, *132*, 13813-13822.
- (6) Julian, L. D.; Springer Berlin Heidelberg: 2013, p 1-47.
- (7) For examples of lanthanide catalyzed intramolecular O-H addition to multiple bonds see (a) Seo, S.; Yu, X.; Marks, T. J. *J. Am. Chem. Soc.* **2008**, *131*, 263-276. (b) Dzudza, A.; Marks, T. J. *Org. Lett.* **2009**, *11*, 1523-1526. (c) Dzudza, A.; Marks, T. J. *Chem.-Eur. J.* **2010**, *16*, 3403-3422.
- (8) Fiege, H.; Voges, H.-W.; Hamamoto, T.; Umemura, S.; Iwata, T.; Miki, H.; Fujita, Y.; Buysch, H.-J.; Garbe, D.; Paulus, W. In *Ullmann's Encyclopedia of Industrial Chemistry*; Wiley-VCH Verlag GmbH & Co. KGaA: 2000.
- (9) Williamson, A. *Philosophical Magazine* **1850**, *37*, 350-356.
- (10) Sowa, F. J.; Hinton, H. D.; Nieuwland, J. A. *J. Am. Chem. Soc.* **1932**, *54*, 3694-3698.
- (11) Yang, C.-G.; He, C. *J. Am. Chem. Soc.* **2005**, *127*, 6966-6967.
- (12) Rosenfeld, D. C.; Shekhar, S.; Takemiya, A.; Utsunomiya, M.; Hartwig, J. F. *Org. Lett.* **2006**, *8*, 4179-4182.
- (13) Li, Z.; Zhang, J.; Brouwer, C.; Yang, C.-G.; Reich, N. W.; He, C. *Organic Letters* **2006**, *8*, 4175-4178.
- (14) Hintermann, L. In *C-X Bond Formation*; Vigalok, A., Ed.; Springer Berlin Heidelberg: 2010; Vol. 31, p 123-155.
- (15) Dang, T. T.; Boeck, F.; Hintermann, L. *J. Org. Chem.* **2011**, *76*, 9353-9361.
- (16) Yamamoto, H.; Futatsugi, K. *Angew. Chem., Intl. Ed.* **2005**, *44*, 1924-1942.
- (17) After this manuscript was submitted for publication, a report by Sevov and Hartwig on a Segphos-iridium catalyzed olefin hydroaryloxylation appeared: Sevov, C. S.; Hartwig, J. F. *J. Am. Chem. Soc.* **2013**, *135*, 9303-9306.
- (18) Some of this work has been presented preliminarily: Haibach, M. C.; Li, B.; Wang, D. Y.; Guan, C.; Krogh-Jespersen, K.; Goldman, A. S. Abstracts of Papers, 245th ACS National Meeting & Exposition, New Orleans, LA, United States, April 7-11, 2013, INOR-130.
- (19) Choi, J.; Choliy, Y.; Zhang, X.; Emge, T. J.; Krogh-Jespersen, K.; Goldman, A. S. *J. Am. Chem. Soc.* **2009**, *131*, 15627-15629.
- (20) Kundu, S.; Choi, J.; Wang, D. Y.; Choliy, Y.; Emge, T. J.; Krogh-Jespersen, K.; Goldman, A. S. *J. Am. Chem. Soc.* **2013**, *135*, 5127-5143.

- (21) See Supporting Information for details.
- (22) Kundu, S.; Choliy, Y.; Zhuo, G.; Ahuja, R.; Emge, T. J.; Warmuth, R.; Brookhart, M.; Krogh-Jespersen, K.; Goldman, A. S. *Organometallics* **2009**, *28*, 5432-5444.
- (23) Zhu, K.; Achord, P. D.; Zhang, X.; Krogh-Jespersen, K.; Goldman, A. S. *J. Am. Chem. Soc.* **2004**, *126*, 13044-13053.
- (24) Ahuja, R.; Punji, B.; Findlater, M.; Supplee, C.; Schinski, W.; Brookhart, M.; Goldman, A. S. *Nature Chem.* **2011**, *3*, 167-171.
- (25) Choi, J.; MacArthur, A. H. R.; Brookhart, M.; Goldman, A. S. *Chem. Rev.* **2011**, *111*, 1761-1779.
- (26) Haibach, M. C.; Kundu, S.; Brookhart, M.; Goldman, A. S. *Acc. Chem. Res.* **2012**, *45*, 947-958.
- (27) Pincer iridium dihydrides and tetrahydrides are well known to undergo dehydrogenation by olefin, and are therefore presumed to act simply as precursors of the corresponding (pincer)Ir fragment. Likewise, the ethylene adducts and the hydrido chlorides in the presence of strong base are known precursors of the same fragment. (a) Gupta, M.; Hagen, C.; Kaska, W. C.; Cramer, R. E.; Jensen, C. M. *J. Am. Chem. Soc.* **1997**, *119*, 840-841. (b) Renkema, K. B.; Kissin, Y. V.; Goldman, A. S. *J. Am. Chem. Soc.* **2003**, *125*, 7770-7771. (c) Götter-Schnetmann, I.; White, P.; Brookhart, M. *J. Am. Chem. Soc.* **2004**, *126*, 1804-1811.
- (28) (ⁱPrPCOP)IrH₄ was generated from the reported (ⁱPrPCOP)Ir(C₂H₄) complex and H₂ at room temperature. See the Supplementary Information for experimental details and spectral data.
- (29) Dehydroalkoxylation, catalyzed by lanthanide triflates and thermodynamically driven by hydrogenation of the olefin product catalyzed by Pd nanoparticles (at 110 °C in the case of acyclic ethers) was recently reported by Marks and co-workers: Atesin, A. C.; Ray, N. A.; Stair, P. C.; Marks, T. J. *J. Am. Chem. Soc.* **2012**, *134*, 14682-14685.
- (30) Afeefy, H. Y.; Liebman, J. F.; Stein, S.E. "Neutral Thermochemical Data" in NIST Chemistry WebBook, NIST Standard Reference Database Number 69, Eds. P.J. Linstrom and W.G. Mallard, National Institute of Standards and Technology, Gaithersburg MD, 20899, <http://webbook.nist.gov>, (retrieved February 11, 2013)
- (31) Conversion from a mixture of products to exclusively (ⁱPrPCOP)Ir(η²-propene) is observed upon raising the temperature from ambient to 120 °C. It seems safe to assume that at 150 °C, the temperature of most of our experimental runs, the major species is still predominantly the same propene complex. Unfortunately, however, the temperature limits of our NMR spectrometers did not allow observation at this temperature. (Note that when the temperature is taken back down to ambient in between intervals of heating at 150 °C, the original mixture is again observed, which, on warming to 120 °C in the NMR spectrometer, again yields exclusively (ⁱPrPCOP)Ir(η²-propene)).
- (32) Schwartz, J.; Labinger, J. A. *Angew. Chem., Int. Ed.* **1976**, *15*, 333-340.
- (33) Reger, D. L.; Culbertson, E. C. *Inorg. Chem.* **1977**, *16*, 3104-3107.

- (34) Some excellent lead references to organometallic C-H addition, with particular emphasis on selectivity: (a) Bennett, J. L.; Vaid, T. P.; Wolczanski, P. T. *Inorg. Chim. Acta.* **1998**, *270*(1-2), 414-423 (b) Wick, D. D.; Jones, W. D. *Organometallics* **1999**, *18*, 495-505. (c) Asbury, J. B.; Hang, K.; Yeston, J. S.; Cordaro, J. G.; Bergman, R. G.; Lian, T. *J. Am. Chem. Soc.* **2000**, *122*, 12870 - 12871 and references 4-11 therein. (d) Vetter, A. J.; Flaschenriem, C.; Jones, W. D. *J. Am. Chem. Soc.* **2005**, *127*, 12315-12322. (e) Balcells, D.; Clot, E.; Eisenstein, O. *Chem. Rev.* **2010**, *110*, 749-823.
- (35) Hartwig, J. F. In *Organotransition Metal Chemistry*; University Science Books: Sausalito, CA, 2010, p 85-146.
- (36) Bryndza, H. E. *Organometallics* **1985**, *4*, 406-8.
- (37) Woerpel, K. A.; Bergman, R. G. *J. Am. Chem. Soc.* **1993**, *115*, 7888-7889.
- (38) Zhao, P.; Incarvito, C. D.; Hartwig, J. F. *J. Am. Chem. Soc.* **2006**, *128*, 9642-9643.
- (39) Tye, J. W.; Hartwig, J. F. *J. Am. Chem. Soc.* **2009**, *131*, 14703-14712.
- (40) Hartwig, J. F. *Nature* **2008**, *455*, 314-322

Computational Details

DFT calculations¹ employed the M06-L exchange-correlation functionals.² The electronic environment was modeled using the following scheme: for Ir, we applied the Hay-Wadt relativistic effective (small) core potential³ and the LANL2TZ basis set^{4a} augmented by a diffuse d-type function (exponent = 0.07645);^{4b} all other atoms (P, O, C and H) were assigned 6-311G(d,p) basis sets.⁵ Calculations were performed on the actual molecular species used in the experiments, i.e. pincers retained the bulky *i*Pr groups on P. Standard optimization procedures were employed to obtain the geometries and electronic energies for stationary points. Normal mode analysis was performed for each species and the resulting set of vibrational frequencies was employed (without scaling) to determine zero-point energy corrections. Enthalpies (H) and Gibbs' free energies (G; T = 298.15 K, P = 1 atm) were obtained from the electronic energies (E) using standard statistical mechanical expressions.⁶ The free energies quoted in the manuscript text and figures have been modified to correspond to a standard state of T = 423 K (150 °C) and a concentration of 1 M (~ 34.7 atm at T = 423 K) for all species participating in the reaction using standard thermodynamic corrections.⁶ All calculations have been performed using the Gaussian 09 collection of computer programs.⁷

Tables of Energetic Quantities

Table S1. Potential energies, enthalpies, entropies and free energies for the proposed 1,2-Ir-O addition pathway for hydrophenoxylation of propene by (ⁱPrPCOP)Ir to afford the observed product *i*-PrOAr (Figure 6).^a

Proposed addition pathway for hydrophenoxylation of olefin ($:=C_3H_6$) by (ⁱ PrPCOP)Ir ($:=[Ir]$) to afford $(CH_3)_2C-OAr$ ($:=i-PrOAr$)	ΔE	ΔH	ΔS	ΔG
[Ir] + olefin + PhOH	0.0	0.0	0.0	0.0
[Ir](olefin) + PhOH	-38.5	-39.3	-42.3	-21.4
TS: OH Addition + olefin	-14.2	-15	-36.1	0.2
[Ir](H)(OPh) + olefin	-35.6	-36.5	-41.2	-19.0
[Ir](H)(OPh)(olefin) (red path)	-48.4	-50.1	-81.8	-15.5
[Ir](H)(OPh)(olefin) (blue path)	-44.1	-45.8	-80.4	-11.8
TS: Olefin Insertion (red path)	-29.0	-30.7	-83.6	4.7
TS: Olefin Insertion (blue path)	-24.5	-26.2	-81.2	8.1
[Ir](H)(CH ₂ CHMeOPh) (red path)	-34.7	-36.4	-80.0	-2.5
[Ir](H)(CH ₂ CHMeOPh) (blue path)	-35.4	-37.1	-84.8	-1.2
TS: Reductive Elimination (red path)	-20.3	-22.0	-76.8	10.5
TS: Reductive Elimination (blue path) ^b	-21.4	-23.1	-80.7	11.1
[Ir] + <i>i</i> -PrOPh	-15.9	-16.8	-35.9	-1.6

^a Units are kcal/mol for ΔE , ΔH , and ΔG ; units are cal/(deg•mol) for ΔS . The standard state for concentrations is 1 M for each species participating in the reaction; T = 423.15 K. ^b We believe this **blue path** TS for RE would readily interconvert to the lower energy TS found for the **red path**. Hence only one TS for RE is indicated in Figure 6.

Table S2. Potential energies, enthalpies, entropies and free energies for the hypothetical 2,1-Ir-O addition pathway for hydrophenoxylation of propene by (ⁱPrPCOP)Ir to afford the non-observed species *n*-PrOAr (Figure 8).^a

Hypothetical addition pathway for hydrophenoxylation of olefin ($=C_3H_6$) by (ⁱ PrPCOP)Ir ($=[Ir]$) to afford ($CH_3CH_2CH_2OPh$) ($=n$ -PrOAr)	ΔE	ΔH	ΔS	ΔG
[Ir] + olefin + PhOH	0.0	0.0	0.0	0.0
[Ir](olefin) + PhOH	-38.5	-39.3	-42.3	-21.4
TS: OH Addition + olefin	-14.2	-15.0	-36.1	0.2
[Ir](H)(OPh) + olefin	-35.6	-36.5	-41.2	-19.0
[Ir](H)(OPh)(olefin) (red path)	-48.8	-50.5	-81.2	-16.2
[Ir](H)(OPh)(olefin) (blue path)	-45.0	-46.7	-80.2	-12.8
TS: Olefin Insertion (red path)	-22.0	-23.7	-81.0	10.5
TS: Olefin Insertion (blue path)	-19.2	-20.9	-81.7	13.7
[Ir](H)(CHMeCH ₂ OPh) (red path)	-30.1	-31.8	-85.9	4.5
[Ir](H)(CHMeCH ₂ OPh) (blue path)	-30.1	-31.8	-85.9	4.5
TS: Reductive Elimination (red path)	-15.5	-17.2	-85.0	18.8
TS: Reductive Elimination (blue path) ^b	-15.3	-17.0	-81.2	17.4
[Ir] + <i>n</i> -PrOPh	-12.7	-13.6	-35.2	1.3

^a Units are kcal/mol for ΔE , ΔH , and ΔG ; units are cal/(deg•mol) for ΔS . The standard state for concentrations is 1 M for each species participating in the reaction; T = 423.15 K. ^b We believe this **blue path** TS for RE would readily interconvert to the lower energy TS found for the **red path**. Hence only one TS for RE is indicated in Figure 8.

Table S3. Potential energies, enthalpies, entropies and free energies for the proposed pathway for hydrophenoxylation of ethylene by (ⁱPrPCOP)Ir (Figure 9).

Proposed pathway for hydrophenoxylation of olefin (:=C ₂ H ₄) by (ⁱ PrPCOP)Ir (:=[Ir]) to afford (CH ₃ CH ₂ OPh) (:= <i>ether</i>)	ΔE	ΔH	ΔS	ΔG
[Ir] + olefin + PhOH	0.0	0.0	0.0	0.0
[Ir](olefin) + PhOH	-40.4	-41.3	-32.8	-27.4
TS: OH Addition + olefin	-14.2	-15.0	-36.1	0.2
[Ir](H)(OPh) + olefin	-35.6	-36.5	-41.2	-19.0
[Ir](H)(OPh)(olefin)	-50.0	-51.7	-77.4	-18.9
TS: β -OPh Elimination	-28.5	-30.2	-77.5	2.6
[Ir](H)(CH ₂ CH ₂ OPh)	-35.7	-37.4	-78.4	-4.2
TS: Reductive Elimination	-22.4	-24.1	-76.2	8.1
[Ir] + <i>ether</i>	-17.0	-17.8	-32.3	-4.2

^a Units are kcal/mol for ΔE , ΔH , and ΔG ; units are cal/(deg•mol) for ΔS . The standard state for concentrations is 1 M for each species participating in the reaction; T = 423.15 K.

Table S4. Potential energies, enthalpies, entropies and free energies using M06-L functionals for the proposed 1,2-Ir–O addition pathway for reaction of 3,5-dimethylphenol (ArOH) and propene.

Proposed addition pathway for hydroaryloxylation of C ₃ H ₆ by (ⁱ PrPCOP)Ir ([Ir]) to afford (CH ₃) ₂ CH-O(3,5-di-MePh) (<i>i</i> -PrOAr)	ΔE	ΔH	ΔS	ΔG
[Ir] + C ₃ H ₆ + ArOH	0.00	0.00	0.00	0.00
[Ir](C ₃ H ₆) + ArOH	-35.83	-36.51	-44.85	-17.53
[Ir](C ₃ H ₆) + olefin	-20.40	-19.72	-35.01	-4.90
TS: OH Addition + olefin	-13.58	-13.31	-37.63	2.61
[Ir](H)(C ₃ H ₆) + olefin	-38.67	-38.61	-44.32	-19.86
[Ir](H)(OAr)(C ₃ H ₆)	-47.82	-48.29	-88.47	-10.85
TS: Olefin Insertion	-28.43	-28.94	-83.72	6.49
[Ir](H)(CH ₂ CHMe-OAr)	-34.07	-34.88	-85.95	1.49
TS: Reductive Elimination	-22.14	-22.52	-80.46	11.53
[Ir] + <i>i</i> -PrOAr	-16.06	-16.66	-36.82	-1.08

^a Units are kcal/mol for ΔE , ΔH , and ΔG ; units are cal/(deg•mol) for ΔS . The standard state for concentrations is 1 M for each species participating in the reaction; T = 423.15 K.

Table S5. Potential energies, enthalpies, entropies and free energies obtained using M06 functionals for the proposed 1,2-Ir–O addition pathway for hydrophenoxylation of propene by (ⁱPrPCOP)Ir to afford the observed product *i*-PrOPh.^a

Proposed addition pathway for hydrophenoxylation of C ₃ H ₆ by (ⁱ PrPCOP)Ir ([Ir]) to afford (CH ₃) ₂ C–OPh (<i>i</i> -PrOPh)	ΔE	ΔH	ΔS	ΔG
[Ir] + C ₃ H ₆ + PhOH	0.0	0.0	0.0	0.0
[Ir](C ₃ H ₆) + PhOH	-37.1	-37.8	-44.6	-19.0
[Ir](HOPh) + C ₃ H ₆	-20.3	-19.7	-37.2	-4.0
TS: OH Addition + C ₃ H ₆	-10.1	-9.9	-37.8	6.1
[Ir](H)(OPh) + C ₃ H ₆	-34.9	-35.0	-41.7	-17.3
[Ir](H)(OPh)(C ₃ H ₆) (<i>trans</i> path ^b)	-44.3	-44.6	-83.4	-9.3
[Ir](H)(OPh)(C ₃ H ₆) (<i>cis</i> path)	-41.0	-41.7	-82.3	-6.9
TS: Olefin Insertion (<i>trans</i> path)	-24.4	-25.6	-87.2	11.3
TS: Olefin Insertion (<i>cis</i> path)	-20.5	-21.5	-87.6	15.6
[Ir](H)(CH ₂ CHMeOPh) (<i>trans</i> path)	-32.4	-33.7	-87.9	3.5
[Ir](H)(CH ₂ CHMeOPh) (<i>cis</i> path)	-33.0	-34.0	-87.0	2.8
TS: Reductive Elimination (<i>trans</i> path)	-21.4	-22.4	-84.3	13.3
TS: Reductive Elimination (<i>cis</i> path) ^c	-23.5	-24.5	-82.8	10.5
[Ir] + <i>i</i> -PrOPh	-17.8	-18.4	-35.6	-3.4
TS:C-O Elimination (Fig 1a), <i>i</i> -PrOPh formed	1.0	0.8	-78.3	33.9

TS:C-O Elimination (Fig 1a), <i>n</i> -PrOPh formed	5.4	5.1	-76.8	37.6
--	-----	-----	-------	------

^a Units are kcal/mol for ΔE , ΔH , and ΔG ; units are cal/(deg•mol) for ΔS . The standard state for concentrations is 1 M for each species participating in the reaction; T = 423.15 K. ^b The *trans* and *cis* paths refer to C₃H₈ binding *trans* and *cis* to the ^{iPr}PCOP phenyl ring. ^c We believe this *cis* TS for RE would readily interconvert to the lower energy TS found for the *trans* path.

Computational Section References

1. Parr, R.G. & Yang, W. *Density-Functional Theory of Atoms and Molecules* (University Press: Oxford, 1989).
2. Zhao, Y. & Truhlar, D. G. The M06 suite of density functionals for main group thermochemistry, thermochemical kinetics, noncovalent interactions, excited states, and transition elements: two new functionals and systematic testing of four M06-class functionals and 12 other functional. *Theo. Chem. Acc.* **120**, 215-241 (2008).
3. Hay, P.J. & Wadt, W.R. Ab-initio Effective Core Potentials for Molecular Calculations – Potentials for K to Au Including the Outermost Core Orbitals. *J. Chem. Phys.* **82**, 299–310 (1985).
4. (a) Roy, L. E., Hay, P. J. & Martin, R. L. Revised Basis Sets for the LANL Effective Core Potentials. *J. Chem. Theory Comput.* **4**, 1029-1031 (2008). (b) Value obtained as one-half times the exponent of the outermost d-type function in the LANL2TZ basis set for Ir.
5. (a) K. Raghavachari, K., Binkley, J. S., Seeger, R., & J. A. Pople, J. A. Self-Consistent Molecular Orbital Methods. 20. Basis set for correlated wave-functions. *J. Chem. Phys.* **72**, 650-654 (1980). (b) McLean, A. D. & Chandler, G. S. Contracted Gaussian-basis sets for molecular calculations. 1. 2nd row atoms, Z=11-18. *J. Chem. Phys.* **72**, 5639-5648 (1980).
6. McQuarrie, D.A. *Statistical Thermodynamics* (Harper and Row: New York, 1973).
7. Gaussian 09, Revision A.02, Frisch, M. J.; Trucks, G. W.; Schlegel, H. B.; Scuseria, G. E.; Robb, M. A.; Cheeseman, J. R.; Scalmani, G.; Barone, V.; Mennucci, B.; Petersson, G.. A.; Nakatsuji, H.; Caricato, M.; Li, X.; Hratchian, H. P.; Izmaylov. A. F.; Bloino, J; Zheng, G.; Sonnenberg, J. L.; Hada, M.; Ehara, M.; Toyota, K.; Fukuda, R.; Hasegawa, J.; Ishida, M.; Nakajima, T.; Honda, Y.; Kitao, O.; Nakai, H.; Vreven, T.; Montgomery, Jr., J. A.; Peralta, J. E.; Ogliaro, F.; Bearpark, M.; Heyd, J. J.; Brothers. E.; Kudin, K. N.; Staroverov, V. N.; Kobayashi, R.; Normand, J.; Raghavachari, K.; Rendell, A.; Burant, J. C.; Iyengar, S. S.; Tomasi, J.; Cossi, M.; Rega, N.; Millam, J. M.; Klene, M.; Knox, J. E.; Cross, J. B.;

Bakken, V.; Adamo, C.; Jaramillo, J.; Gomperts, R.; Stratmann, R. E.; Yazyev, O.; Austin, A. J.; Cammi, R.; Pomelli, C.; Ochterski, J. W.; Martin, R. L.; Morokuma, K.; Zakrzewski, V. G.; Voth, G. A.; Salvador, P.; Dannenberg, J. J.; Dapprich, S.; Daniels, A. D.; Farkas, O.; Foresman, J. B.; Ortiz, J. V.; Cioslowski, J.; and Fox, D. J., Gaussian, Inc., Wallingford CT, 2009.

Chapter 3

Computational Study of PNP Pincer Iridium Catalyzed Alkene Hydrogenation

Majority of this chapter is reproduced with permission from

**Synthesis and Characterization of Carbazolide-Based Iridium PNP Pincer
Complexes. Mechanistic and Computational Investigation of Alkene
Hydrogenation: Evidence for an Ir(III)/Ir(V)/Ir(III) Catalytic Cycle**

Chen Cheng, Bong Gon Kim, Damien Guironnet, Maurice Brookhart, Changjian Guan,

David Y. Wang, Karsten Krogh-Jespersen, and Alan S. Goldman

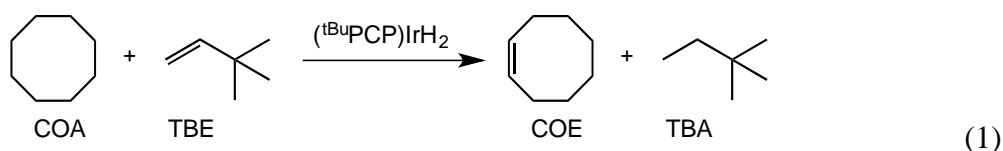
J. Am. Chem. Soc., **2014**, 136, 6672–6683

Copyright © 2013 American Chemical Society

Introduction

Dehydrogenation of alkanes to alkenes using homogeneous catalysts has received intense interest in recent years.¹⁻⁴ Dehydrogenation reactions can be run in an “acceptorless” mode,⁵ but most commonly the reaction is run as a transfer dehydrogenation where a sacrificial alkene is used as a hydrogen acceptor. Transfer dehydrogenation is one of the two key reactions in the dual catalytic system used to achieve alkane metathesis, a potentially important reaction for converting low molecular weight hydrocarbons to higher molecular weight hydrocarbons useful for fuels.⁶⁻⁸ Conversion of linear alkanes to aromatics under homogeneous conditions has also been achieved via multiple transfer dehydrogenations coupled with electrocyclic ring closure of intermediate trienes.⁹

While a number of early reported systems based on late transition metal complexes showed promise,¹⁰ a major breakthrough was the discovery by Kaska and Jensen that the iridium pincer complex $[\text{C}_6\text{H}_3\text{-}2,6\text{-(CH}_2\text{P}(t\text{-Bu})_2)_2]\text{IrH}_2$, $(^t\text{BuPCP})\text{IrH}_2$, catalyzes the transfer dehydrogenation reaction between cyclooctane (COA) and *t*-butylethylene (TBE) to form cyclooctene (COE) and *t*-butylethane (TBA) with high turnover numbers at 200 °C (eq 1);¹¹ this reaction is often regarded as a benchmark for screening catalysts for transfer dehydrogenation.



Following this initial report, extensive investigations of transfer dehydrogenations using the $(^t\text{BuPCP})\text{IrH}_2$ pincer complex and many other PCP-type

derivatives have been reported.¹²⁻¹⁷ The three most well examined frameworks, “PCP”, “POCOP”^{18,19} and “PCOP”⁷, are shown in Fig. 1. Extensive screening reactions, mechanistic studies and DFT investigations of these systems have been reported.^{14,19-24}

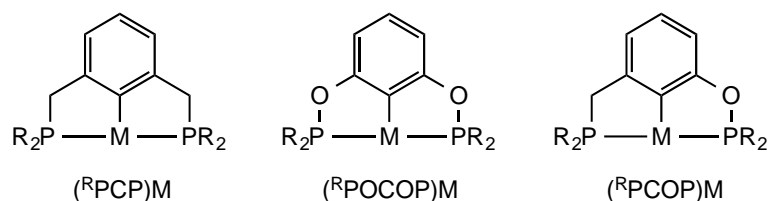
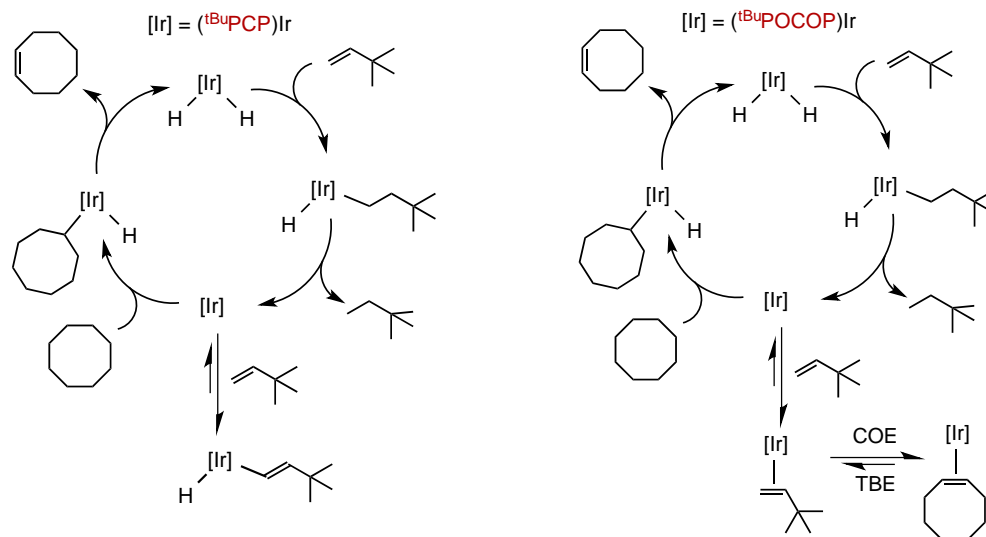


Figure 1. Common PCP-type pincer complexes.

The basic mechanism established for transfer dehydrogenation using the COA/TBE system is shown in Scheme 1. In the case of the (^tBuPCP)Ir system, at low TBE concentration the catalyst resting state is the dihydride and the turnover-limiting step is hydrogenation of TBE, while at high TBE concentration the resting state is the vinyl hydride and dehydrogenation is turnover-limiting.²² For the (^tBuPOCOP)Ir system, the resting state is the alkene complex and dehydrogenation is turnover-limiting.¹⁹

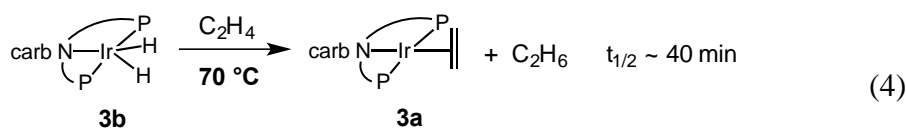
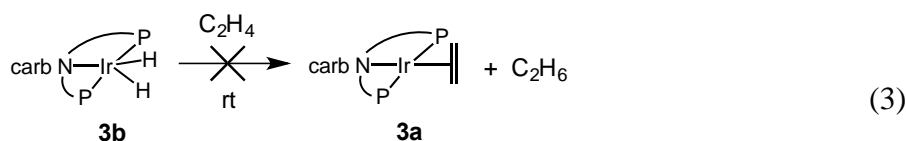
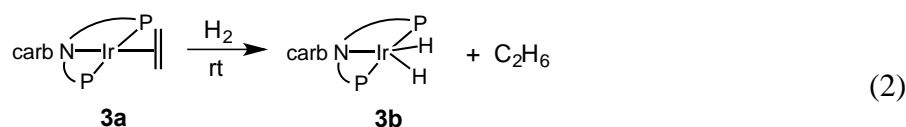
Scheme 1. Hydrogen transfer between COA and TBE using PCP- and POCOP-iridium pincer complexes.



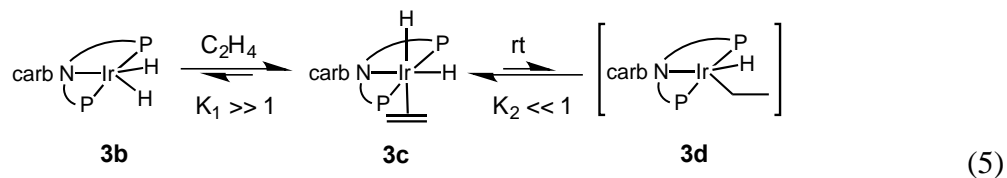
Convenient rates for transfer dehydrogenation for the PCP and POCOP systems occur at temperatures in the range of ca. 125 °C – 200 °C. Thus, temperatures employed for alkane metathesis using these catalysts must also be in this range despite the fact that the molecular olefin metathesis co-catalysts often decompose rapidly at these elevated temperatures and operate more effectively at lower temperatures.²⁵ In part for this reason, it is desirable to develop new transfer dehydrogenation catalysts that function at lower temperatures.

DFT calculations have shown that the thermodynamic favorability of oxidative addition of non-polar substrates, including H_2 and RH , to the fragment XML_2 ($\text{M} = \text{Ir}$, Rh) increases as the sigma-donating ability of X decreases.^{26,27} The direction of this effect is opposite that which is generally accepted for oxidative addition, and, moreover, the magnitude is surprisingly large. For example, addition of $\text{CH}_3\text{-H}$ to $\text{Ir}(\text{PH}_3)_2\text{F}$ is

room temperature in the absence of H₂ over 24 hours (eq 3). Experiment shows that hydrogenation of C₂H₄ with **3b** under a C₂H₄ atmosphere (eq 4) proceeding at 70 °C has a half-life of ca. 40 min, which converts to a barrier of $\Delta G^\ddagger \sim 26$ kcal/mol. This behavior is in dramatic contrast to the ^tBuPOCOP iridium(III) dihydride complex which hydrogenates a much bulkier alkene, COE, at -70 °C.¹⁹ (^tBuPCP)IrH₂ also reacts with the bulky TBE to give TBA under relatively mild conditions (ca. 55 °C) and with 1-alkenes rapidly even at sub-ambient temperatures.^{22,31}



The iridium dihydride **3b** binds C₂H₄ immediately and forms an Ir(III) ethylene dihydride species, **3c**, with *cis*-dihydride geometry at -50 °C (eq 5). This reaction is reversible and thermodynamically favored ($K_1 \gg 1$, eq 5). The free energy barrier for exchange of free C₂H₄ with **3c** at -20 °C was estimated to be ~13 kcal/mol and a large positive ΔS^\ddagger value (~40 cal K⁻¹ mol⁻¹) was determined for the exchange. The rate of exchange was found to be independent of the C₂H₄ concentration, which is consistent with a dissociative mechanism for C₂H₄ exchange.

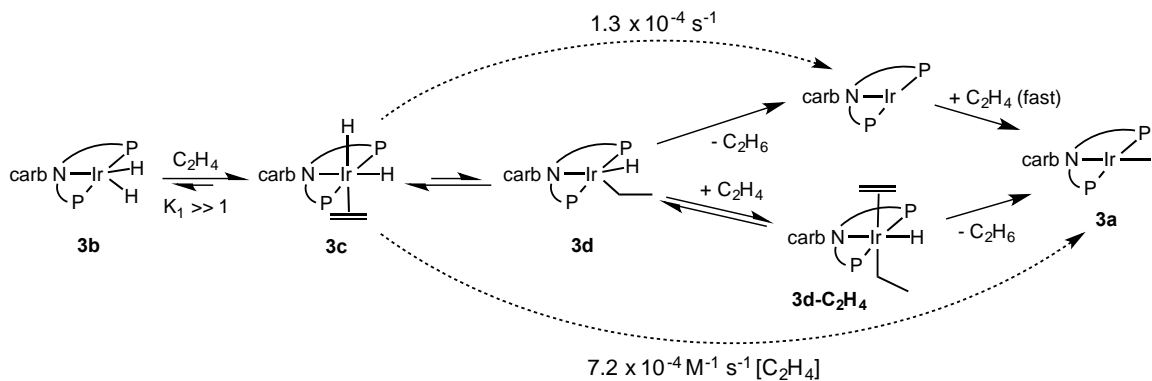


The ethylene dihydride complex **3c** is the resting state under C_2H_4 atmosphere at room temperature. A reversible insertion of C_2H_4 ligand on **3c** into Ir-H bond was observed at room temperature, and thus strongly suggests that the rate-limiting step for hydrogenation of C_2H_4 with **3b** under excess C_2H_4 is reductive elimination of C_2H_6 . The barrier of C_2H_4 insertion reaction was estimated at $\Delta G^\ddagger \approx 21$ kcal/mol at -10 °C, with a small $\Delta\Delta S^\ddagger$ value of ca. 3 e.u., consistent with an intramolecular rearrangement reaction. Kinetic experiments revealed that the rate of stoichiometric hydrogenation of C_2H_4 with dihydride **3b** under excess C_2H_4 (eq 4) is dependent on $[C_2H_4]$ in the range 0.05-0.9 M at 75 °C according to eq 6.

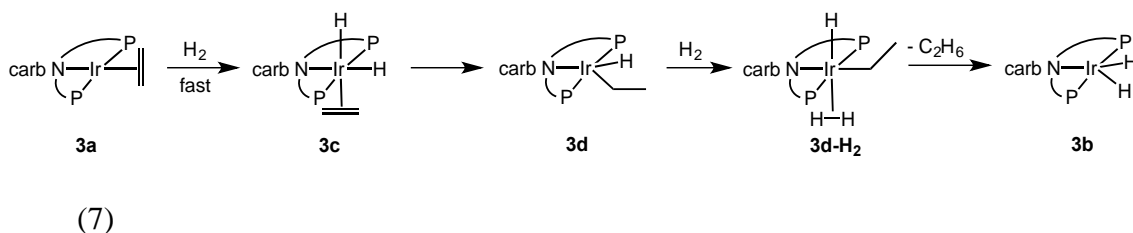
$$k_{\text{obs}} = 1.3 \times 10^{-4} \text{ s}^{-1} + 7.2 \times 10^{-4} \text{ M}^{-1} \text{ s}^{-1} [C_2H_4] \quad (6)$$

The non-zero value of k_{obs} in the limit as $[C_2H_4]$ approaches zero is consistent with a unimolecular pathway that proceeds via elimination of ethane from **3d**. The $[C_2H_4]$ -dependent term suggests that the major pathway under high C_2H_4 pressure involves, in addition to the ethylene molecule that rapidly coordinates to give **3c**, a second molecule of ethylene in the transition state for reductive elimination of ethane from **3d**; this would be consistent with formation of the six-coordinate species $(^{\text{carb}}\text{PNP})\text{Ir}(\text{H})(\text{C}_2\text{H}_5)(\text{C}_2\text{H}_4)$ (**3d-C₂H₄**) prior to ethane elimination (Scheme 3).

Scheme 3. Proposed pathways (unimolecular and bimolecular) for the reaction of **3c** with C_2H_4 to yield **3a** and C_2H_6 (rate constants determined at 75 °C)



In the hydrogenation of ethylene complex **3a** with H_2 to form dihydride **3b** and ethane, ethylene dihydride **3c** was formed as resting state, and it converts to dihydride **3b** under 1 atm H_2 in ca. 5 min at 25 °C. These observations suggest that the ethyl hydride complex **3d**, formed by migratory insertion of **3c**, is trapped by H_2 to form a six-coordinate dihydrogen complex, **3d-H₂**, and that this complex undergoes elimination of ethane at a rate much greater than ethane elimination from the five-coordinate **3d** (eq 7).



Acceleration by H_2 of propene and TBE hydrogenation by the carbazole-based dihydride **3b** was also observed. The catalyst resting state in each of these hydrogenations is the dihydride complex **3b**. These observations further support the contention that alkane elimination from the iridium center in the carbazole system is facilitated by H_2 .

Results and Discussion

The results of DFT calculations on the reaction of carbazole iridium dihydride **3b** with ethylene are consistent with and quite helpful in explaining the experimental observations. We applied the M11 functional in electronic structure calculations.³³ The pincer ligands retained the bulky *i*-Pr groups on phosphorus. Enthalpies (H°) and Gibbs free energies (G° ; $T = 298.15$ K, $P = 1$ atm) were obtained from the electronic energies (E) using standard statistical mechanical expressions. Complete computational details are provided in the Supporting Information.

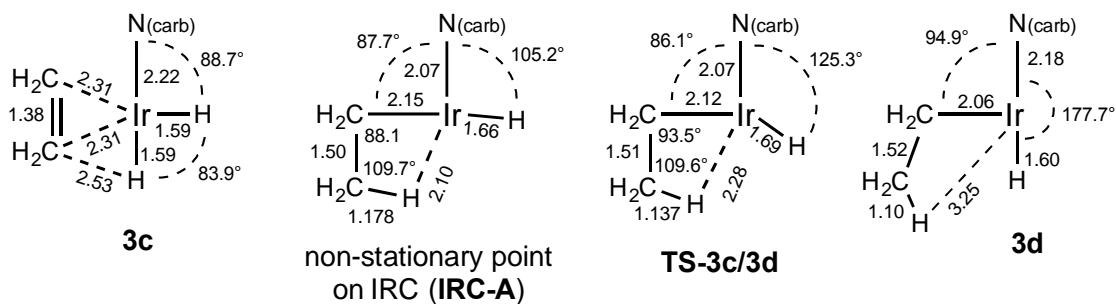
a. Reaction of dihydride 3b with ethylene to afford ethyl hydride 3d. In accord with experiment, the reaction of **3b** with ethylene is calculated to yield the cis-dihydride ethylene complex **3c**. The addition is calculated to be exergonic and the kinetic barrier to this reaction is calculated to be quite low, $\Delta G^\ddagger = 5.0$ kcal/mol, consistent with the immediate formation of **3c** observed upon addition of ethylene to a solution of **3b**. The calculated free energy of olefin addition ($\Delta G^\circ_{\text{calc}} = -2.9$ kcal/mol) is about at the upper limit consistent with experiment, since the observed equilibrium lies fully to the right indicating that $\Delta G^\circ < \text{ca. } -3$ kcal/mol. The calculated barrier to dissociation, $\Delta G^\ddagger = 7.9$ kcal/mol, is somewhat lower than the barrier of ca. 13 kcal/mol indicated by the experimentally determined rate of exchange with free ethylene. These results may suggest that ligand binding energies are understated by the computational method. It is worth noting, as we compare associative vs. dissociative reaction pathways below, that this propensity would only lead to a computational bias in favor of dissociative pathways.

In contrast to the kinetically facile addition of ethylene to **3b** to give the cis-dihydride ethylene complex **3c** ($\Delta G^\ddagger = 5.0$ kcal/mol), ethylene addition to give the *trans*

dihydride is calculated to have an extremely high kinetic barrier, ca. 46 kcal/mol, as well as somewhat unfavorable thermodynamics ($\Delta G^{\circ}_{\text{calc}} = +9.1$ kcal/mol).³⁴ In agreement with these calculated values, the trans-dihydride was never observed experimentally in the course of this work.

Locating a plausible TS for the seemingly simple insertion reaction of the coordinated ethylene of **3c** into the Ir-H bond turned out to be computationally intricate. The product of olefin insertion, ethyl hydride **3d**, is a pentacoordinate metal d^6 species and hence susceptible to *pseudo* second-order Jahn-Teller effects; accordingly, several square-pyramidal (SQP) or trigonal-bipyramidal (TBP) structures may exist for **3d**.³⁵ The lowest energy conformer of **3d** is SQP with ethyl apical and the carbazolide nitrogen and hydride ligands oriented trans to each other ($\angle\text{N-Ir-H} = 177.7^\circ$, see Scheme 4); this is a T_C structure in the notation of Eisenstein and Pelissier.³⁶ The T_C conformer of **3d** is 6.1 kcal/mol above **3c** in free energy; other SQP structures located, namely T_H and T_{Ncarb} , are found 9.7 kcal/mol and 35.5 kcal/mol above **3c**, respectively. A TBP structure, denoted Y_{Ncarb} ($\angle\text{H-Ir-C} = 75.9^\circ$), is 8.1 kcal/mol above **3c**.

Scheme 4. Species on the reaction pathway from **3c** to **3d**. Metrics are shown (bond lengths in Å) for the coordination sphere excluding the coordinating P atoms (i.e. for the ligands in the approximate plane bisecting the P-Ir-P axis).



Some geometrical parameters pertaining to the lowest energy conformers of **3c**, **3d**, and the TS of lowest energy connecting them, **TS-3c/3d**, are shown in Scheme 4. In **TS-3c/3d** the C-H bond is nearly fully formed ($d(\text{C-H}) = 1.137 \text{ \AA}$) and the Ir-H distance ($d(\text{Ir-H}) = 2.28 \text{ \AA}$) remains well below the sum of the van der Waals radii of Ir and H (3.1 \AA^{37}), suggesting the presence of an agostic interaction. Examination of the reaction coordinate evaluated at **TS-3c/3d** shows predominantly a swinging motion of the hydride ligand, i.e. a substantial increase of the N-Ir-H angle when progressing toward **3d**, with a smaller component best described as loss of the agostic interaction (see Scheme 4; cf. **TS-3c/3d** and **IRC-A**).

The olefin insertion reaction (**3c** \rightarrow **3d**) thus proceeds through structures which, although not certifiable as stationary points, appear classifiable as iridium ethyl hydrides with a β -hydrogen agostic interaction. Following the intrinsic reaction coordinate (IRC)³⁸ from transition state **TS-3c/3d** (Scheme 4) for a few steps in the direction of **3c** leads, for example, through non-stationary structure **IRC-A** (2.7 kcal/mol below **TS-3c/3d**) with

metric parameters $d(\text{Ir-H}(\text{Me})) = 2.10 \text{ \AA}$; $d(\text{C-H}) = 1.178 \text{ \AA}$; $d(\text{C-C}) = 1.50 \text{ \AA}$; and $\text{>Ir-C-C} = 88.1^\circ$. The Wiberg bond-index between Ir and the migrating H is 0.75 in **3c**, 0.16 in **IRC-A**, 0.09 in **TS-3c/3d**, and 0.004 in the T_C **3d** conformer.³⁹ Despite this clear indication that significant Ir-H bonding is maintained along a major portion of the reaction coordinate, an iridium ethyl hydride with a β -hydrogen agostic interaction could not be located as an energy minimum.

Disturbingly, the free energy of **TS-3c/3d** is calculated to be 32.8 kcal/mol above that of **3c**, while the experimental value, implied by the rate of H/D exchange observed for **3c-d₂**, is only 21 kcal/mol. Single point calculations (M11 optimized geometries) at the MP2 level predict an even higher barrier (44.0 kcal/mol). Other commonly used ‘Minnesota functionals’ such as M11-L, M06-L, or M06 produced TS structures very similar to **TS-3c/3d** but their free energies were only 23.6, 27.7, and 25.9 kcal/mol, respectively, above **3c**.⁴⁰ The overestimation of the barrier by single-determinant based methods may reflect that proper descriptions of the potential energy surfaces and electronic states of $d^6 \text{ML}_5$ -type species require minimally the use of two-configuration wavefunctions.⁴¹ Whether a multi-configuration approach would produce a TS structure and energy for olefin insertion significantly different from **TS-3c/3d** is, however, well outside the scope of the present work.⁴²

b. Reaction of ethyl hydride 3d under an ethylene atmosphere.

b.1. The unassisted (dissociative) pathway. For the PCP-type (phenyl-based) pincer analogues of complex **3d**, calculations indicate that reductive elimination with loss of ethane is exergonic. For example, using the computational methods applied to the present (^{carb}PNP)Ir system we calculate that ΔG° for loss of ethane from

(ⁱPrPCP)Ir(ethyl)(H) is -2.5 kcal/mol ($\Delta H^\circ = +10.1$ kcal/mol). In contrast, loss of ethane from ^{carb}PNP iridium ethyl hydride complex **3d** is predicted to be endergonic by 15.6 kcal/mol ($\Delta H^\circ = 28.9$ kcal/mol), representing a very pronounced difference of 18 kcal/mol for C-H elimination/addition. The barrier to reductive C-H coupling in **3d** is calculated as $\Delta G^\ddagger = 16.6$ kcal/mol (Figure 4); this coupling leads to a C-H sigma-bond complex, **3e**, with free energy 22.1 kcal/mol above **3c**. The ethane molecule in **3e** is bound quite strongly; ΔH° for dissociation to yield **3f** is 11.9 kcal/mol.

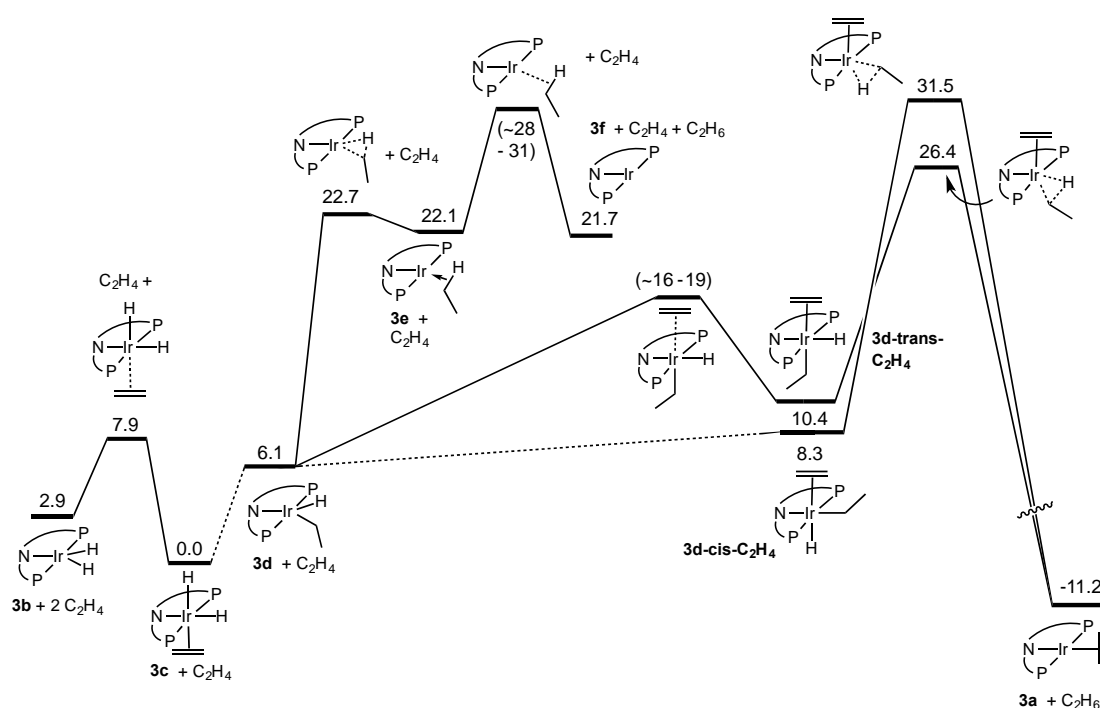


Figure 4. Calculated free energies (kcal/mol) for the hydrogenation of ethylene by **3b** under 1 atm ethylene at 25 °C.

We have not been able to locate a proper transition state on the potential energy surface for dissociation of ethane from the C-H sigma-bond complex **3e** but we can provide an estimate for the effective free energy barrier. We assume that $\Delta H^\ddagger \approx 11.9$

kcal/mol (equal to ΔH° , and thus presumably a *lower limit* since this assumes that $\Delta H^\ddagger = 0$ for the back reaction), and that ΔS^\ddagger for this unimolecular, dissociative, process is in the range of 10 – 20 eu. This yields a range of values for ΔG^\ddagger for ethane loss from **3e** at 25 °C of 5.9 kcal/mol to 8.9 kcal/mol or, in effect, a transition state with free energy 28 to 31 kcal/mol above that of resting state **3c**.

At 75 °C, the temperature at which the $[C_2H_4]$ -dependence was experimentally determined, the resulting rate equation (eq 8) indicates a first-order rate constant of $1.3 \times 10^{-4} \text{ s}^{-1}$ for **3c** undergoing overall ethylene insertion and ethane loss; this rate corresponds to $\Delta G^\ddagger_{\text{exp}} = 26.7 \text{ kcal/mol}$. At this temperature, the calculated free energy of **3e** is 21.7 kcal/mol above **3c** (the value is 22.1 kcal/mol at 25 °C). Again assuming that $\Delta H^\ddagger \approx 11.9 \text{ kcal/mol}$ for ethane loss from **3e**, and $\Delta S^\ddagger = 10 - 20 \text{ eu}$, the estimated free energy (relative to **3c**) of the effective TS for ethane loss is 33.6 kcal/mol (21.7 kcal/mol + 11.9 kcal/mol) minus 3.5 to 7.0 kcal/mol (10 to 20 eu at 75 °C); this is equal to 26.6 to 30.1 kcal/mol, in full agreement with the experimental value of 26.7 kcal/mol. As this experimental value at 75 °C is at the low end of the range estimated/calculated at that temperature, one would assume a value at the low end of the estimated/ calculated range upon extrapolation to 25 °C, which would correspond to a value of ca. 28 kcal/mol.

b.2. The ethylene-assisted (associative) pathway. Addition of ethylene to ethyl hydride **3d**, can give two isomers, **3d-cis-C₂H₄** and **3d-trans-C₂H₄**, where the ethylene and ethyl groups are mutually cis or trans, respectively, with free energies 2.2 kcal/mol and 4.3 kcal/mol above that of **3d** plus free C₂H₄. A proper transition state for the addition was not located but incremental scans of the potential energy surfaces reveal that both additions proceed with virtually no energy barrier. The free energy of the TS (or the

effective TS) may be estimated using the same procedure as outlined above for dissociation of ethane from **3e** (in this case proceeding in the reverse direction). The enthalpy of ethylene loss from **3d-trans-C₂H₄** is calculated to be 11.9 kcal/mol (coincidentally equal to the value for ethane loss from **3e**); if ΔS^\ddagger is again estimated to be in the range of 10-20 eu, then ΔG^\ddagger lies in the range 5.9-8.9 kcal/mol, which places the TS (for ethylene loss from **3d-trans-C₂H₄** or ethylene addition to **3d**) at ~16 to 19 kcal/mol above the resting state **3c** plus ethylene at 25 °C (Fig. 4).

Reductive elimination from six-coordinate d⁸ complexes is generally not a facile process⁴³ and indeed ΔG^\ddagger for elimination from **3d-trans-C₂H₄** is substantial, 16.0 kcal/mol at 25 °C, with a TS that is 26.4 kcal/mol above the free energy of **3c** plus ethylene (1 atm) (Fig. 4). At 75 °C, the value is 28.9 kcal/mol at 1 atm ethylene, or 26.5 kcal/mol at 1 mol/L (28 atm at 75 °C), in excellent agreement with the second-order rate constant of $7.2 \times 10^{-4} \text{ M}^{-1} \text{ s}^{-1}$ obtained at this temperature (eq 8) which corresponds to $\Delta G^\ddagger_{\text{exp}} = 25.5 \text{ kcal/mol}$.

Reductive elimination of ethane from **3d-trans-C₂H₄** is strongly exergonic ($\Delta G^\circ = -21.6 \text{ kcal/mol}$) in striking contrast with the value for elimination from five-coordinate ethyl hydride **3d**, $\Delta G^\circ = +13.6 \text{ kcal/mol}$. The transition state for the uphill reductive coupling by **3d** is, however, calculated to be somewhat lower than reductive coupling by **3d-trans-C₂H₄**. Reductive *elimination* (i.e. loss of ethane), however, is significantly *less* favorable from **3d**. This can be explained in terms of the free energy of reductive elimination ($\Delta G^\circ = 13.6 \text{ kcal/mol}$) to give **3e**, combined with the thermodynamic barrier to loss of ethane from ethane complex **3e** ($\Delta H^\circ = 11.9 \text{ kcal/mol}$). Alternatively, and perhaps most simply, the barrier may be explained by considering the high

endothermicity of ethane loss from **3d**; $\Delta H^\circ = +28.9$ kcal/mol (or +36.7 kcal/mol relative to resting state **3c**). Even a total entropic contribution as great as $\Delta S^\ddagger = +30$ eu in the rate-determining step only lowers ΔG^\ddagger to ca. 28 kcal/mol above **3c**. Consequently, it is ultimately the unfavorable thermodynamics (specifically the high positive enthalpy) that results in a very high kinetic barrier for the unassisted elimination. In the case of the ethylene assisted pathway, the overall thermodynamics of elimination (driven by ethylene coordination) are quite favorable. Thus, while there is a fairly high kinetic barrier to elimination from six-coordinate **3d-trans-C₂H₄**, in the presence of ethylene (ca. 1 atm or greater) the associative pathway is still the more favorable one with $\Delta G^\ddagger = 26.4$ kcal/mol relative to **3c**, in excellent agreement with the experimentally determined dependence of rate on [C₂H₄].

Finally, we note that we have searched extensively (without success) for a TS corresponding to an ethylene-assisted pathway that might be described as the displacement of coordinated ethane in complex **3e** by ethylene. But even if an independent TS of this type were located, its calculated Gibbs free energy would undoubtedly be higher than that calculated for the TS for elimination of ethane from **3d-trans-C₂H₄** (26.4 kcal/mol relative to **3c**) if only due to the unfavorable entropic term of a bimolecular reaction (> ca. 7 kcal/mol at 25 °C) added to the free energy of complex **3e** (22.1 kcal/mol relative to **3c**).

c. Reaction of ethyl hydride 3d under an H₂ atmosphere. The experimental kinetics indicate that an H₂-assisted pathway for the release of ethane from ethylene dihydride complex **3c** is even more favorable than the ethylene-assisted pathway. The DFT calculations strongly support this conclusion. As discussed above, the unassisted

pathway (involving dissociative loss of ethane from **3d**) appears to have a free energy barrier (25 °C) of ca. 28 kcal/mol relative to resting state **3c**, or 22 kcal/mol above ethyl hydride **3d**. In the presence of an H₂ atmosphere, the five-coordinate unsaturated ethyl hydride complex **3d** is calculated to add H₂ with no barrier on the potential energy surface (just as it readily adds ethylene), to afford a dihydrogen complex with the dihydrogen ligand trans or cis to the ethyl group (**3d-trans-(H₂)** or **3d-cis-(H₂)**, respectively), which, coincidentally, has a free energy 4.9 kcal/mol above that of **3c** in both cases (Fig. 5). If $\Delta H^\ddagger = \Delta H^\circ \sim 11$ kcal/mol for the reverse reaction (loss of dihydrogen from **3d-trans-(H₂)** or **3d-cis-(H₂)**) and if ΔS^\ddagger is estimated to be in the range of 10–20 eu, then the effective TS for the H₂ elimination/addition has a free energy of 10–13 kcal above **3c**. This corresponds to a free energy of 4–7 kcal/mol above that of **3d**, which is fully consistent with an approximately diffusion-controlled reaction (e.g. a diffusion-controlled rate of ca. $10^{10} \text{ M}^{-1} \text{ s}^{-1}$,⁴⁴ and a concentration of 0.041 M, equivalent to 1 atm, corresponds to a pseudo-first-order rate constant of $4 \times 10^8 \text{ s}^{-1}$ and $\Delta G^\ddagger = 5.7$ kcal/mol at 25 °C).

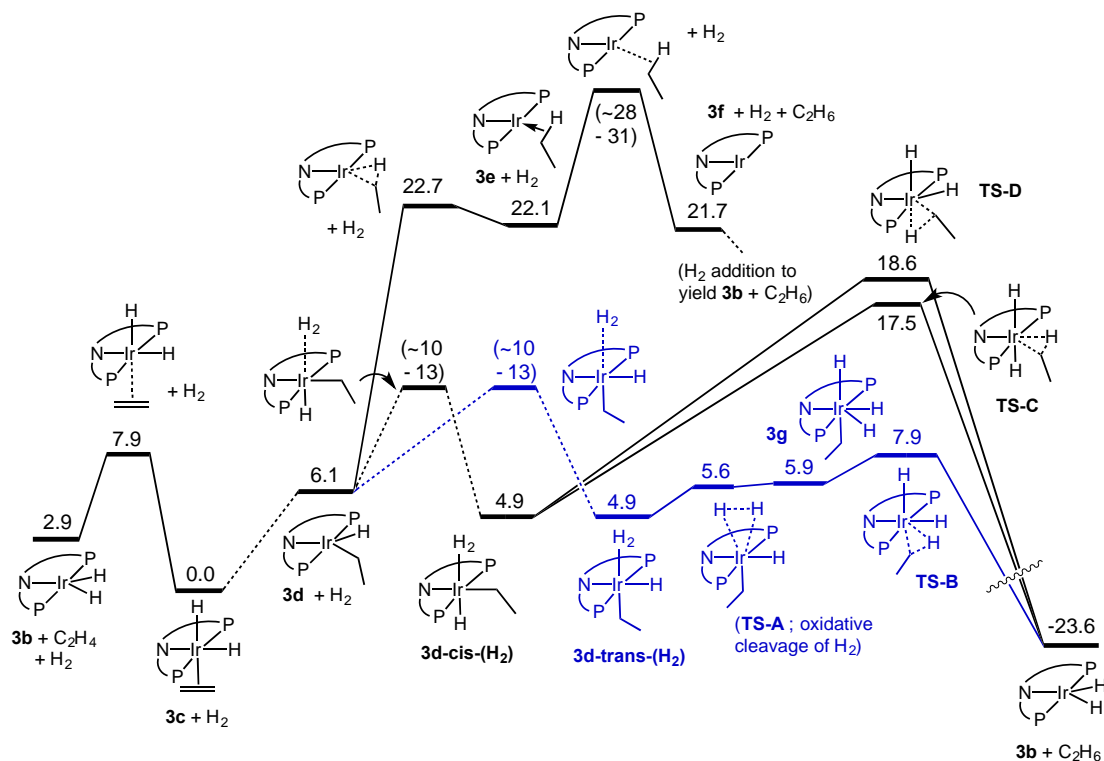
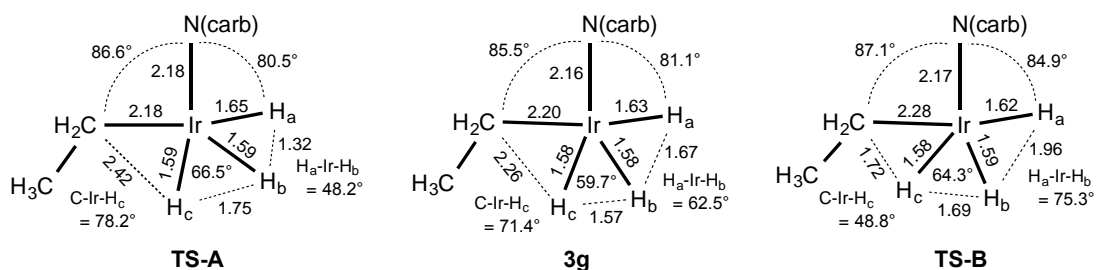


Figure 5. Calculated free energies (kcal/mol) for hydrogenation of ethylene by **3b** under 1 atm H_2 (favored path in blue).

3d-trans-(H₂) readily converts to an Ir(V) species, **3g** (with $\Delta G^\circ = 1.0$ kcal/mol) in a nearly barrierless transition. The TS for this conversion, **TS-A**, is a mere 0.7 kcal/mol higher in electronic energy, E , than **3g**. Species **3g** is actually slightly higher than **TS-A** in free energy and even enthalpy (due to inclusion of zero point energies). It is thus questionable whether **3g** can even be characterized as a true intermediate. Importantly, however, no matter whether it is a minimum or a non-stationary point on the reaction coordinate, the Ir(V) species **3g** connects to Ir(III) species **3b** via **TS-B** to lose ethane; the barrier to this transformation is only 2.0 kcal/mol (Figure 5). Scheme 5 illustrates the geometry of these species on the reaction coordinate. The full Ir(V) character of **3g** is

clear from its lack of any close inter-hydride or carbon-hydride contacts. It can be seen that the reaction coordinate comprises almost exclusively a movement of H_b away from H_a combined with the movement of H_c toward the α -carbon of the ethyl group. These motions occur concomitantly although the motion of H_b is somewhat more pronounced at earlier points on the reaction coordinate (cf. **TS-A** and **3g**), while the motion of H_c is somewhat more pronounced later (cf. **3g** and **TS-B**).

Scheme 5. Species on the reaction pathway from **3d-trans-(H₂)** to dihydride **3b**. Metrics are shown (bond lengths in Å) for the coordination sphere excluding the coordinating P atoms (i.e. for the ligands in the approximate plane bisecting the P-Ir-P axis).



In the pathway calculated to be most favorable for the H₂-assisted C-H elimination, the hydrogen undergoing C-H elimination (H_c in Scheme 5) is derived from the hydride ligand of **3d**, rather than from the incoming H₂ molecule. A pathway in which the ethane hydrogen is derived from the incoming H₂ was calculated, but its TS for elimination (**TS-C**) has a free energy of 17.5 kcal/mol which, though not prohibitively high, is significantly above that of **TS-B** (7.9 kcal/mol). **TS-C** might be viewed as being a point on a σ -CAM (sigma-complex assisted metathesis) pathway.⁴⁵ Note that although **TS-C** is higher in energy than **TS-B**, the σ -CAM-type pathway is apparently not

intrinsically unfavorable. In fact, **TS-C** is calculated to be slightly lower in energy than **TS-D**, a C-H elimination TS which, like **TS-C**, connects to **3d-cis-(H₂)** but in **TS-D** the eliminating H atom is derived from a hydride ligand of **3b**. (Thus, of the two pathways examined for H₂-assisted C-H elimination from the intermediate **3d-cis-(H₂)**, the σ -CAM pathway is the slightly more favorable).

It is interesting to note that (PONOP)Ir(CH₃)(H)⁺ (PONOP = 2,6-bis(di-*tert*-butylphosphinito)pyridine), isoelectronic with **3d**, adds H₂ to form dihydrogen adduct (PONOP)Ir(CH₃)(H)(η^2 -H₂)⁺, which can be observed by low temperature NMR spectroscopy.⁴⁶ The H₂ ligand is trans to the terminal hydride. Elimination of methane from (PONOP)Ir(CH₃)(H)⁺ occurs by a σ -CAM mechanism in which the hydrogen that is eliminated originates from the η^2 -H₂ ligand in analogy to the conversion of **3d-cis-(H₂)** to **3b** plus C₂H₆ via **TS-C**. The barrier to elimination from the dihydrogen complex (PONOP)Ir(CH₃)(H)(η^2 -H₂)⁺ is significantly lower (17.9 kcal/mol) than the direct elimination of methane from methyl hydride (PONOP)Ir(CH₃)(H)⁺, consistent with DFT computations for the carbazolidone analog in Fig. 5.

The comparison of the H₂-assisted path for ethane elimination with the ethylene-assisted path is informative. Addition of either H₂ or ethylene to **3d** proceeds without any significant kinetic or thermodynamic barrier. Both of the resulting adducts are coordinatively saturated 18-valence-electron complexes. Since the ethane product is derived from the ethyl and hydride ligands of **3d**, not from the incoming dihydrogen, the H₂-assisted pathway can be viewed as a displacement reaction in analogy with the reaction with ethylene. Elimination from the six-coordinate d⁶ ethylene adducts, however, has a substantial kinetic barrier, ca. 16 kcal/mol in the most favorable case, reflecting the

general and well-explained⁴⁷ behavior of such species. In contrast, upon addition of H₂, the barrier to ethane loss is quite low. This is attributable to the ability of the added H₂ (in contrast with ethylene) to undergo oxidative cleavage, to give an Ir(V) species, **3g**; C-H reductive elimination from **3g** is not subject to the same barriers as elimination from a six-coordinate d⁶ complex (the C-H reductive coupling by **3g** is formally analogous to the reverse of the nearly barrierless oxidative cleavage of H₂ that leads from **3d-trans-(H₂)** to **3g**). While **3g** is calculated to be an Ir(V) intermediate, one could easily envision a pathway in which ethane elimination proceeds concertedly with H-H oxidative cleavage; but, regardless of whether the transitional Ir(V) species is an energy minimum or not, whereas the ethylene-assisted pathway (or the unassisted pathway) is an Ir(III)/Ir(I) cycle, the H₂-assisted pathway would be best described as Ir(III)/Ir(V). Thus, the *unassisted* elimination of ethane has a high barrier attributable to the thermodynamic unfavorability of three-coordinate Ir(I) relative to Ir(III) in the case of the carbazole-PNP complex. The *ethylene-assisted pathway* has a somewhat lower barrier (ca. 26 kcal/mol) attributable to the kinetics of interconversion between octahedral Ir(III) and square-planar Ir(I). The H₂-assisted pathway faces neither of these difficulties. Accordingly, the kinetics of the H₂-assisted pathway are apparently limited only by the kinetics of formation of **3d** (i.e. insertion of ethylene into the Ir-H bond of **3c**), and it thus proceeds at a rate comparable to H/D exchange by **3c-d₂**.

Figure 6 illustrates the displacement of ethane from **3d** by ethylene and by H₂ in the same energy diagram for comparison.

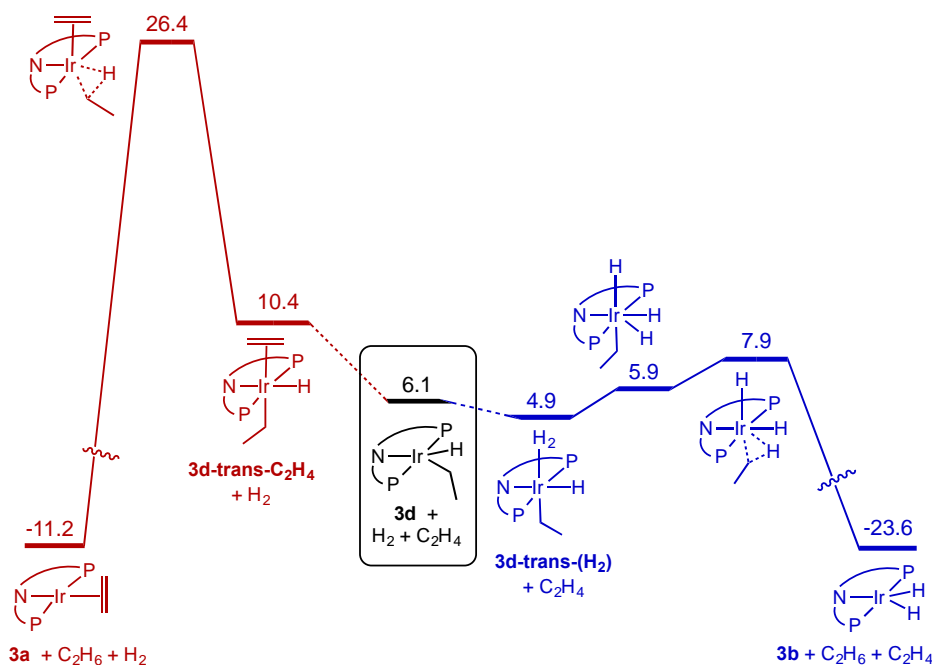


Figure 6. Comparison of ethane elimination from **3d** promoted by addition of H₂ (blue) and promoted by addition of ethylene (red).

Conclusions

The much poorer sigma-donating ability of the central nitrogen atom (relative to the central carbon atom of iridium PCP and iridium POCOP systems) in the iridium carbazolidone system studied here gives rise to a stronger preference for the Ir(III) oxidation state, relative to Ir(I), for the carbazolidone system. For example the enthalpy of ethane loss from five-coordinate ethyl hydride **3d** is calculated to be 28.9 kcal/mol vs. 10.1 kcal/mol from (ⁱPrPCP)Ir(H)Et. The free energy of **3d** is calculated as 6.1 kcal/mol above that of the six-coordinate ethylene *cis*-dihydride resting state, **3c**, and thus the overall barrier to “unassisted” release of ethane from **3c** is quite high.

The high barrier to ethane elimination from **3d** results in unusual features with respect to hydrogenation of olefins by these complexes. The (^{carb}PNP)Ir dihydride, **3b**, readily adds ethylene to give **3c**. This is rapidly followed by olefin insertion to give the ethyl hydride, **3d**, as shown by rapid H/D exchange between hydride ligands and ethylene hydrogens. Although direct elimination of ethane from **3d** has a very high barrier, **3d** can easily trap ethylene. The resulting six-coordinate adduct, specifically the isomer **3d-trans-C₂H₄**, has a significant kinetic barrier to elimination ($\Delta G^\ddagger = 16$ kcal/mol). Nevertheless the overall calculated barrier of 26.4 kcal/mol is less than that predicted for a direct ethane elimination pathway, and indeed the absolute value of this barrier and the predicted dependence on ethylene pressure is in excellent agreement with the experimental rate and the kinetic dependence on ethylene pressure. A similar “ethylene-promoted” reductive elimination from the facially-substituted cationic iridium complex $L_3IrH_2(C_2H_4)^+$ ($L = PPhMe_2$) has been noted by Caulton.⁴⁸

The effect of hydrogen on lowering the overall barrier to hydrogenation of ethylene by **3c** is even more pronounced than the effect of ethylene. DFT calculations suggest that the ethyl hydride adds H₂ to form the η^2 -dihydrogen complex, **3d-trans-(H₂)**; this barrierless step is followed by rapid reductive elimination of ethane proceeding via an Ir(V) intermediate, with an extremely low overall barrier, $\Delta G^\ddagger = 3$ kcal/mol. This lower barrier for reductive elimination relative to the ethylene-promoted pathway may be explained in terms of the carbazolid pincer engendering a strong preference for the Ir(III) oxidation state vs. Ir(I), the lack of any species with Ir(I) character along the reaction coordinate, and the fact that there is no net change in the oxidation state upon release of ethane from the dihydrogen complex, **3d-H₂**.

Experimental and computational studies suggest that cationic LL'Ir⁺ Crabtree-type hydrogenation catalysts⁴⁹ can function via Ir(III)/Ir(V)/Ir(III) cycles. Brandt et al.⁵⁰ carried out computational and experimental studies on a cationic phosphanooxazoline iridium catalyst⁵¹ that supported an olefin hydrogenation cycle in which an unsaturated Ir(III) olefin dihydride species is the catalyst resting state and hydrogenation proceeds via addition of H₂ to form an Ir(III) olefin η²-dihydrogen dihydride complex, followed by migratory insertion and oxidative cleavage of the dihydrogen ligand to yield an Ir(V) alkyl trihydride. Facile elimination of alkane from this Ir(V) species followed by coordination of olefin closes the catalytic cycle. Similar conclusions were reached by Cui et. al.⁵² in their study of cationic Ir(III) hydrogenation catalysts employing bidentate N-heterocyclic carbene-oxazoline ligands. In a study of the hydrogenation of ethylene by (triphos)Ir(C₂H₄)₂⁺ Bianchini has suggested that both ethylene and H₂ can accelerate the reductive elimination of ethylene based on the half-order pressure dependence of both hydrogen and ethylene on the rate of hydrogenation.⁵³

The hydrogen-induced acceleration of olefin hydrogenation by dihydride **3b** is even more dramatic in the case of more hindered olefins. Neither propylene nor *t*-butylethylene form stable adducts with **3b**, and neither reacts with **3b** to give alkane even at temperatures up to 100 °C. Deuterium labeling shows that olefin binding and insertion occurs and alkyl hydrides are readily formed reversibly at room temperature, but apparently even at 100 °C the barrier to reductive elimination is too high to complete the hydrogenation reaction. These olefins, however, are rapidly hydrogenated at room temperature under hydrogen, presumably via addition of hydrogen to the corresponding alkyl hydride complex.

Our studies of the hydrogenations explain why the carbazolide complex is ineffective for catalytic transfer dehydrogenation. Under transfer dehydrogenation conditions there is no free hydrogen present and thus the required hydrogenation step in the cycle has an exceptionally high barrier. In comparison with the much more effective PCP-type pincer complexes, the difference is ultimately attributable to the very unfavorable thermodynamics of the Ir(III)→Ir(I) transformations, particularly elimination of alkane from the five-coordinate alkyl hydride **3d** (the high barrier may also be expressed in terms of the very unfavorable thermodynamics of transfer of hydrogen from the Ir(III) dihydride to olefin). Notably, preference for the *higher* oxidation state is in turn attributable to the much *poorer* sigma-donating ability of the carbazolide nitrogen relative to that of the coordinating carbon of the PCP-type pincers. As the carbazole ligand biases the system strongly in favor of the +3 vs. +1 oxidation state, future work with this ligand will focus on rhodium, since, in the case of PCP-type pincer ligands, the Rh(III) state is not sufficiently accessible to allow an effective catalytic cycle based on the Rh(I)/Rh(III) couple.

References

- (1) Findlater, M.; Choi, J.; Goldman, A. S.; Brookhart, M. *Catal. Met. Complexes* **2012**, *38*, 113-141.
- (2) Choi, J.; MacArthur, A. H. R.; Brookhart, M.; Goldman, A. S. *Chem. Rev.* **2011**, *111*, 1761-1779.
- (3) Huang, Z.; Brookhart, M.; Goldman, A. S.; Kundu, S.; Ray, A.; Scott, S. L.; Vicente, B. C. *Adv. Synth. Catal.* **2009**, *351*, 188-206.
- (4) Morales-Morales, D. *Iridium Complexes in Organic Synthesis* **2009**, 325-344.
- (5) Xu, W.; Rosini, G. P.; Gupta, M.; Jensen, C. M.; Kaska, W. C.; Krogh-Jespersen, K.; Goldman, A. S. *Chem. Commun.* **1997**, 2273-2274.
- (6) Goldman, A. S.; Roy, A. H.; Huang, Z.; Ahuja, R.; Schinski, W.; Brookhart, M. *Science* **2006**, *312*, 257-261.
- (7) Nawara-Hultsch, A. J.; Hackenberg, J. D.; Punji, B.; Supplee, C.; Emge, T. J.; Bailey, B. C.; Schrock, R. R.; Brookhart, M.; Goldman, A. S. *ACS Catalysis* **2013**, *3*, 2505-2514.
- (8) Haibach, M. C.; Kundu, S.; Brookhart, M.; Goldman, A. S. *Acc. Chem. Res.* **2012**, *45*, 947-958.
- (9) Ahuja, R.; Punji, B.; Findlater, M.; Supplee, C.; Schinski, W.; Brookhart, M.; Goldman, A. S. *Nature Chem.* **2011**, *3*, 167-171.
- (10) (a) Crabtree, R. H.; Mihelcic, J. M.; Quirk, J. M. *J. Am. Chem. Soc.* **1979**, *101*, 7738-7739. (b) Burk, M. J.; Crabtree, R. H. *J. Am. Chem. Soc.* **1987**, *109*, 8025-32. (c) Maguire, J. A.; Boese, W. T.; Goldman, A. S. *J. Am. Chem. Soc.* **1989**, *111*, 7088-7093. (d) Maguire, J. A.; Petrillo, A.; Goldman, A. S. *J. Am. Chem. Soc.* **1992**, *114*, 9492-9498.
- (11) Gupta, M.; Hagen, C.; Flesher, R. J.; Kaska, W. C.; Jensen, C. M. *Chem. Commun.* **1996**, 2083-2084.
- (12) Liu, F.; Goldman, A. S. *Chem. Commun.* **1999**, 655-656.
- (13) Haenel, M. W.; Oevers, S.; Angermund, K.; Kaska, W. C.; Hua-Jun Fan; Hall, M. B. *Angew. Chem., Intl. Ed.* **2001**, *40*, 3596-3600.
- (14) Götter-Schnetmann, I.; White, P.; Brookhart, M. *J. Am. Chem. Soc.* **2004**, *126*, 1804-1811.
- (15) Kuklin, S. A.; Sheloumov, A. M.; Dolgushin, F. M.; Ezernitskaya, M. G.; Peregudov, A. S.; Petrovskii, P. V.; Koridze, A. A. *Organometallics* **2006**, *25*, 5466-5476.
- (16) Kundu, S.; Choliy, Y.; Zhuo, G.; Ahuja, R.; Emge, T. J.; Warmuth, R.; Brookhart, M.; Krogh-Jespersen, K.; Goldman, A. S. *Organometallics* **2009**, *28*, 5432-5444.
- (17) Punji, B.; Emge, T. J.; Goldman, A. S. *Organometallics* **2010**, *29*, 2702-2709.
- (18) Morales-Morales, D.; Redon, R.; Yung, C.; Jensen, C. M. *Inorg. Chim. Acta.* **2004**, *357*, 2953-2956.
- (19) Götter-Schnetmann, I.; Brookhart, M. *J. Am. Chem. Soc.* **2004**, *126*, 9330-9338.

- (20) Krogh-Jespersen, K.; Czerw, M.; Kanzelberger, M.; Goldman, A. S. *J. Chem. Inf. Comput. Sci.* **2001**, *41*, 56-63.
- (21) Krogh-Jespersen, K.; Czerw, M.; Summa, N.; Renkema, K. B.; Achord, P. D.; Goldman, A. S. *J. Am. Chem. Soc.* **2002**, *124*, 11404-11416.
- (22) Renkema, K. B.; Kissin, Y. V.; Goldman, A. S. *J. Am. Chem. Soc.* **2003**, *125*, 7770-7771.
- (23) Götter-Schnetmann, I.; White, P. S.; Brookhart, M. *Organometallics* **2004**, *23*, 1766-1776.
- (24) Goettker-Schnetmann, I.; Heinekey, D. M.; Brookhart, M. *J. Am. Chem. Soc.* **2006**, *128*, 17114-17119.
- (25) (a) Malcolmson, S. J.; Meek, S. J.; Sattely, E. S.; Schrock, R. R.; Hoveyda, A. H. *Nature* **2008**, *456*, 933-937. (b) Ibrahim, I.; Yu, M.; Schrock, R. R.; Hoveyda, A. H. *J. Am. Chem. Soc.* **2009**, *131*, 3844-3845. (c) Flook, M. M.; Jiang, A. J.; Schrock, R. R.; Muller, P.; Hoveyda, A. H. *J. Am. Chem. Soc.* **2009**, *131*, 7962-7963.
- (26) Wang, D. Y.; Choliy, Y.; Krogh-Jespersen, K.; Hartwig, J. F.; Goldman, A. S. *Abstracts of Papers, 240th ACS National Meeting, Boston, MA, United States, August 22-26, 2010*, INOR-5.
- (27) Wang, D. Y.; Krogh-Jespersen, K.; Goldman, A. S. *Abstracts of Papers, 244th ACS National Meeting & Exposition, Philadelphia, PA, United States, August 19-23, 2012*, INOR-587.
- (28) (a) Ozerov, O. V.; Guo, C.; Papkov, V. A.; Foxman, B. M. *J. Am. Chem. Soc.* **2004**, *126*, 4792-4793. (b) Weng, W.; Guo, C.; Moura, C.; Yang, L.; Foxman, B. M.; Ozerov, O. V. *Organometallics* **2005**, *24*, 3487-3499. (c) Gatard, S.; Celenligil-Cetin, R.; Guo, C.; Foxman, B. M.; Ozerov, O. V. *J. Am. Chem. Soc.* **2006**, *128*, 2808-2809. (d) Weng, W.; Guo, C.; Celenligil-Cetin, R.; Foxman, B. M.; Ozerov, O. V. *Chem. Commun.* **2006**, 197-199.
- (29) The pKa values are in DMSO. Source:
<http://www.chem.wisc.edu/areas/reich/pkatable/index.htm>
- (30) Britovsek, G. J. P.; Gibson, V. C.; Hoarau, O. D.; Spitzmesser, S. K.; White, A. J. P.; Williams, D. J. *Inorg. Chem.* **2003**, *42*, 3454-3465.
- (31) Lee, D. W.; Kaska, W. C.; Jensen, C. M. *Organometallics* **1998**, *17*, 1-3.
- (32) While the stable isomer of (^{carb}PNP)IrH₂(C₂H₄) is the cis isomer, **3c**, treatment of (^tBuPCP)IrH₂ with ethylene at -90 °C results in formation of the trans dihydride (^tBuPCP)IrH₂(C₂H₄). The increased stability of the cis dihydride in the case of the carbazole system is likely in part due to the decreased trans effect of the carbazolide nitrogen in **3a** relative to the sp² carbon the (PCP)Ir complex thereby favoring the cis dihydride structure which places hydride trans to nitrogen, although the greater steric demand of t-Bu vs. i-Pr groups likely also plays an important role. Other iridium ethylene dihydride complexes of which we are aware are the facially substituted cationic L₃IrH₂(C₂H₄)⁺ where the hydrides are forced to be cis. See: (a) Barbaro, P.; Bianchini, C.; Meli, A.; Peruzzini, M.; Vacca, A.; Vizza, F. *Organometallics* **1991**,

- 10, 2227-2238. (b) Garcia-Camprubi, A.; Martin, M.; Sola, E. *Inorg. Chem.* **2010**, *49*, 10649-10657.
- (33) Peverati, R.; Truhlar, D. G. *J. Phys. Chem. Lett.* **2011**, *2*, 2810-2817.
- (34) Biswas, S.; Zhou, T.; Wang, D. Y.; Hackenberg, J.; Nawara-Hultzs, A.; Schrock, R. R.; Brookhart, M.; Krogh-Jespersen, K.; Goldman, A. S. *Abstracts of Papers, 245th ACS National Meeting & Exposition, New Orleans, LA, United States, April 7-11, 2013*, INOR-681. The origin of the kinetic barrier will be discussed in detail in a forthcoming publication.
- (35) Jean, Y.; Eisenstein, O. *Polyhedron* **1988**, *7*, 405-407.
- (36) Riehl, J. F.; Jean, Y.; Eisenstein, O.; Pelissier, M. *Organometallics* **1992**, *11*, 729-737.
- (37) The van der Waals radii of Ir and H are reported as 202 pm and 110 pm, respectively. <http://periodic.lanl.gov/index.shtml>
- (38) Hratchian, H. P.; Schlegel, H. B. *J. Chem. Theory Comput.* **2004**, *1*, 61-69.
- (39) Wiberg, K. B. *Tetrahedron* **1968**, *24*, 1083-1096.
- (40) The present authors are not qualified to comment with authority on the probable causes for this significant disagreement among the functionals. We note, however, that M11 is a range-separated hybrid functional containing a contribution of 42.8% Hartree-Fock (HF) exchange to the short-range interelectronic interactions but 100% HF exchange to the long-range interactions, whereas M11-L is a local functional with a dual-range local exchange functional (i.e. 0% HF exchange). M06-L is also a local functional, whereas M06 is a hybrid functional with 27% HF exchange; neither M06-L nor M06 features range-separation. It is tempting to associate the exceedingly large barrier produced by the M11 functionals, relative to the barriers predicted by M11-L, M06-L, and M06 functionals and experiment, with differences in the treatment of electron exchange and, in particular, the large admixture of HF exchange present in M11.
- (41) See, e.g. Bersuker, I. B., "The Jahn-Teller Effect: Implications in Electronic Structure Calculations" in Piecuch, P.; Maruani, J.; Delgado-Barrio, G.; Wilson, S., Ed. *Progress in Theoretical Chemistry and Physics*, Vol. 19, Springer New York, 2009, pp 343-362.
- (42) The barrier predicted by M11-L (23.6 kcal/mol) is in fact very close to the experimental value (21 kcal/mol). We note that M11-L is intended to '...provide broad accuracy for both single-configurational and multiconfigurational molecules and for solid-state lattice constants.' Peverati, R.; Truhlar, D. C. *J. Phys. Chem. Lett.* **2012**, *3*, 117-124.
- (43) (a) Wick, D. D.; Goldberg, K. I. *J. Am. Chem. Soc.* **1997**, *119*, 10235-10236. (b) Bartlett, K. L.; Goldberg, K. I.; Borden, W. T. *J. Am. Chem. Soc.* **2000**, *122*, 1456-1465. (c) Bartlett, K. L.; Goldberg, K. I.; Borden, W. T. *Organometallics* **2001**, *20*, 2669-2678. (d) Fekl, U.; Goldberg, K. I. *J. Am. Chem. Soc.* **2002**, *124*, 6804-6805.
- (44) Elliot, A. J.; McCracken, D. R.; Buxton, G. V.; Wood, N. D. *J. Chem. Soc. Faraday Trans.* **1990**, *86*, 1539-1547.

- (45) Perutz, R. N.; Sabo-Etienne, S. *Angew. Chem., Intl. Ed.* **2007**, *46*, 2578-2592.
- (46) Campos, J.; Kundu, S.; Pahls, D. R.; Brookhart, M.; Carmona, E.; Cundari, T. R. *J. Am. Chem. Soc.* **2013**, *135*, 1217-1220.
- (47) Saillard, J.; Hoffmann, R. *J. Am. Chem. Soc.* **1984**, *106*, 2006-2026.
- (48) Lundquist, E. G.; Huffman, J. C.; Folting, K.; Caulton, K. G. *Angew. Chem. Intl. Ed. Engl.* **1988**, *27*, 1165-1167.
- (49) Crabtree, R. *Acc. Chem. Res.* **1979**, *12*, 331-337.
- (50) Brandt, P.; Hedberg, C.; Andersson, P. G. *Chem. - Eur. J.* **2003**, *9*, 339-347.
- (51) Helmchen, G. n.; Pfaltz, A. *Acc. Chem. Res.* **2000**, *33*, 336-345.
- (52) Cui, X.; Fan, Y.; Hall, M. B.; Burgess, K. *Chem. - Eur. J.* **2005**, *11*, 6859-6868.
- (53) Bianchini, C.; Farnetti, E.; Graziani, M.; Kaspar, J.; Vizza, F. *J. Am. Chem. Soc.* **1993**, *115*, 1753-1759. The authors note that other mechanistic interpretations are possible.
- (54) Onderdelinden, A. L.; van der Ent, A. *Inorg. Chim. Acta.* **1972**, 420-426.

Computational Details

DFT calculations¹ employed primarily the M06-L² and M11³ exchange-correlation functionals. The electronic environment was modeled using the following scheme: for Ir, we applied the SDD relativistic effective (small) core potential and the associated (6s5p3d) valence basis set;⁴ all other atoms (P, N, C and H) were assigned 6-311G(d,p) basis sets.⁵ Expanded integration grids (integral=ultrafine) were used throughout. Standard optimization procedures were employed to obtain the geometries and electronic energies for stationary points. The calculations were performed on the actual molecular species used in the experiments, except that two Me groups on the backbone inadvertently were replaced by H's; the bulky *i*Pr groups on P were fully retained. Unfortunately, the rotational flexibility of the *i*Pr groups allows the existence of many possible conformers for both minima and transition states; hence, many possibilities (typically 8-10) were examined for each complex (minimum or transition state). These extensive geometry searches were carried out with the efficient, and hence rapidly executing, M06-L functionals.² For each species encountered along the reaction coordinates for ethylene hydrogenation by (^{carb}PNP)Ir(H)₂ (Figs. 4 and 5 in the manuscript), we subsequently re-optimized the one or two lowest energy structures with the recently developed, more comprehensive and detailed M11 functionals.³ For many transition states (TS's), Intrinsic Reaction Coordinate (IRC) following was employed in order to ascertain their true natures, i.e. it was verified which minima a particular TS actually did connect.⁶ Normal mode analysis was performed for all stationary points (minima or TS's), and the resulting set of vibrational frequencies was employed (without scaling) to determine zero-point energy corrections. Enthalpies (H⁰) and Gibbs' free energies (G⁰; T = 298.15 K, P = 1 atm) were obtained from the

electronic potential energies (E) using standard statistical mechanical expressions.⁷ All calculations have been performed using the Gaussian 09 collection of computer programs.⁸

We present energetic results in the form of three Tables. Tables S1 and S2 contain relative energies pertinent to Figures 4 and 5 in the main text, respectively; Table S3 provides absolute energies for relevant minima and transition states. Cartesian coordinates of these stationary points are also presented in tabular form and as .mol files in the Supporting Information supplied with the published manuscript.

Tables of Energetic Quantities

Table S1. Relative potential energies (ΔE), enthalpies (ΔH), entropies (ΔS), and free energies (ΔG) (using the M11 functional) for the proposed hydrogenation reaction of ethylene by (^{carb}PNP)Ir(H)₂ under 1 atm ethylene, Figure 4 in Manuscript. Units are kcal/mol for ΔE , ΔH , and ΔG ; units are cal/(deg•mol) for ΔS . The standard state for concentrations is 1 atm for each species participating in the reaction; T = 298 K. The sequence of species in the Table is arranged to match Figure 4 as closely as possible.

Species	ΔE	ΔH	ΔS	ΔG
3b + 2C ₂ H ₄	19.9	17.3	48.4	2.9
TS-3b-3c + C ₂ H ₄	14.6	12.8	16.5	7.9
3c + C ₂ H ₄	0.0	0.0	0.0	0.0
TS-3c-3d + C ₂ H ₄	36.9	34.9	7.1	32.8
3d + C ₂ H ₄	7.1	7.8	5.5	6.1
TS-3d-3e + C ₂ H ₄	23.0	23.7	3.4	22.7
3e + C ₂ H ₄	22.6	24.8	8.9	22.1
3f + C ₂ H ₄ + C ₂ H ₆	35.8	36.7	50.6	21.7
3d-trans-C₂H₄	-8.6	-4.1	-48.7	10.4
TS-3d-trans-C₂H₄-3a	8.9	11.8	-49.0	26.4
3a + C ₂ H ₆	-16.7	-12.7	-4.8	-11.2
3d-cis-C₂H₄	-8.8	-4.7	-43.5	8.3
TS-3d-cis-C₂H₄-3a	14.4	16.9	-48.8	31.5
3a + C ₂ H ₆	-16.7	-12.7	-4.8	-11.2
3a + C ₂ H ₄ + H ₂	25.5	22.9	25.5	15.2

Table S2. Relative potential energies (ΔE), enthalpies (ΔH), entropies (ΔS), and free energies (ΔG) (using the M11 functional) for the proposed hydrogenation reaction of ethylene by $(^{\text{carb}}\text{PNP})\text{Ir}(\text{H})_2$ under 1 atm H_2 , Figure 5 in Manuscript. Units are kcal/mol for ΔE , ΔH , and ΔG ; units are cal/(deg•mol) for ΔS . The standard state for concentrations is 1 atm for each species participating in the reaction; $T = 298$ K. The sequence of species in the Table is arranged to match Figure 5 as closely as possible.

Species	ΔE	ΔH	ΔS	ΔG
3b + C_2H_4 + H_2	19.9	17.3	48.4	2.9
TS-3b-3c + H_2	14.6	12.8	16.5	7.9
3c + H_2	0.0	0.0	0.0	0.0
TS-3c-3d + H_2	36.9	34.9	7.1	32.8
3d + H_2	7.1	7.8	5.5	6.1
TS-3d-3e + H_2	23.0	23.7	3.4	22.7
3e + H_2	22.6	24.8	8.9	22.1
3f + H_2 + C_2H_6	35.8	36.7	50.6	21.7
3d-cis-H₂	-7.6	-3.7	-28.7	4.9
TS-D	5.8	9.7	-30.1	18.6
3b + C_2H_6	-22.3	-18.2	18.0	-23.6
3d-cis-H₂	-7.6	-3.7	-28.7	4.9
TS-C	4.9	8.2	-31.2	17.5
3b + C_2H_6	-22.3	-18.2	18.0	-23.6
3d-trans-H₂	-7.0	-3.2	-27.0	4.9
TS-A	-5.7	-2.8	-27.9	5.6
3g	-6.4	-2.3	-27.4	5.9
TS-B	-3.8	-0.4	-27.9	7.9
3b + C_2H_6	-22.3	-18.2	18.0	-23.6

Table S3. Total potential energies (E(SCF)), enthalpies (H) and free energies (G) for all species relevant to Figures 4 and 5 in Manuscript. Calculations made use of the M11 functional, the SDD ECP and valence basis set for Ir, and 6-311G(d,p) basis sets for P, N, C, and H. Units are Hartree for E(SCF), H, and G. The standard state for concentration is 1 atm; T = 298 K.

Species	E(SCF)	H	G
3a	-1933.631533	-1932.957244	-1933.053409
3b	-1856.261416	-1855.628401	-1855.724721
3c	-1934.840128	-1934.148476	-1934.247322
3d	-1934.828822	-1934.136122	-1934.237594
3e	-1934.804049	-1934.109002	-1934.212086
3f	-1855.000822	-1854.386031	-1854.483006
3g	-1936.018320	-1935.306944	-1935.407579
3d-cis-C₂H₄	-2013.401151	-2012.648445	-2012.75213
3d-trans-C₂H₄	-2013.400980	-2012.647537	-2012.748752
3d-cis-H₂	-1936.020205	-1935.309141	-1935.409184
3d-trans-H₂	-1936.019263	-1935.308328	-1935.409181
TS-A	-1936.017291	-1935.307684	-1935.408076
TS-B	-1936.014248	-1935.303965	-1935.404392
TS-C	-1936.000361	-1935.290254	-1935.389074
TS-D	-1935.998931	-1935.287904	-1935.387272
TS-3b-3c	-1934.816842	-1934.128026	-1934.234729
TS-3c-3d	-1934.781370	-1934.092825	-1934.195045
TS-3d-3e	-1934.803401	-1934.110766	-1934.211223
TS-3d-cis-C₂H₄-3a	-2013.364267	-2012.613999	-2012.715166
TS-3d-trans-C₂H₄-3a	-2013.373050	-2012.622197	-2012.723284

H ₂	-1.168001	-1.154813	-1.169631
C ₂ H ₄	-78.547078	-78.492457	-78.517968
C ₂ H ₆	-79.782278	-79.703914	-79.729802

Computational Section References

1. Parr, R.G. & Yang, W. *Density-Functional Theory of Atoms and Molecules* (University Press: Oxford, 1989).
2. Zhao, Y. & Truhlar, D. G. *Theo. Chem. Acc.* **120**, 215-241 (2008).
3. Peverati, R.; Zhao, Y.; Truhlar, D. G. *J. Phys. Chem. Lett.* **2011**, 2, 2810-2817;
4. Andrae, D.; Haeussermann, U.; Dolg, M.; Stoll, H.; Preuss, H. *Theor. Chim. Acta* **1990**, 77, 123-141.
5. (a) Raghavachari, K.; Binkley, J. S.; Seeger, R.; Pople, J. A. *Chem. Phys.* **1980**, 72, 650-654 *J. Chem. Phys.* **72**, 650-654 (1980). (b) McLean, A. D; Chandler, G. S. *J. Chem. Phys.* **1980**, 72, 5639-5648.
6. Hratchian, H. P.; Schlegel, H. B. *J. Chem. Theory and Comput.*, **2005**, 1, 61-69.
7. McQuarrie, D.A. *Statistical Thermodynamics* (Harper and Row: New York, 1973).
8. Gaussian 09, Revision D.01, Frisch, M. J.; Trucks, G. W.; Schlegel, H. B.; Scuseria, G. E.; Robb, M. A.; Cheeseman, J. R.; Scalmani, G.; Barone, V.; Mennucci, B.; Petersson, G. A.; Nakatsuji, H.; Caricato, M.; Li, X.; Hratchian, H. P.; Izmaylov, A. F.; Bloino, J.; Zheng, G.; Sonnenberg, J. L.; Hada, M.; Ehara, M.; Toyota, K.; Fukuda, R.; Hasegawa, J.; Ishida, M.; Nakajima, T.; Honda, Y.; Kitao, O.; Nakai, H.; Vreven, T.; Montgomery, J. A., Jr.; Peralta, J. E.; Ogliaro, F.; Bearpark, M.; Heyd, J. J.; Brothers, E.; Kudin, K. N.; Staroverov, V. N.; Kobayashi, R.; Normand, J.; Raghavachari, K.; Rendell, A.; Burant, J. C.; Iyengar, S. S.; Tomasi, J.; Cossi, M.; Rega, N.; Millam, N. J.; Klene, M.; Knox, J. E.; Cross, J. B.; Bakken, V.; Adamo, C.; Jaramillo, J.; Gomperts, R.; Stratmann, R. E.; Yazyev, O.; Austin, A. J.; Cammi, R.; Pomelli, C.; Ochterski, J. W.; Martin, R. L.; Morokuma, K.; Zakrzewski, V. G.; Voth, G. A.; Salvador, P.; Dannenberg, J. J.; Dapprich, S.; Daniels, A. D.; Farkas, Ö.; Foresman, J. B.; Ortiz, J. V.; Cioslowski, J.; Fox, D. J. Gaussian, Inc., Wallingford CT, 2009.

Chapter 4

Computational Study of PNP Pincer Rhodium Catalyzed Alkene

Hydrogenation and Dehydrogenation

Majority of this chapter is reproduced with permission from

Experimental and Computational Study of Alkane Dehydrogenation Catalyzed by a Carbazolide-Based Rhodium PNP Pincer Complex

David B ézier, Changjian Guan, Karsten Krogh-Jespersen,

Alan S. Goldman, and Maurice Brookhart

Chem. Sci., **2016**, *7*, 2579–2586

© The Royal Society of Chemistry 2016

Introduction

Olefins are highly versatile intermediates which can be converted to a wide array of products such as detergents, pharmaceutical intermediates, lubricants, fuels and polymers.¹ Accordingly, there has been growing interest in the homogeneous dehydrogenation of alkanes as a potential highly atom-economic route to olefins.

The first catalytic transfer alkane dehydrogenations were reported independently by Felkin and Crabtree using phosphine-based rhenium, ruthenium and iridium catalysts for a reaction that has become standard for screening transfer dehydrogenations, the use of *t*-butylethylene (TBE) as a hydrogen acceptor to dehydrogenate cyclooctane (COA).² Turnover numbers (TONs) in these systems were limited (< 100 TO) by low catalyst stability. Following these reports, rhodium-based systems were developed independently by the groups of Saito,³ Tanaka⁴ and Goldman⁵ which exhibited high TONs for alkane dehydrogenation; however, formation of the active species, $\text{Rh}(\text{Cl})(\text{PR}_3)_2$, could only be achieved photochemically⁶ or under H_2 atmosphere, limiting the utility of these systems.

The development of the iridium pincer complex ($^{\text{tBu}}\text{PCP}$)IrH₂ by Kaska and Jensen was a breakthrough for the achievement of high TONs in the benchmark COA/TBE system.⁷ More active and stable iridium complexes were next developed through modification of the pincer ligand. Catalysts based on the PCP,⁸ POCOP,⁹ PCOP,¹⁰ Anthraphos^{10a, 11} (Fig. 1) and other¹² frameworks have since been used and studied extensively.

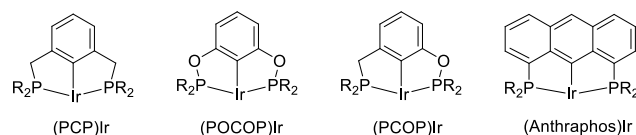
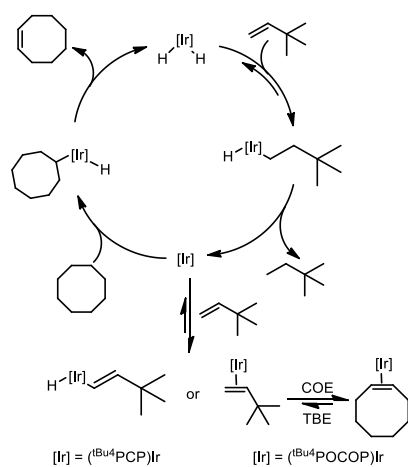


Figure 1. Examples of active PCP iridium pincer complexes for alkane dehydrogenation.

The mechanism of the transfer dehydrogenation of COA with TBE using PCP^{8i, 13} and POCOP^{8i, 9a, 9b} iridium pincer complexes has been thoroughly investigated. The overall catalytic cycle is shown in Scheme 1.

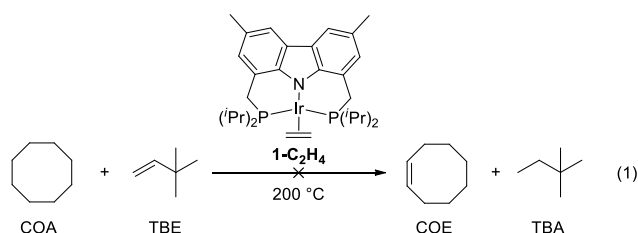
Scheme 1. Mechanism of transfer dehydrogenation of COA with TBE using PCP- and POCOP-iridium complexes



The mechanisms for these two systems are similar. Beginning with the 16-electron iridium dihydride complex, insertion of TBE yields the alkyl hydride complex which undergoes reductive elimination to form the Ir(I) 14-electron species. This complex activates the C-H bond of cyclooctane, followed by β -hydride

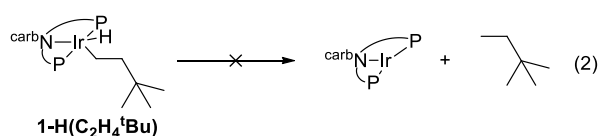
elimination to yield cyclooctene and regenerate the iridium dihydride. At low concentration of TBE, hydrogenation is turnover-limiting for the (PCP)Ir system, and the resting state is (PCP)IrH₂, while at high [TBE], COA dehydrogenation is turnover-limiting and the resting state is the vinyl hydride complex. For the (POCOP)Ir system, dehydrogenation is turnover limiting and alkene (TBE and COE) complexes are the resting states.

DFT calculations have been conducted¹⁴ which indicate that more weakly σ -donating groups at the central position of the pincer ligand favour the thermodynamics of C-H (and H-H) addition to the 14e pincer-Ir fragments. Intrigued by the possible implications for alkane dehydrogenation, we recently synthesized **1-C₂H₄**, an Ir complex of the bis-phosphine carbazolidone pincer, carb-PNP, in which the central coordinating group is an sp² nitrogen which is much less σ -donating than the sp² carbon of PCP pincer ligands. In a previous study, however, **1-C₂H₄** was found to be ineffective as a catalyst for alkane transfer dehydrogenation (eq 1).¹⁵



Experimental and computational studies indicated that hydrogenation of TBE was the rate-limiting step for **1**-catalyzed COA/TBE transfer dehydrogenation. TBE did insert into an Ir-H bond of **1-H₂**, but reductive elimination of alkane from the resulting Ir(III) alkyl hydride, **1-H(C₂H₄^tBu)**, was thermodynamically very

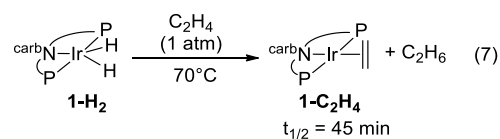
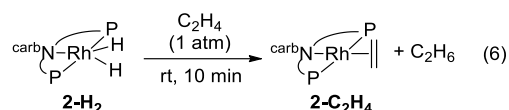
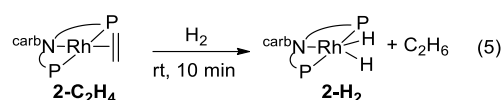
unfavourable (eq 2). Thus, compared with PCP ligands, the carb-PNP ligand was indeed found to strongly favour the Ir(III) alkyl hydride, as well as the Ir(III) dihydride, relative to the 14-electron Ir(I) fragment. But while C-H addition and alkane dehydrogenation by the 14-electron Ir species were favoured by the carb-PNP ligand, the hydrogenation segment of the cycle was disfavoured so strongly that catalytic transfer-dehydrogenation was precluded.



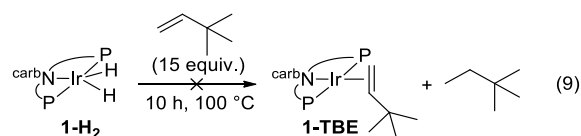
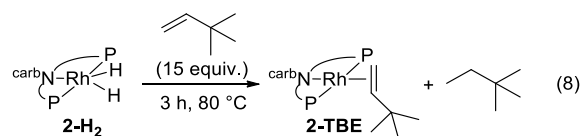
It was previously shown^{8a} that in the case of PCP-type pincer ligands, the Rh(III) state was not sufficiently accessible to allow an effective catalytic cycle based on the Rh(I)/Rh(III) couple. Based on the conclusions reached in the studies with Ir(I), we considered that for carb-PNP complexes of rhodium, the Rh(III) state should be relatively more favourable and thus the system might be active for alkane dehydrogenation.

Here we report a computational study of rhodium complexes (carb-PNP)Rh(ethylene), **2-C₂H₄**, and (carb-PNP)Rh(H)₂, **2-H₂**, and their hydrogenation of ethylene and TBE, in analogy with last chapter's discussion of the (carb-PNP)Ir complexes.¹⁵ These complexes were also investigated for catalytic alkane transfer dehydrogenation. In contrast to the (carb-PNP)Ir analogues, and in accord with the hypothesis proposed above, we find the (carb-PNP)Rh complexes to be quite active as catalysts for COA/TBE transfer-dehydrogenation.

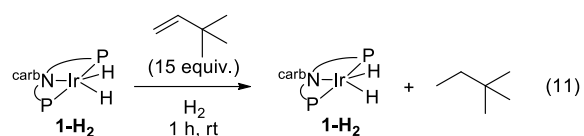
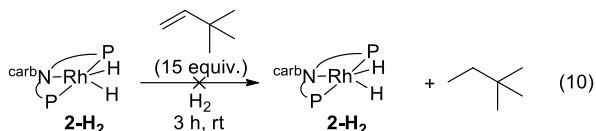
The catalyst complexes **2-C₂H₄** and **2-H₂** were initially tested for hydrogenation under dihydrogen and ethylene atmosphere. Complex **2-C₂H₄** reacts with H₂ at room temperature (rt) for 10 min resulted in the complete conversion to (carb-PNP)Rh(H)₂, **2-H₂** (eq 5). Under 1 atm of ethylene, **2-H₂** was rapidly converted to **2-C₂H₄** at rt (eq 6). This behaviour is in marked contrast to the iridium analogue **1-H₂** which requires a temperature of 70 °C with a half-life of 45 min for the analogous reaction (eq 7).¹⁵



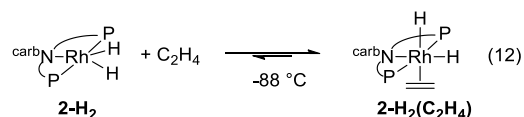
Hydrogenation of TBE by **2-H₂** does not proceed at rt. However, **2-H₂** was converted to (carb-PNP)Rh(TBE), **2-TBE** at 80 °C (eq 8). Thus, hydrogenation of TBE, like ethylene, by **2-H₂** is much more facile than by iridium dihydride **1-H₂**, the latter showing no reactivity after 10 h at 100 °C under the same conditions (eq 9).¹⁵



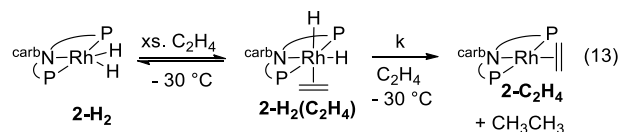
Under an atmosphere of dihydrogen, a solution of **2-H₂** and TBE showed no reaction after 3 h at room temperature (eq. 10). This behaviour contrasts with the iridium dihydride **1-H₂** which rapidly catalyzes the hydrogenation of TBE to TBA at room temperature via an Ir(III)/Ir(V) catalytic cycle (eq 11)¹⁵ assisted by H₂.



Binding of ethylene to **2-H₂** to give **2-H₂(C₂H₄)** is reversible and thermodynamically favoured at low temperature (-88 °C to -70 °C) (eq 12). The free energy barrier for exchange of free ethylene with **2-H₂(C₂H₄)** was estimated to be ≈ 9 kcal/mol.



The rate of the stoichiometric hydrogenation of C₂H₄ by **2-H₂** was found to be first-order in **2-H₂(C₂H₄)**, but independent of the concentration of C₂H₄ in the range 0.05-0.5 M. A first-order rate constant, k, of 2.4 × 10⁻⁴ s⁻¹ was obtained, corresponding to ΔG[‡] = 18 kcal/mol at -30 °C.



It is also shown that migratory insertion is irreversible and is the rate-limiting step in ethylene hydrogenation with $\Delta G^\ddagger = 18$ kcal/mol.¹⁸ The reductive elimination of ethane from the rhodium complex will be shown by DFT calculation to be much more facile than for the iridium analogue, which has a high kinetic barrier ($\Delta G^\ddagger = 20$ -25 kcal/mol).¹⁵

In contrast with the inactive iridium analogue, **2-H₂** and **2-C₂H₄** showed high activity for COA/TBE transfer-dehydrogenation at 200 °C, and suffered catalyst decomposition. However, **2-H₂** was significantly less effective for *n*-octane/TBE transfer-dehydrogenation. The resting states detected were (carb-PNP)Rh(TBE) **2-TBE** and (carb-PNP)RhH₂ (**2-H₂**) in both cases.

Results and Discussion

DFT calculations were conducted on the reactions discussed above using the M06-L density functional and valence basis sets of triple-zeta plus polarization quality (see Supporting Information). We used a model ligand in which the two *i*-Pr groups on each P atom were replaced with a *t*-Bu and a methyl group to give a C₂ symmetric diastereomer. Since metal-bound P^{*i*}Pr₂ groups typically adopt a conformation in which one of the two methynyl C-H bonds points toward the metal center while the other points away, the P^{*t*}BuMe group mimics the steric effect of the P^{*i*}Pr₂ group. The P^{*t*}BuMe group, however, offers the advantage of avoiding the many local (non-global) conformational minima, which we have encountered in calculations of pincers with P^{*i*}Pr₂ groups (see Supporting Information for a computational assessment of this model). In addition, our model does not include the two methyl groups at the positions para to the carbazolide N atom. We refer to

this ligand as carb-PNP' and the model compounds as derivatives of **2'** to distinguish them from the experimental complexes related to **2**.

The results of the calculations proved quite valuable in attempting to interpret the experimental results. A free energy diagram for the reaction of dihydride **2'**-H₂ with ethylene at -30 °C is shown in Fig. 2. Note that at -80 °C, the calculations indicate that ethylene binds to **2**-H₂, to give **2'**-H₂(C₂H₄), exoergically ($\Delta G = -0.7$ kcal/mol), in agreement with the observation illustrated in eq 12. At -30 °C, the observed equilibrium suggests that ΔG is slightly positive and indeed, the calculated free energy of binding is $\Delta G = 1.5$ kcal/mol. At -30 °C, the barrier to the reaction of ethylene dihydride complex **2'**-H₂(C₂H₄) to give the three-coordinate (carb-PNP')Rh (**2'**) and ethane is calculated to be 16.1 kcal/mol, in good agreement with the experimental value for **2**-H₂(C₂H₄) of $\Delta G^\ddagger = 18$ kcal/mol.

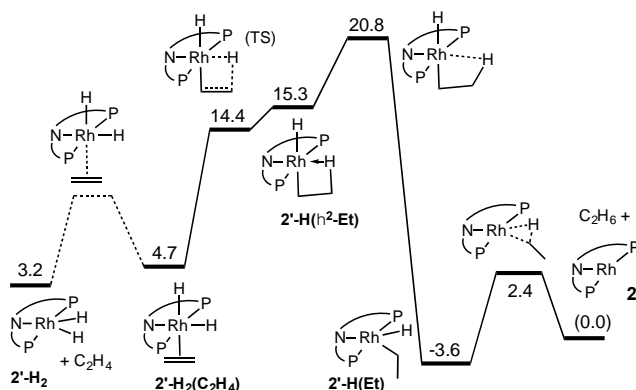


Fig. 2. Calculated free energies (kcal/mol) for reaction of **2'**-H₂ with ethylene at -30 °C

H/D exchange of **2'**-D₂(C₂H₄) with C₂H₄ is not observed in the course of the hydrogenation reaction. This would typically be interpreted to suggest that

migratory insertion of ethylene is irreversible and is the rate-limiting step of the reaction, followed by fast elimination of ethane. The calculations, however, yield a somewhat different explanation. Insertion of C₂H₄ into a Rh-H bond of **2'**-H₂ leads to a β-agostic ethyl complex (PNP)RhH(η²-Et), **2'**-H(η²-Et), with a nearly fully formed C-H bond (d = 1.23 Å; see Figures 3 and 4).¹⁹ The TS for this insertion process at -30 °C has a free energy 9.7 kcal/mol above that of **2'**-H₂(C₂H₄) while the free energy of the agostic product is 10.6 kcal/mol higher than **2'**-H₂(C₂H₄). (Although it has a *lower free energy*, *G*, the *electronic energy*, *E*, of the TS leading to the agostic intermediate is *higher* than that of the agostic intermediate, as required of a proper TS on the potential energy surface). Accordingly, the barrier to the back-reaction of this process (i.e. **2'**-H(η²-Et) → **2'**-H₂(C₂H₄)) is negligible.

The short Rh-H distance of 1.75 Å in **2'**-H(η²-Et) indicates a very strong agostic interaction. The H atom is located trans to the weak-trans-influence carbazole nitrogen, while the α-carbon is trans to a strong-trans-influence hydride ligand; this result is consistent with conclusions of an earlier study of the relationship between agostic bond strengths and the respective trans influences of ancillary ligands.²⁰

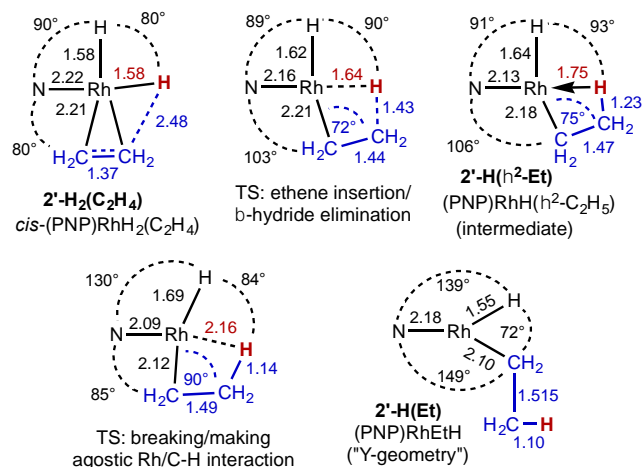


Fig. 3. Structural parameters, in the plane bisecting the P-Rh-P axis, along the pathway for the insertion of ethylene into a Rh-H bond of **2'-H₂(C₂H₄)**.

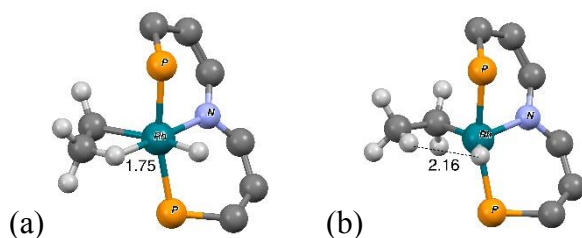


Fig. 4. "3-D" models of (a) agostic intermediate **2'-H(η²-Et)** and (b) ring-opening transition state **TS(2'-H(η²-Et)/2'-H(Et))**. Peripheral atoms omitted for clarity. Rh-H distances in Å

Loss of the agostic interaction in **2'-H(η²-Et)** has a barrier $\Delta G^\ddagger = 5.5$ kcal/mol (Fig. 2). The product of this ring-opening, **2'-H(Et)**, is 18.9 kcal/mol lower in free energy than agostic **2'-H(η²-Et)**. Since this is formally only a bond breaking reaction, with no concomitant bond making, a negative value of ΔG , and particularly such a strongly negative value (-18.9 kcal/mol), is quite striking. This result can be explained, however, in terms of the geometry of reactant and product. In **2'-H(η²-**

Et), the strong-trans-influence agostic ethyl group α -carbon is positioned trans to the strong-trans-influence hydride ligand. In contrast, **2'-H(Et)** adopts a so-called Y-geometry,²¹ in which the C_{α} -Rh-H angle, instead of being ca. 180° (mutually trans) is only 72° , while the N-Rh- C_{α} angle (106° in **2'-H(η^2 -Et)**) is 149.0° (Fig. 3). As a result, **2'-H(Et)** has a very short Rh-C bond (2.095 \AA vs 2.175 \AA in **2'-H(η^2 -Et)**) and a much shorter Rh-H bond (1.546 \AA vs. 1.640 \AA) than is found in **2'-H(η^2 -Et)**.

The barrier to elimination of ethane from **2'-H(Et)** is only $\Delta G^{\ddagger} = 6.0 \text{ kcal/mol}$ as compared with 24.4 kcal/mol for the reverse reaction, i.e. re-formation of the agostic bond to give **2'-H(η^2 -Et)**. Thus the "ring-opening" of **2'-H(η^2 -Et)** is the rate-determining step for the overall loss of ethane from dihydride ethylene complex **2'-H₂(C₂H₄)**. Attempts to locate a TS for rotation around the ethylene C-C bond of agostic complex **2'-H(η^2 -Et)** only led to loss of the agostic interaction to give **2'-H(Et)**. Thus, although insertion of ethylene into a Rh-H bond of **2'-H₂(C₂H₄)** is fully reversible, the calculations predict that it should not lead to exchange between hydride (or deuteride) and ethylene H atoms, in accord with the observed lack of H/D exchange between **2-D₂** and C₂H₄.

The reaction of dihydride **2-H₂** with TBE, as noted above, does not proceed at room temperature in contrast with the reaction with ethylene, which occurs at -30°C . The TBE reaction proceeds slowly at 80°C ; the timescale corresponds to a free energy barrier of ca. $26\text{-}27 \text{ kcal/mol}$, about $8\text{-}9 \text{ kcal/mol}$ greater than the reaction with ethylene. The reaction is calculated to proceed via a pathway analogous to that for ethylene. An agostic analogue to **2'-H(η^2 -Et)** is calculated to form with a free

energy 24.2 kcal/mol higher than **2-H₂** plus TBE, followed by a rate-determining ring-opening with a TS that is 3.3 kcal/mol higher. The overall barrier for the reaction is thus $\Delta G^\ddagger = 27.5$ kcal/mol, about 10 kcal/mol greater than the reaction barrier with ethylene, and in very good agreement with experiment. While the Ir analogue was previously shown to react with TBE via an Ir(III)/Ir(V) pathway requiring the presence of H₂, no acceleration by H₂ is observed in the present Rh system. This is consistent with the calculated barrier for elimination of *n*-hexane from (carb-PNP')Rh(t-butylvinyl)(H), $\Delta G^\ddagger = 5.9$ kcal/mol, which is far lower than the barrier calculated for the back-reaction ($\Delta G^\ddagger = 28.6$ kcal/mol).

The calculations also provide insight into the much greater rate of dehydrogenation of COA compared with *n*-octane. (Free energy values are shown in Fig. 5, expressed relative to **2'** plus the free alkane and calculated for T = 473 K in the gas phase with pressures that correspond to the molarity of the respective pure liquid alkanes.) Oxidative addition of the C-H bond of COA has a calculated barrier ca. 4 kcal/mol higher than that of *n*-octane. However, the TS for formation of the β -agostic species (carb-PNP')RhH(η^2 -1-octyl), which is rate-determining for *n*-octane dehydrogenation, is 5.4 kcal/mol higher than the TS for formation of the corresponding β -agostic cyclooctyl complex. This may be explained in terms of the eclipsed interactions required by the formation of agostic complex (carb-PNP')RhH(η^2 -1-octyl) (see Fig. 4a for the ethyl analogue). Such unfavourable interactions are also present in the TS for formation of (carb-PNP')RhH(η^2 -cyclooctyl). However, in the case of COA, unlike *n*-octane, these eclipsed interactions are already present in the alkane substrate (being responsible for the

well known ring strain of COA) as well as in the non-agostic C-H addition product. Thus, relative to these free species and the non-agostic alkyl hydride, the TS for agostic bond formation for COA is significantly lower in energy than that for *n*-octane. It may be relevant in this context that unlike the case for *n*-octane or ethane, the agostic cyclooctyl complex (the analogue of **2'**-H(η^2 -Et)) appears to be a distinct minimum on the free energy surface (Fig. 5), and not only a minimum on the electronic energy surface.

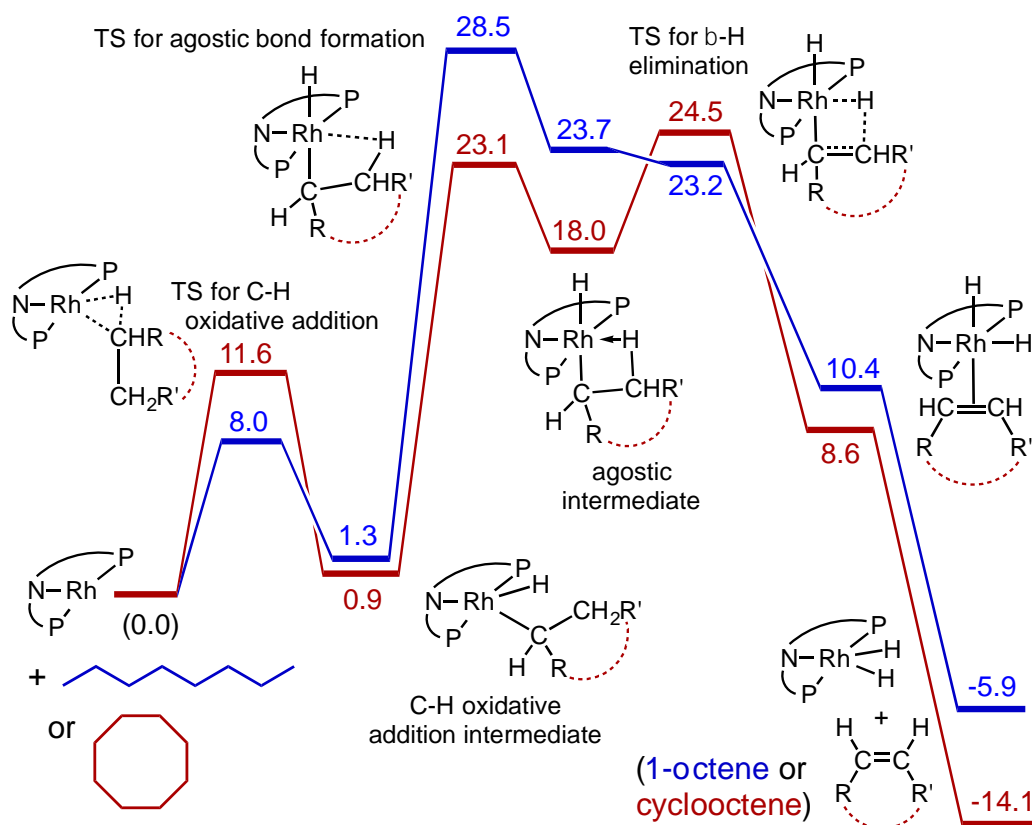


Fig. 5. Calculated free energies (kcal/mol) for reaction of **2** with *n*-octane (blue) and with cyclooctane (red) at 200 °C (gas phase, pressures corresponding to molarity of pure liquid)

On the dehydrogenation pathway the step subsequent to formation of the agostic intermediate is β -H-elimination. In the case of *n*-octane dehydrogenation the TS for this step, TS(**2'-H**(η^2 -**1-Oc**)/**2'-H**(**1-Oc**)), has a much lower free energy (23.2 kcal/mol) than the TS for the (rate-determining) formation of the agostic complex (28.5 kcal/mol). In contrast, β -H elimination of the agostic cyclooctyl complex (carb-PNP')RhH(η^2 -cyclooctyl) is calculated to have a TS slightly higher in free energy (24.5 kcal/mol) than the TS for formation of the agostic complex (23.1 kcal/mol), although this difference is quite small (and probably too small to be meaningful for the comparison of such different species).

Interestingly, the free energy of the TS for β -H elimination of the cyclooctyl complex (24.5 kcal/mol) is *higher* than that for the 1-octyl complex (23.2 kcal/mol). Likewise (but not surprisingly), as noted above, the TS for C-H addition of COA is of higher free energy than that for *n*-octane. These steps, C-H addition and β -H elimination, are the steps most commonly considered in the context of alkane dehydrogenation (while their microscopic reverse reactions are regarded similarly for olefin hydrogenation). But although the higher reactivity of COA vs. *n*-alkanes is a staple of organometallic-catalyzed alkane dehydrogenation, in the present system the TSs of both of these steps are calculated to be *higher* in free energy for the dehydrogenation of COA than of *n*-octane. The higher reactivity of COA vs. *n*-octane in the present system, according to our calculations, is a result of only the lower energy of the unanticipated transition state for the formation of an agostic interaction in the case of COA.

Conclusions

The iridium dihydride complex **1-H₂** based on the carbazole bis-phosphine ligand was previously reported to be ineffective as a transfer-dehydrogenation catalyst. This was found to be ultimately attributable to the very high energy of the (carb-PNP)Ir(I) complex relative to (carb-PNP)Ir(III). Thus, potential hydrogen acceptors such as TBE inserted into an Ir-H bond (maintaining the Ir(III) oxidation state) but the barrier to subsequent elimination to give the Ir(I) product was prohibitively high while deinsertion was much more favourable. Hydrogenation by H₂ was effected, but this was found to proceed via an Ir(III)/Ir(V) pathway involving addition of H₂ to the Ir(III) alkyl hydride; such a path is not viable for alkane dehydrogenation.

As the M(I)/M(III) thermodynamics are biased more towards M(I) in the case of Rh than Ir,²² we suspected the relatively high stability of a Rh(III) analogue would not preclude, and might even favour, transfer dehydrogenation. Indeed the complex **2-H₂** is found to be an active catalyst for the dehydrogenation of COA with TBE achieving TOFs up to 10 min⁻¹, similar to the catalyst (^tBu⁴PCP)IrH₂.⁷ To our knowledge this is the first example of a highly active rhodium-based alkane transfer-dehydrogenation catalyst that does not require light or H₂ atmosphere. However, decomposition of the catalyst at 200 °C limits the catalyst efficiency.

n-Octane dehydrogenation proceeded more slowly than COA dehydrogenation. DFT calculations indicate that the slower rate for *n*-octane is attributable to the barrier to a rate-determining step not heretofore given consideration in the context of alkane dehydrogenation (or its microscopic reverse,

in the case of alkene hydrogenation), namely the formation of an agostic intermediate, (carb-PNP')RhH(η^2 -1-octyl), subsequent to C-H addition. Even so the reaction is not prohibitively slow; however, the combination of relatively rapid decomposition at 200 °C and the relatively slow dehydrogenation rate leads to very limited TONs. The development of more stable rhodium pincer complexes based on a similar framework is currently underway.

References

- 1) K. Weissermel and H.-J. Arpe, in *Industrial Organic Chemistry*, Wiley-VCH Verlag GmbH, 2008, pp. 59.
- 2) (a) M. Findlater, J. Choi, A. Goldman and M. Brookhart, in *Alkane C-H Activation by Single-Site Metal Catalysis*, ed. P. J. Pérez, Springer Netherlands, 2012, vol. 38, ch. 4, pp. 113; (b) J. Choi, A. H. R. MacArthur, M. Brookhart and A. S. Goldman, *Chem. Rev.*, 2011, **111**, 1761; (c) J. Choi and A. Goldman, in *Iridium Catalysis*, ed. P. G. Andersson, Springer Berlin Heidelberg, 2011, vol. 34, ch. 6, pp. 139; (d) D. Morales-Morales, *Iridium Complexes Org. Synth.*, 2009.
- 3) K. Nomura and Y. Saito, *J. Chem. Soc., Chem. Commun.*, 1988, 161.
- 4) T. Sakakura, T. Sodeyama, Y. Tokunaga and M. Tanaka, *Chem. Lett.*, 1988, 263.
- 5) (a) J. A. Maguire, W. T. Boese and A. S. Goldman, *J. Am. Chem. Soc.*, 1989, **111**, 7088; (b) J. A. Maguire, W. T. Boese, M. E. Goldman and A. S. Goldman, *Coord. Chem. Rev.*, 1990, **97**, 179; (c) J. A. Maguire and A. S. Goldman, *J. Am. Chem. Soc.*, 1991, **113**, 6706; (d) J. A. Maguire, A. Petrillo and A. S. Goldman, *J. Am. Chem. Soc.*, 1992, **114**, 9492; (e) K. Wang, M. E. Goldman, T. J. Emge and A. S. Goldman, *J. Organomet. Chem.*, 1996, **518**, 55.
- 6) A. D. Chowdhury, N. Weding, J. Julis, R. Franke, R. Jackstell and M. Beller, *Angew. Chem. Int. Ed.*, 2014, **53**, 6477.
- 7) M. Gupta, C. Hagen, R. J. Flesher, W. C. Kaska and C. M. Jensen, *Chem. Commun.*, 1996, 2083.

- 8) (a) W.-w. Xu, G. P. Rosini, K. Krogh-Jespersen, A. S. Goldman, M. Gupta, C. M. Jensen and W. C. Kaska, *Chem. Commun.*, 1997, 2273; (b) M. Gupta, W. C. Kaska and C. M. Jensen, *Chem. Commun.*, 1997, 461; (c) D. W. Lee, W. C. Kaska and C. M. Jensen, *Organometallics*, 1998, **17**, 1; (d) F. Liu, E. B. Pak, B. Singh, C. M. Jensen and A. S. Goldman, *J. Am. Chem. Soc.*, 1999, **121**, 4086; (e) S. Kundu, Y. Choliy, G. Zhuo, R. Ahuja, T. J. Emge, R. Warmuth, M. Brookhart, K. Krogh-Jespersen and A. S. Goldman, *Organometallics*, 2009, **28**, 5432; (f) B. Punji, T. J. Emge and A. S. Goldman, *Organometallics*, 2010, **29**, 2702; (g) J. J. Adams, N. Arulsamy and D. M. Roddick, *Organometallics*, 2012, **31**, 1439; (h) K. Krogh-Jespersen, M. Czerw, K. Zhu, B. Singh, M. Kanzelberger, N. Darji, P. D. Achord, K. B. Renkema and A. S. Goldman, *J. Am. Chem. Soc.*, 2002, **124**, 10797; (i) K. Zhu, P. D. Achord, X. Zhang, K. Krogh-Jespersen and A. S. Goldman, *J. Am. Chem. Soc.*, 2004, **126**, 13044; (j) A. Ray, K. Zhu, Y. V. Kissin, A. E. Cherian, G. W. Coates and A. S. Goldman, *Chem. Commun.*, 2005, 3388; (k) S. A. Kuklin, A. M. Sheloumov, F. M. Dolgushin, M. G. Ezernitskaya, A. S. Peregudov, P. V. Petrovskii and A. A. Koridze, *Organometallics*, 2006, **25**, 5466.
- 9) (a) I. Gottker-Schnetmann, P. White and M. Brookhart, *J. Am. Chem. Soc.*, 2004, **126**, 1804; (b) I. Gottker-Schnetmann and M. Brookhart, *J. Am. Chem. Soc.*, 2004, **126**, 9330; (c) I. Götter-Schnetmann, P. S. White and M. Brookhart, *Organometallics*, 2004, **23**, 1766; (d) D. Morales-Morales, R. o. Redón, C. Yung and C. M. Jensen, *Inorg. Chim. Acta*, 2004, **357**, 2953.
- 10) (a) R. Ahuja, B. Punji, M. Findlater, C. Supplee, W. Schinski, M. Brookhart and A. S. Goldman, *Nat. Chem.*, 2011, **3**, 167; (b) A. J. Nawara-Hultsch, J. D.

Hackenberg, B. Punji, C. Supplee, T. J. Emge, B. C. Bailey, R. R. Schrock, M. Brookhart and A. S. Goldman, *ACS Catal.*, 2013, **3**, 2505.

11) (a) M. W. Haenel, S. Oevers, K. Angermund, W. C. Kaska, H.-J. Fan and M. B. Hall, *Angew. Chem. Int. Ed.*, 2001, **40**, 3596; (b) T. W. Lyons, D. Guironnet, M. Findlater and M. Brookhart, *J. Am. Chem. Soc.*, 2012, **134**, 15708; (c) S. Kundu, T. W. Lyons and M. Brookhart, *ACS Catalysis*, 2013, **3**, 1768.

12) (a) Y. Shi, T. Suguri, C. Dohi, H. Yamada, S. Kojima and Y. Yamamoto, *Chem. Eur. J.*, 2013, **19**, 10672; (b) W. Yao, Y. Zhang, X. Jia and Z. Huang, *Angew. Chem. Int. Ed.*, 2014, **53**, 1390; (c) D. B ézier and M. Brookhart, *ACS Catalysis*, 2014, **4**, 3411.

13) (a) K. B. Renkema, Y. V. Kissin and A. S. Goldman, *J. Am. Chem. Soc.*, 2003, **125**, 7770; (b) M. Kanzelberger, B. Singh, M. Czerw, K. Krogh-Jespersen and A. S. Goldman, *J. Am. Chem. Soc.*, 2000, **122**, 11017; (c) K. Krogh-Jespersen, M. Czerw, N. Summa, K. B. Renkema, P. D. Achord and A. S. Goldman, *J. Am. Chem. Soc.*, 2002, **124**, 11404; (d) K. Krogh-Jespersen, M. Czerw and A. S. Goldman, *J. Mol. Catal. A: Chem.*, 2002, **189**, 95.

14) D. Y. Wang, Y. Choliy, M. C. Haibach, J. F. Hartwig, K. Krogh-Jespersen and A. S. Goldman, *J. Am. Chem. Soc.* 2016, **138**, 149.

15) C. Cheng, B. G. Kim, D. Guironnet, M. Brookhart, C. Guan, D. Y. Wang, K. Krogh-Jespersen and A. S. Goldman, *J. Am. Chem. Soc.*, 2014, **136**, 6672.

16) (a) O. V. Ozerov, C. Guo, V. A. Papkov and B. M. Foxman, *J. Am. Chem. Soc.*, 2004, **126**, 4792; (b) W. Weng, C. Guo, C. Moura, L. Yang, B. M. Foxman and O. V. Ozerov, *Organometallics*, 2005, **24**, 3487; (c) S. Gatard, R. Çelenligil-Çetin, C. Guo, B. M. Foxman and O. V. Ozerov, *J. Am. Chem. Soc.*, 2006, **128**, 2808; (d) W. Weng,

C. Guo, R. Celenligil-Cetin, B. M. Foxman and O. V. Ozerov, *Chem. Commun.*, 2006, 197.

17) Due to decomposition of **2-H₂** at 80 °C, **2-TBE** was formed in a 50% yield. After 3 h at 80 °C, **2-TBE** was the only species detected by ³¹P NMR, however the ¹H NMR showed the presence of other non identified compounds.

18) Since exchange with excess free C₂H₄ is rapid, if ethylene insertion into the Rh-D bond of **2-D₂(C₂H₄)** were reversible, the major expected product would be the C₂H₄ (d₀) complex with incorporation of H into the hydride positions as indicated in eq 15.

19) M. Brookhart, M. L. H. Green and G. Parkin, *Proc. Natl. Acad. Sci.*, 2007, **104**, 6908.

20) F. Hasanayn, P. Achord, P. Braunstein, H. J. Magnier, K. Krogh-Jespersen and A. S. Goldman, *Organometallics*, 2012, **31**, 4680.

21) (a) Y. Jean and O. Eisenstein, *Polyhedron*, 1988, **7**, 405; (b) I. E.-I. Rachidi, O. Eisenstein and Y. Jean, *New. J. Chem.*, 1990, **14**, 671; (c) J. F. Riehl, Y. Jean, O. Eisenstein and M. Pelissier, *Organometallics*, 1992, **11**, 729.

22) J. P. Collman, *Acc. Chem. Res.*, 1968, **1**, 136.

Computational Details

All electronic structure calculations employed the DFT method¹ and the M06-L² functional. The electronic environment was modeled using the following scheme: for Rh, we applied the SDD relativistic effective (small) core potential and the associated (6s5p3d) valence basis set,³ augmented with an f-type function and a complete set of diffuse spdf functions;⁴ all-electron 6-311G(d,p) basis sets were applied to all other atoms.⁵ Reactant, transition state and product geometries were fully optimized and characterized by normal mode analysis. Expanded integration grid sizes (pruned (99,590) atomic grids invoked using the integral=ultrafine keyword) were applied to increase numerical accuracy and stability in both geometry optimizations and normal mode analysis.⁶ The (unscaled) vibrational frequencies formed the basis for the calculation of vibrational zero-point energy (ZPE) corrections; standard thermodynamic corrections (based on the harmonic oscillator/rigid rotor approximations and ideal gas behavior) were made to convert from purely electronic energies (E) to (standard) enthalpies (H) and Gibbs free energies (G; P = 1 atm, T = 298 K).⁷ All calculations were executed using the GAUSSIAN 09 series of computer programs.⁸

Computational Section References

1. W. Koch and M. C. Holthausen, *A Chemist's Guide to Density Functional Theory*, Wiley, New York, 2001.
2. Y. Zhao and D. G. Truhlar, *J. Chem. Phys.*, 2006, **125**, 194101/194101-194101/194118.
3. D. Andrae, U. Haeussermann, M. Dolg, H. Stoll and H. Preuss, *Theor. Chim. Acta*, 1990, **77**, 123-141.
4. M. A. Iron, A. C. B. Lucassen, H. Cohen, M. E. van der Boom and J. M. L. Martin, *J. Am. Chem. Soc.*, 2004, **126**, 11699-11710.
5. (a) R. Ditchfield, W. J. Hehre and J. A. Pople, *J. Chem. Phys.* 1971, **54**, 724-728. (b) P. C. Hariharan and J. A. Pople, *Molecular Physics* 1974, **27**, 209-214. (c) K. Raghavachari, J. S. Binkley, R. Seeger and J. A. Pople, *J. Chem. Phys.* 1980, **72**, 650-654. (d) A. D. McLean and G. S. Chandler, *J. Chem. Phys.* 1980, **72**, 5639-5648
6. Æ. Frisch, M. J. Frisch, F. R. Clemente and G. W. Trucks, *Gaussian 09 User's Reference*, 147.
7. D. A. McQuarrie, *Statistical Thermodynamics*, Harper and Row, New York, 1973.
8. M. J. Frisch, G. W. Trucks, H. B. Schlegel, G. E. Scuseria, M. A. Robb, J. R. Cheeseman, G. Scalmani, V. Barone, B. Mennucci, G. A. Petersson, H. Nakatsuji, M. Caricato, X. Li, H. P. Hratchian, A. F. Izmaylov, J. Bloino, G. Zheng, J. L. Sonnenberg, M. Hada, M. Ehara, K. Toyota, R. Fukuda, J. Hasegawa, M. Ishida, T. Nakajima, Y. Honda, O. Kitao, H. Nakai, T. Vreven, J. J. A. Montgomery and J. E. O. Peralta, F.; Bearpark, M.; Heyd, J. J.; Brothers, E.; Kudin, K. N.; Staroverov, V. N.; Kobayashi, R.; Normand, J.; Raghavachari, K.; Rendell, A.; Burant, J. C.; Iyengar, S. S.; Tomasi, J.; Cossi, M.; Rega, N.; Millam, N. J.; Klene, M.; Knox, J. E.; Cross, J. B.; Bakken, V.; Adamo, C.; Jaramillo, J.; Gomperts, R.; Stratmann, R. E.; Yazyev, O.; Austin, A. J.; Cammi, R.; Pomelli, C.; Ochterski, J. W.; Martin, R. L.; Morokuma, K.; Zakrzewski, V. G.; Voth, G. A.; Salvador, P.; Dannenberg, J. J.; Dapprich, S.; Daniels, A. D.; Farkas, Ö.; Foresman, J. B.; Ortiz, J. V.; Cioslowski, J.; Fox, D. J., *Gaussian 09, Revision D.01*, Gaussian, Inc., Wallingford, CT, 2009.

Chapter 5

Computational Study of Alkane Dehydrogenation Reaction

Co-Catalyzed by Pincer Iridium Complexes and Lewis Acids

A manuscript based on the work described in this chapter of the dissertation has been submitted for publication on 12/20/2016 as

β -Hydride Elimination and C-H Activation by an Iridium Acetate Complex, Catalyzed by Lewis Acids. Alkane Dehydrogenation Co-Catalyzed by Lewis Acids and (Phebox)Ir

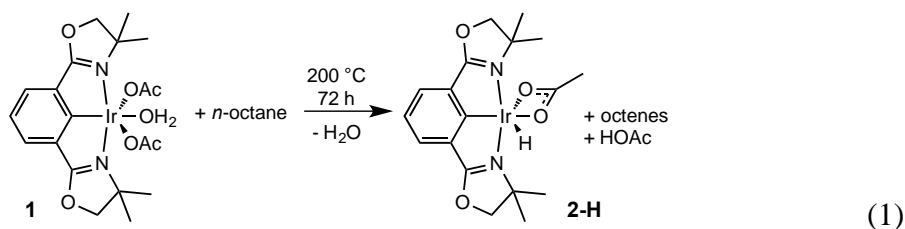
Yang Gao, Changjian Guan, Meng Zhou, Akshai Kumar, Karen Goldberg,

Ashley M. Wright, Karsten Krogh-Jespersen and Alan S. Goldman

Introduction

The selective catalytic dehydrogenation of alkanes and alkyl groups has great potential with respect to the synthesis of fuels and both commodity and fine chemicals. Transition metal based catalysts have shown considerable promise in this context, affording high turnover numbers and the very desirable selectivity for dehydrogenation of the terminal position. To date such catalysts have generally involved electron-rich highly unsaturated (14-electron) metal centers in low oxidation states.¹⁻³

In 2012, Nishiyama reported that (Phebox)Ir(OAc)₂(OH₂) (**1**) activates the terminal C-H bond of *n*-octane to form (Phebox)Ir(OAc)(*n*-octyl) (**2-Oc**) at 160 °C in the presence of potassium carbonate.⁴ The Goldberg lab reported that if **1** is heated in *n*-octane to 200 °C (without added base), (Phebox)Ir(OAc)(H) (**2-H**) and free octenes are obtained (eq 1). This reaction, shown in eq 1, is the stoichiometric (heterolytic) dehydrogenation of *n*-octane by an Ir-OAc unit.⁵ The higher temperature of 200 °C, relative to the C-H activation at 160 °C, was apparently necessary to induce β-H elimination of **2-Oc**.

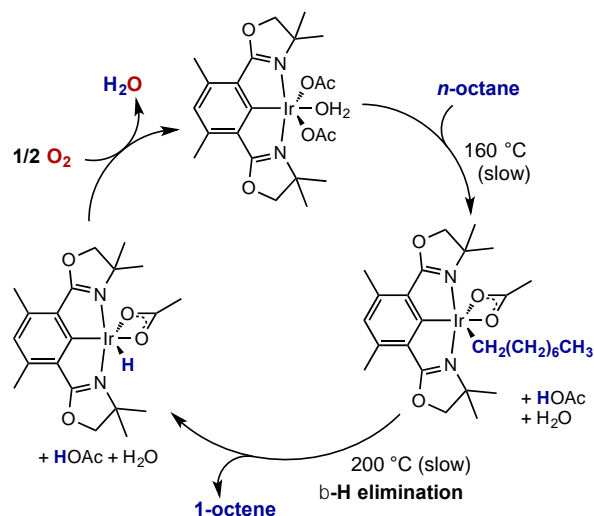


Notably, the reaction shown in eq 1 was not inhibited by the presence of N₂ or water,⁵ in contrast with the well-known catalytic dehydrogenation of *n*-alkanes by R⁴PCP (R⁴PCP = 2,6-(R₂PCH₂)₂C₆H₃) pincer iridium complexes^{1,2} (the rate of eq 1 was even slightly promoted by the presence of water). Nishiyama proposed that alkane activation

by **1** proceeded via a concerted metallation-deprotonation (CMD) mechanism;^{4,6-9} this proposal was later supported by DFT calculations by Cundari and co-workers.¹⁰ We considered that the difference between the alkane reactions of (^{R4}PCP)Ir and (Phebox)Ir, with respect to inhibition by N₂ or water, might be explained in terms of the intermediacy of Ir(I) intermediates in the case of (^{R4}PCP)Ir and the lack thereof in the case of (Phebox)Ir.

Subsequently, the Goldberg lab reported that **2-H** reacts with O₂ in the presence of acetic acid to regenerate **1**.¹¹ In combination with eq 1 this reaction would constitute a catalytic cycle for the dehydrogenation of *n*-octane using O₂ as a hydrogen acceptor, as illustrated in Scheme 1. On a practical level this represents a very attractive alternative to the use of olefinic hydrogen acceptors commonly employed with pincer Ir catalysts. Fundamentally, it further underscores a contrast with (^{R4}PCP)Ir catalysts which are highly sensitive to oxygen.¹² More generally, it highlights the potential advantages of catalytic cycles for Ir-catalyzed dehydrogenation that do not proceed via low-oxidation-state (Ir(I)) species.

Scheme 1. Hypothetical Cycle for Dehydrogenation of *n*-Octane by O₂, Catalyzed by (Phebox)Ir(acetate) Complexes, Based on Individually Observed Stoichiometric Reactions



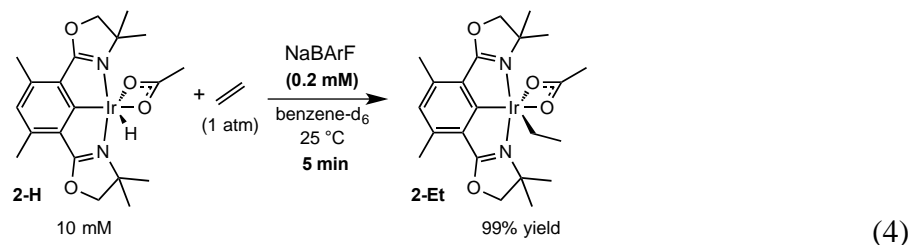
Unfortunately, although the reaction of **2-H** with O₂ proceeded cleanly at room temperature, at the high temperature (200 °C) required for the reaction shown in eq 1 (which comprises two of the steps of the catalytic cycle shown in Scheme 1), decomposition occurred in the presence of O₂. Thus, it was not possible to achieve the catalytic oxidation of alkanes to alkenes by O₂ as indicated in Scheme 1.

A catalytic cycle for alkane dehydrogenation based on only high-oxidation state species offers tantalizing possibilities. The use of O₂ as acceptor, and the tolerance for N₂, H₂O and other possible impurities is indicated above; this proposal is supported by reports by Roddick of pincer-ligated Ru- and Os-based alkane dehydrogenation catalysts that are much less sensitive to N₂, water, and even O₂ than (PCP)Ir catalysts.¹³ In addition, such catalysts might circumvent other issues that plague cycles based on low oxidation state species (including but not limited to Ir(I)), such as catalyst inhibition by the olefin product. Many potential tandem systems can be envisioned that are based on

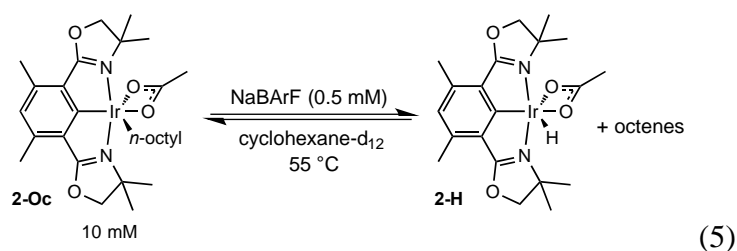
dehydrogenation and a secondary olefin functionalization, but the corresponding reagents (or co-catalysts) would likely not be tolerated by (PCP)Ir or other low oxidation state intermediates. High-oxidation-state catalysts might also be less susceptible to inhibition by functional groups, allowing dehydrogenation of potential substrates more complex than alkanes.

With the above points in mind we have begun to explore routes to promoting the kinetics of dehydrogenation (e.g. eq 1) by (Phebox)Ir species. Here we report that Lewis acids are found to increase by orders of magnitude the rate of the step in Scheme 1 with the highest barrier, β -H elimination by **2-alkyl**. In addition, C-H activation by **2-H** is promoted by Lewis acids. We report that **2-H** catalyzes acceptorless dehydrogenation and that the rate of this reaction is substantially increased by the presence of Na^+ .

Na^+ promoted Ir-H addition to olefins. Under 1 atm ethylene, a benzene- d_6 solution of **2-H** and $\text{NaBAR}^{\text{F}_4}$ (BAR^{F_4} = tetrakis[(3,5-trifluoromethyl)phenyl]borate) undergoes insertion reaction, and within 5 min, **2-H** is converted to **2-Et** as the only product in 99% yield (eq 4). The catalytic role of sodium cation is confirmed by a total inhibition of the reaction if 15-crown-5 (12 mM) ether was added to an identical solution prior to addition of ethylene. $\text{NaBAR}^{\text{F}_4}$ was also found to catalyze insertion of other *n*-alkenes, such as propene, 1-pentene, and 1-octene, into the Ir-H bond of **2-H**. The kinetics of the $\text{NaBAR}^{\text{F}_4}$ -catalyzed insertions of ethylene and propene into the Ir-H bond of **2-H** were found to be zero order in **2-H** in ethylene and propene insertion reactions. This is easily attributed to the catalyst ($\text{NaBAR}^{\text{F}_4}$) being saturated with substrate (**2-H**).



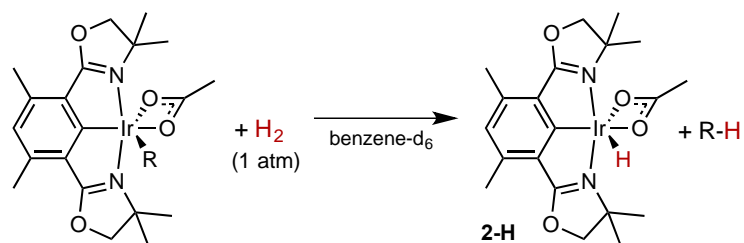
Na⁺ promoted β -hydride elimination. For the dehydrogenation of *n*-octane by (Phebox)Ir(OAc)₂(H₂O) to give **2-H** plus octenes (eq 1), β -hydride elimination of the intermediate **2-Oc** was found to be the rate-determining step,⁵ only proceeding at a significant rate at ca. 200 °C. It is found that in presence of NaBARF^F₄, a cyclohexane-d₁₂ solution of **2-Oc** undergoes β -hydride elimination readily at 55 °C, to give 30% conversion after 30 min (eq 5).



Na⁺ promoted C-H Addition or Elimination. The ability of a Lewis acid to open a coordination site in **2-H** or **2-R** to promote olefin insertion or β -H elimination, respectively, raised the question as to whether Lewis acids could catalyze other reactions that might require a vacant coordination site. C-H bond activation was of particular interest in the context of this class of complexes and this work. To explore this possibility we initially studied the (energetically downhill) microscopic reverse, a C-H bond elimination, specifically the hydrogenolysis of an Ir-C bond (eq 7).



In accord with the above hypothesis, the rate of reaction between **2-alkyl** and H₂ was substantially increased by the presence of NaBARF₄. In the absence of NaBARF₄, **2-Et** did not react to any significant extent under an atmosphere of H₂ at room temperature. At 50 °C, hydrogenolysis to afford **2-H** and ethane occurred, but in only 3% yield after 24 h. In contrast, in the presence of NaBARF₄ (1.2 mM), the reaction proceeded at 25 °C to give 75% yield of **2-H**. Considering the fact that analysis of the NaBARF₄-catalyzed reaction of **2-Et** or **2-Pr** with H₂ is complicated by NaBARF₄ catalyzed β-H elimination reactions, **2-Me** was tested for similar hypothesis reaction. As with **2-Et** and **2-Pr**, no reaction of **2-Me** with H₂ was observed in the absence of NaBARF₄ at 25 °C, whereas in the presence of NaBARF₄ the complex was converted to **2-H** (75% yield) and methane.



R = Et	50 °C, 24 h	3% yield
R = Et	NaBARF ₄ 25 °C, 24 h	75% yield
R = Pr	NaBARF ₄ 25 °C, 12 h	75% yield

(8)

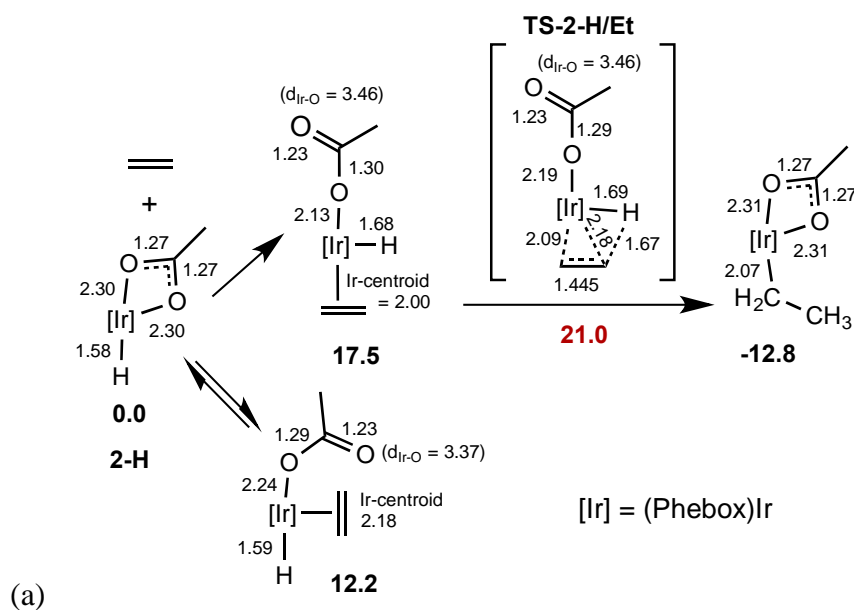
Results and Discussion

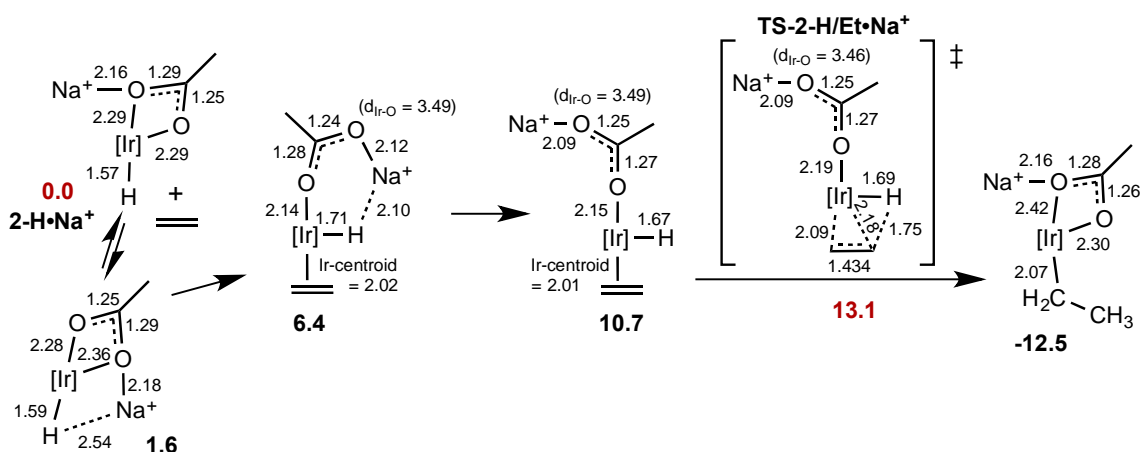
DFT calculation was conducted on olefin insertion/β-hydride elimination reactions on these systems. Since **2-H** is an 18e complex, it may be expected that opening a coordination site would be required to allow the insertion of ethylene into the Ir-H bond or, at the very least, that the availability of a vacant site would facilitate such an insertion.

With that in mind, we considered that the catalytic effect of Lewis acids on the insertion/ β -H elimination reaction might be attributable to dechelation of an acetate ligand via coordination at oxygen. To further explore this possibility, a series of electronic structure (DFT) calculations were carried out on the full metal pincer-ligand systems using the M06-L functional,²⁰ the SDD effective core potential on Ir,²¹ and valence basis sets of triple-zeta plus polarization quality on all other atoms (see Supporting Information for full computational details).²¹⁻²⁵ For the uncatalyzed reaction, Figure 7(a), the addition of an ethylene molecule to **2-H**, trans to the phebox coordinating carbon (along with dechelation of the acetate ligand) is computed to be endergonic by ca. 12.2 kcal/mol as shown. We were unable to locate a proper TS on the potential energy surface for ethylene insertion into the Ir-H bond for this intermediate. When ethylene coordinates cis to the phebox coordinating carbon, the calculations verify that in the ethylene insertion transition state, **TS-2-H/Et**, the acetate ligand is indeed coordinated in a κ^1 fashion (Ir-O distances are 2.19 Å and 3.46 Å; Figure 7(a)). However, the calculations predict that the barrier to ethylene insertion, unassisted by Lewis acid, is only 21.0 kcal/mol (Figure 7), well below that indicated by experiment (ca. 32 kcal/mol; see above). The origin of this discrepancy is not clear but the calculated barrier to the actual insertion step, subsequent to ethylene coordination, is only $\Delta G^\ddagger = 3.5$ kcal/mol, and is probably understated by the calculations.²⁶

Coordination of Na^+ to **2-H** is calculated to lower the barrier to ethylene insertion into the Ir-H bond to 13.1 kcal/mol (Figure 7(b)), a decrease of 7.9 kcal/mol, corresponding to a predicted increase in rate by a factor of ca. 10^5 relative to the uncatalyzed reaction. The Ir-O distances (2.19 Å and 3.47 Å) and the geometry of the Ir-

H-ethene unit in the Na^+ -coordinated TS are essentially the same as in the TS for the Na^+ -free TS; the difference in the overall free energy barrier is chiefly due to the difference in energy of the respective ethylene adduct intermediates relative to the respective κ^2 -acetate precursors **2-H** and **2-H $\cdot\text{Na}^+$** (6.8 kcal/mol). In accord with our hypothesis, the Na^+ cation in the TS is tightly coordinated to the O atom not bound to Ir, with $d_{\text{Na-O}} = 2.085 \text{ \AA}$. These data strongly support the proposition that the origin of the catalytic effect of the Na^+ ion is straightforward, specifically, binding to the acetate terminal oxygen and thereby favoring the κ^1 versus κ^2 binding that is required by the insertion (or β -H elimination) transition state.²⁷





(b)

Figure 7. Free energies (kcal/mol) and selected bond lengths (Å) of intermediates and transition state for ethylene insertion into the Ir-H bond of **2-H**. (a) Unassisted by Lewis acid. (b) Promoted by Na⁺.

Oxidative addition to Cp*Ir(I) fragments,²⁹⁻³¹ are the iconic examples of alkane C-H bond activation, first reported by Bergman in 1982. However, reports³² of alkane C-H activation by Cp*Ir(III) complexes followed very soon thereafter. Since then, although Ir(I) has perhaps maintained its lead status in this area, C-H activation by Ir(III) has become increasingly well established^{33,34}, including within catalytic cycles for hydrogenation and dehydrogenation.³⁵⁻³⁸

DFT calculations suggest that the uncatalyzed hydrogenolysis of **2-Me** proceeds via a CMD-type mechanism. Dechelation of the acetate ligand and addition of H₂ trans to the methyl group gives an intermediate (Phebox)Ir(Me)(κ¹-OAc)(H₂) (**4a**) with a fairly low free energy, 10.2 kcal/mol relative to **2-Me** (Figure 10). Transfer of a proton from the coordinated H₂ to the acetate ligand gives the acetic acid complex (Phebox)Ir(Me)[OC(OH)Me](H) (**5a-syn**), which is also relatively low in free energy

(13.2 kcal/mol); this proton transfer is virtually barrierless ($\Delta G^\ddagger = 0.2$ kcal/mol in the reverse, endoergic direction). Rotation around the Ir-O bond of the acetic acid complex would then give the rotamer of (Phebox)Ir(Me)[OC(OH)Me](H) (**5a-anti**), with a free energy of 22.4 kcal/mol. **5a-anti** can undergo protonolysis of the Ir-Me group (the reverse of a CMD activation mechanism); this CMD-type reaction also has a very low barrier ($\Delta G^\ddagger = 0.6$ kcal/mol). The required rotation around the Ir-O bond to give **5a-anti**, however, is sterically very hindered and we are unable to find an accessible intramolecular pathway for this reaction. Alternatively, the isomerization can be achieved via loss of acetic acid and then re-coordination to provide the anti orientation. The coordination of acetic acid could also lead to coordination isomer **5b** which can undergo Ir-Me protonolysis. Likewise, addition of H₂ trans to the Phebox aryl group of **2-Me**, to give **4b** and then **5c**, followed by loss of acetic acid would also give the same intermediate, (Phebox)Ir(Me)(H) (**6**), plus free acetic acid. From either intermediate (**5a-syn** or **5c**), however, loss of acetic acid carries a significant energetic cost; the free energy of **6** plus free acetic acid is calculated as 29.5 kcal/mol. One might envision more facile pathways for the net rotation reaction, **5a-syn** to **5a-anti**, e.g., intramolecular proton transfer (O2-O1) accompanied by slippage of Ir in the reverse direction, but as of yet we have been unable to locate such a TS by computational means. These results are, at least qualitatively, consistent with the experimental observation of a slow hydrogenolysis of **2-Me** in the absence of NaBAR^F₄, to give a 3% yield in 24 h at 50 °C, which implies a barrier of $\Delta G^\ddagger \sim 29$ kcal/mol.

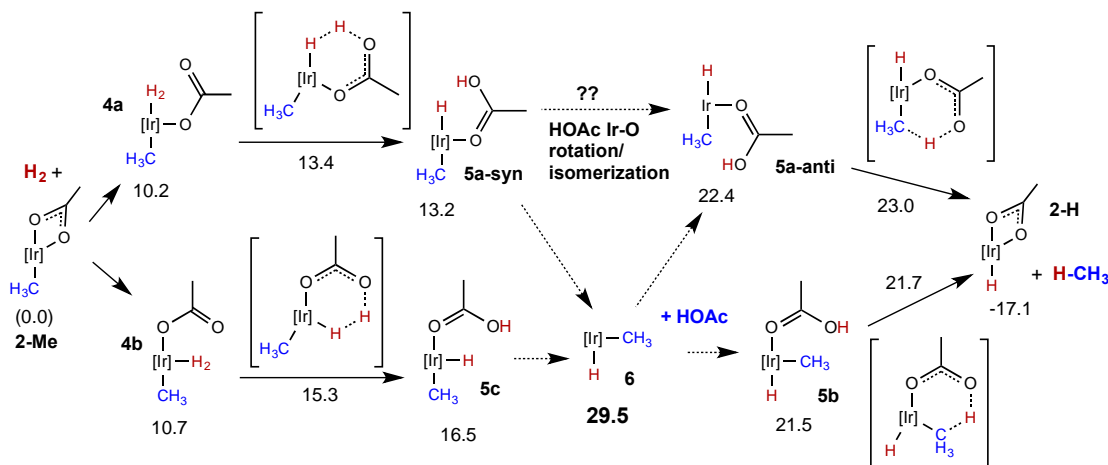


Figure 10. CMD-type pathways for hydrogenolysis of the Ir-C bond of **2-Me** (unassisted by Lewis acid); calculated free energies (kcal/mol) of intermediates and transition states indicated.

Two alternative pathways for the uncatalyzed hydrogenolysis of **2-Me**, which do not involve CMD, have also been calculated. Each pathway involves initial coordination of H_2 to the Ir center, producing intermediates **4b** or **4c** respectively, in which CH_3 is coordinated trans to the Phebox aryl and to the acetate group, respectively (Figure 11). **4c** is much higher in free energy than isomers **4a** or **4b** (32.2 kcal/mol vs. 10.2 and 10.7 kcal/mol, respectively) consistent with a mutually trans arrangement of the strong-trans-influence aryl and methyl groups. **4c** undergoes oxidative cleavage of the coordinated dihydrogen (Figure 11, top path) with virtually no barrier, to give an Ir(V) intermediate, **7** ($d_{\text{HH}} = 1.44 \text{ \AA}$) with free energy 31.3 kcal/mol above reactants (the TS for this reaction is actually lower in free energy than the connected intermediates, although it is a maximum (a first order saddle point) on the electronic potential energy surface). One of the hydride ligands then swings toward the Me group, proceeding through a TS on the potential energy surface with free energy 31.2 kcal/mol above reactants, essentially equal to the free energy of **7**. The TS for hydride insertion reveals $d_{\text{HH}} = 1.57 \text{ \AA}$, and incipient C-H

bond formation as indicated by a short C-H distance ($d_{\text{CH}} = 1.88 \text{ \AA}$) and the Ir-Me bond bending slightly to allow C-H bond formation (Ir-C-H angles = 116.9° , 116.2° , 99.2°). As indicated in Figure 11 (upper path), the energy surface is quite flat between the initial dihydrogen adduct **4c** and the C-H bond formation TS.

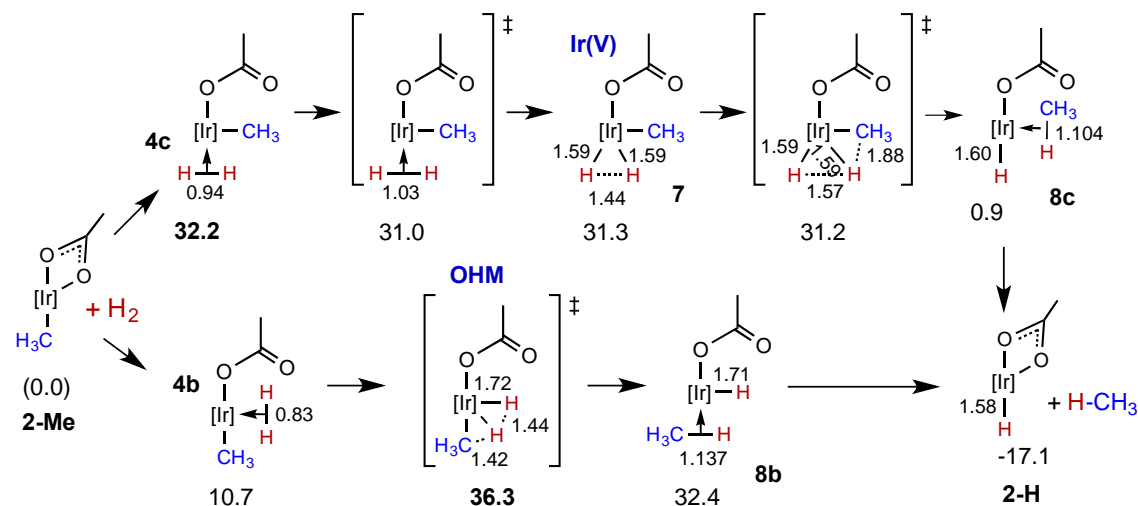


Figure 11. Non-CMD (OHM or Ir(V)) pathways for hydrogenolysis of **2-Me** (unassisted by Lewis acid) via H₂ adducts **4b** or **4c**; calculated free energies (kcal/mol) and selected internuclear distances (Å) indicated.

In the case of the other, closely related, pathway, (Figure 11, lower path), the H₂ coordinates trans to the Phebox aryl group, rather than trans to the acetate ligand, to give the dihydrogen complex **4b**. This pathway then also proceeds through a species that is Ir(V) in character, but it is a TS, with free energy 36.3 kcal/mol above the reactants. No Ir(V) intermediate was located; thus this appears to be an example of an oxidative hydrogen migration (OHM) pathway.³⁴ Both of these non-CMD pathways are calculated to have higher overall barriers ($\Delta G^\ddagger > 32 \text{ kcal/mol}$ and $>36 \text{ kcal/mol}$, respectively) than the CMD pathway of Figure 10 ($\Delta G^\ddagger = 29.5 \text{ kcal/mol}$), even if the CMD pathway must proceed through loss of acetic acid to achieve the net rotation around the Ir-O bond.

We initially considered that a Na⁺-catalyzed pathway might proceed analogously to the uncatalyzed pathway, with Na⁺ simply favoring the ring-opened intermediates and/or TS's; this was essentially the case for the insertion/ β -H elimination reactions discussed above. The situation, however, is apparently not so simple for hydrogenolysis. If we consider the reverse reaction, the CMD activation of methane (**2-H** to **5a-anti** or **5b**), coordination of Na⁺ facilitates the dechelation of acetate, but it *strongly lowers the basicity of the unbound O atom*. As a result, the proton transfer from the incoming methane has a TS that is substantially *higher* in free energy (32.3 kcal/mol relative to **2-Me** plus H₂) than the corresponding TS unbound to Na⁺ (23.0 kcal/mol; Figure 10). Moreover, the step that was apparently rate-limiting in the uncatalyzed case, namely rotation about the Ir-O bond, would still be required subsequent to CMD activation of methane. Thus, rather than introducing a lower barrier to the CMD-type pathway, coordination of Na⁺ at the terminal oxygen to promote dechelation is calculated to leave the highest barrier unchanged, while introducing a new, even *higher*, barrier to the overall reaction.

Thus, dechelation of the acetate ligand, required for the CMD pathways of Figure 10, is favored by Na⁺ coordination but the advantage is more than offset by the resulting decrease in basicity of the resulting κ^1 -acetate terminal oxygen. In the (non-CMD) Ir(V) and OHM pathways (Figure 11) however, no such counteracting effect of Na⁺ coordination is expected. Coordination of Na⁺ to an acetate O atom favors the thermodynamics of dechelation by 5.7 kcal/mol in the case of **4c**, and 8.6 kcal/mol in the case of **4b** (Figure 12). Both species then undergo Ir-Me hydrogenolysis via an oxidative hydrogen migration pathway (the Na⁺-coordinated analogue of the Ir(V) intermediate in

Figure 11 is not a stationary point on the potential energy surface). The calculated barriers are approximately equal, with the pathway proceeding through **4b** calculated to have the slightly lower overall free energy barrier of 24.5 kcal/mol. This is ca. 8 kcal/mol lower than the overall barrier of the more favorable of the unassisted *non*-CMD pathways of Figure 11. It is also more favorable than the (unassisted) CMD-type pathway (Figure 10), which is calculated to be the most favorable pathway in the absence of Na⁺ with a barrier of 29.5 kcal/mol.

The sodium cation presumably facilitates the OHM pathway of Figures 11 and 12 primarily by favoring the κ^1 -acetate configuration. In the case of the lower pathway of Figure 12, however, (proceeding via **4b•Na⁺**) the Na⁺ ion appears to play an additional role by interacting with the incipient hydride of the TS connecting **4b•Na⁺** with **8b•Na⁺**. In all the κ^1 -acetate complexes shown in Figure 2, the Na⁺ is positioned over the Phebox phenyl ring (Na⁺-centroid distances of ca. 2.5 Å are shown in Figure 12), except for **8b•Na⁺** and the TS which leads to it. In **8b•Na⁺** the calculated Na-H (hydride) distance is particularly short at 2.05 Å. Accordingly, an isomer of **8b•Na⁺** in which the Na⁺ cation is located near the Phebox aryl group (Na⁺-centroid distance = 2.50 Å) is 5.9 kcal/mol higher in free energy than **8b•Na⁺**. In the case of the TS connecting **4b•Na⁺** with **8b•Na⁺** H-H bonding is still significant and the H atom does not have full hydride character; nevertheless, the TS shown in Figure 12 is still calculated to be 2.2 kcal/mol lower in free energy than a conformer of this TS in which the Na⁺ is interacting with the aryl ring (Na⁺-centroid distance = 2.53 Å).

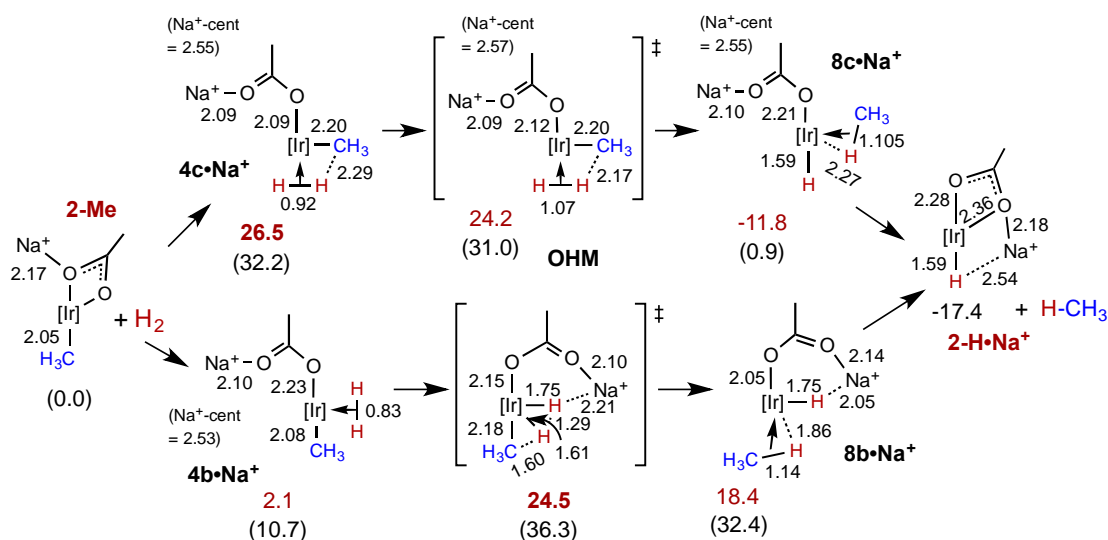


Figure 12. Na⁺-catalyzed hydrogenolysis of **2-Me** proceeding via H₂ adducts **4b•Na⁺** or **4c•Na⁺**; free energies (kcal/mol) and selected internuclear distances (Å) of intermediates and transition states indicated. Energies of analogous species in the unassisted pathway (Figure 11) are shown (in parentheses) for comparison. "Na⁺-cent" is the calculated distance between the Na⁺ cation and the centroid of the Phebox phenyl ring; this is given for all species for which such an interaction is calculated (distance < 3.5 Å).

Thus, while the sodium ion does not promote the more favorable unassisted pathways (CMD, Figure 10), it is calculated to lower the barrier to the OHM pathway (Figure 11) to a level below that of the unassisted CMD pathway. Results of kinetic isotope experiments, in which **2-Me** reacted with either H₂ or D₂ (eq 8), support the proposal that the Na⁺-catalyzed and unassisted reactions proceed via qualitatively different pathways (or at least different rate-determining TSs). For the unassisted reaction, the kinetic isotope effect (KIE) of eq 8 is found to be inverse, $k_{\text{H}_2}/k_{\text{D}_2} = 0.72$, consistent with a rate-determining step in which the H-H (or D-D) bond has been broken and Ir-H(D) and O-H(D) bonds have been formed. The Na⁺-catalyzed reaction, by contrast, reveals a normal albeit very small KIE, $k_{\text{H}_2}/k_{\text{D}_2} = 1.1$. The directions of both of

these KIEs are consistent with the DFT calculations on the respective proposed pathways.³⁹

Conclusions

Transition metal acetate complexes have received great attention in recent years, in part thanks to the ability to activate C-H bonds via a CMD mechanism.⁶⁻⁹ The present system, Nishiyama's Phebox iridium acetate complex, represents an important example of this phenomenon. Here we discussed DFT calculation on two of the most relevant and fundamental organometallic reactions with this complex: olefin insertion and C-H addition (and their respective microscopic reverse reactions) catalyzed by Na⁺. The results of DFT calculations indicate that the Lewis acid catalysts primarily operate via coordination to an acetate oxygen atom which promotes the opening of a vacant coordination site. For C-H addition, the calculations indicate that acetate dechelation by Na⁺ promotes a non-CMD, high-oxidation state pathway. Further investigation is ongoing to determine the scope of the applicability of such Lewis acids in the context of transition metal acetate chemistry, as well as attempts to apply the understanding gained in this work toward the development of new, non-acetate, catalysts.

References

- (1) Kumar, A.; Goldman, A. S. In *Top. Organomet. Chem.*; van Koten, G., Gossage, R. A., Eds.; Springer International Publishing: 2016; Vol. 54, p 307-334.
- (2) Choi, J.; MacArthur, A. H. R.; Brookhart, M.; Goldman, A. S. *Chem. Rev.* **2011**, *111*, 1761-1779.
- (3) Dobereiner, G. E.; Crabtree, R. H. *Chem. Rev.* **2010**, *110*, 681-703.
- (4) Ito, J.-i.; Kaneda, T.; Nishiyama, H. *Organometallics* **2012**, *31*, 4442-4449.
- (5) Allen, K. E.; Heinekey, D. M.; Goldman, A. S.; Goldberg, K. I. *Organometallics* **2013**, *32*, 1579-1582.
- (6) Gorelsky, S. I.; Lapointe, D.; Fagnou, K. *J. Am. Chem. Soc.* **2008**, *130*, 10848-10849.
- (7) Lapointe, D.; Fagnou, K. *Chem. Lett.* **2010**, *39*, 1118-1126.
- (8) Ackermann, L. *Chem. Rev.* **2011**, *111*, 1315-1345.
- (9) Gorelsky, S. I. *Coord. Chem. Rev.* **2013**, *257*, 153-164.
- (10) Pahls, D. R.; Allen, K. E.; Goldberg, K. I.; Cundari, T. R. *Organometallics* **2014**, *33*, 6413-6419.
- (11) Allen, K. E.; Heinekey, D. M.; Goldman, A. S.; Goldberg, K. I. *Organometallics* **2014**, *33*, 1337-1340.
- (12) Williams, D. B.; Kaminsky, W.; Mayer, J. M.; Goldberg, K. I. *Chem. Commun.* **2008**, 4195-4197.
- (13) The stability of Roddick's pincer-ligated Ru and Os alkane dehydrogenation catalysts toward N₂, water, and to some extent even O₂ may be attributable to the electron-poor nature of the pincer ligands which contain perfluoroalkyl groups. It may also be attributable to the oxidation states of the catalytic species, which are probably no lower than M(II), and which is isoelectronic to the Ir(III) discussed in this work. (a) Gruver, B. C.; Adams, J. J.; Warner, S. J.; Arulsamy, N.; Roddick, D. M. *Organometallics* **2011**, *30*, 5133-5140. (b) Gruver, B. C.; Adams, J. J.; Arulsamy, N.; Roddick, D. M. *Organometallics* **2013**, *32*, 6468-6475.
- (14) Choi, J.; Goldman, A. S. *Top. Organomet. Chem.* **2011**, *34*, 139-168.
- (15) A closely related cationic complex, (pybox)Ir(C₂H₄)₂, has been previously reported: D éz, J.; Gamasa, M. P.; Gimeno, J.; Paredes, P. *Organometallics* **2005**, *24*, 1799-1802.
- (16) See Supporting Information for details.
- (17) Kundu, S.; Choliy, Y.; Zhuo, G.; Ahuja, R.; Emge, T. J.; Warmuth, R.; Brookhart, M.; Krogh-Jespersen, K.; Goldman, A. S. *Organometallics* **2009**, *28*, 5432-5444.
- (18) Punji, B.; Emge, T. J.; Goldman, A. S. *Organometallics* **2010**, *29*, 2702-2709.
- (19) We considered that NaBARF was soluble in benzene, even if very slightly, but that due to ion-pairing perhaps the signal was too broad to be observed in the ¹H NMR spectrum. We therefore added NaBARF to benzene, filtered, and then added **2-H** and then ethylene. No reaction was observed, and the spectrum of **2-H** was no different than in benzene that had not been exposed to NaBARF, of the indicating that the solubility was much less than even the 0.2 mM that was in solution in the experiment of eq 4.
- (20) Zhao, Y.; Truhlar, D. G. *J. Chem. Phys.* **2006**, *125*, 194101/1-194101/18.

- (21) Andrae, D.; Haeussermann, U.; Dolg, M.; Stoll, H.; Preuss, H. *Theor. Chim. Acta* **1990**, *77*, 123-41.
- (22) Iron, M. A.; Lucassen, A. C. B.; Cohen, H.; van der Boom, M. E.; Martin, J. M. L. *J. Am. Chem. Soc.* **2004**, *126*, 11699-11710.
- (23) Ditchfield, R.; Hehre, W. J.; Pople, J. A. *J. Chem. Phys.* **1971**, *54*, 724-728.
- (24) Hariharan, P. C.; Pople, J. A. *Mol. Phys.* **1974**, *27*, 209-214.
- (25) Raghavachari, K.; Binkley, J. S.; Seeger, R.; Pople, J. A. *J. Chem. Phys.* **1980**, *72*, 650-654.
- (26) We also investigated the predictions of other functionals, using the same basis set as in the M06-L calculations described in the text. Briefly, the barrier (ΔG^\ddagger , kcal/mol) to ethylene insertion calculated by various popular functionals span an energy range of more than 10 kcal/mol, viz. 21.0 (M06-L); 18.2 (M06); 29.0 (M11-L); 18.8 (M11); 22.7 (PBE); and 29.0 (B3LYP). Inclusion of Grimme's D3 dispersion treatment as a single-point correction (<http://www.thch.uni-bonn.de/tc/>, accessed September 2016. D3 scaling parameters not available for the M11-L and M11 functionals) lowers the barriers (kcal/mol) further to 19.5 (M06-L); 16.1 (M06); 16.5 (PBE); and 21.6 (B3LYP). Thus, DFT calculations generally favor free energy barrier values significantly lower than the experimental result. Bulk solvation effects computed via a continuum dielectric model with benzene as the model solvent tend to increase the computed barrier for ethylene insertion slightly (~1 kcal/mol or less).
- (27) We also considered that the Na⁺ ion might form a complex with a benzene solvent molecule, i.e. the effective Lewis acid was modeled as a Na⁺:benzene complex. This does not significantly influence the reaction energetics, only slightly raising the barrier to ethylene insertion from 13.1 kcal/mol (Figure 7(b)) to 13.8 kcal/mol. Nicholas, J. B.; Hay, B. P.; Dixon, D. A. *J. Phys. Chem. A* **1999**, *103*, 1394-1400.
- (28) Labinger, J. A.; Bercaw, J. E. *Organometallics* **1988**, *7*, 926-8.
- (29) Janowicz, A. H.; Bergman, R. G. *J. Am. Chem. Soc.* **1982**, *104*, 352-354.
- (30) Hoyano, J. K.; Graham, W. A. G. *J. Am. Chem. Soc.* **1982**, *104*, 3723-3725.
- (31) Arndtsen, B. A.; Bergman, R. G.; Mobley, T. A.; Peterson, T. H. *Acc. Chem. Res.* **1995**, *28*, 154-162.
- (32) Burger, P.; Bergman, R. G. *J. Am. Chem. Soc.* **1993**, *115*, 10462-3.
- (33) For some examples of C-H addition to give Ir(V) and closely related reactions see: (a) Klei, S. R.; Tilley, T. D.; Bergman, R. G. *J. Am. Chem. Soc.* **2000**, *122*, 1816-1817. (b) Kawamura, K.; Hartwig, J. F. *J. Am. Chem. Soc.* **2001**, *123*, 8422-8423. (c) Krogh-Jespersen, K.; Czerw, M.; Kanzelberger, M.; Goldman, A. S. *J. Chem. Inf. Comput. Sci.* **2001**, *41*, 56-63. (d) Mohammad, H. A. Y.; Grimm, J. C.; Eichele, K.; Mack, H.-G.; Speiser, B.; Novak, F.; Quintanilla, M. G.; Kaska, W. C.; Mayer, H. A. *Organometallics* **2002**, *21*, 5775-5784. (e) Krogh-Jespersen, K.; Czerw, M.; Summa, N.; Renkema, K. B.; Achord, P. D.; Goldman, A. S. *J. Am. Chem. Soc.* **2002**, *124*, 11404-11416. (f) Webster, C. E.; Hall, M. B. *Coord. Chem. Rev.* **2003**, *238-239*, 315-331. (g) Brandt, P.; Hedberg, C.; Andersson, P. *G. Chem. - Eur. J.* **2003**, *9*, 339-347. (h) Lam, W. H.; Lam, K. C.; Lin, Z.; Shimada, S.; Perutz, R. N.; Marder, T. B. *Dalton Trans.* **2004**, 1556-1562. (i) Bernskoetter, W. H.; Lobkovsky, E.; Chirik, P. J. *Organometallics* **2005**, *24*, 4367-4373. (j) Roseblade, S. J.; Pfaltz, A. *C. R. Chim.* **2007**, *10*, 178-187. (k)

- Hopmann, K. H.; Bayer, A. *Organometallics* **2011**, *30*, 2483-2497. (l) Gruber, S.; Pfaltz, A. *Angew. Chem., Intl. Ed.* **2014**, *53*, 1896-1900. (m) Polo, V.; Al-Saadi, A. A.; Oro, L. A. *Organometallics* **2014**, *33*, 5156-5163. (n) Shin, K.; Park, S.-W.; Chang, S. *J. Am. Chem. Soc.* **2015**, *137*, 8584-8592.
- (34) (a) Oxgaard, J.; Muller, R. P.; Goddard, W. A.; Periana, R. A. *J. Am. Chem. Soc.* **2004**, *126*, 352-363. (b) Oxgaard, J.; Periana, R. A.; Goddard, W. A., III *J. Am. Chem. Soc.* **2004**, *126*, 11658-11665.
- (35) (a) Fan, Y.; Cui, X.; Burgess, K.; Hall, M. B. *J. Am. Chem. Soc.* **2004**, *126*, 16688-16689. (b) Cui, X.; Fan, Y.; Hall, M. B.; Burgess, K. *Chem.-Eur. J.* **2005**, *11*, 6859-6868.
- (36) Cheng, C.; Kim, B. G.; Guironnet, D.; Brookhart, M.; Guan, C.; Wang, D. Y.; Krogh-Jespersen, K.; Goldman, A. S. *J. Am. Chem. Soc.* **2014**, *136*, 6672-6683.
- (37) Mazuela, J.; Norrby, P.-O.; Andersson, P. G.; Pàmies, O.; Diéguez, M. *J. Am. Chem. Soc.* **2011**, *133*, 13634-13645.
- (38) Rimoldi, M.; Fodor, D.; van Bokhoven, J. A.; Mezzetti, A. *Chem. Commun.* **2013**, *49*, 11314-11316.
- (39) The factors determining the values of isotope effects for H₂ addition to transition metal complexes are complex, and a full analysis of the predicted isotope effects for these reactions is beyond the scope of this paper, particularly considering that the calculations do not yield unambiguous predictions for the rate-determining transition state within each set of pathways. For in-depth discussion of isotope effects for H₂ addition to transition metal complexes, see: (a) Parkin, G. *Acc. Chem. Res.* **2009**, *42*, 315-325. (a) Janak, K. E.; Parkin, G. *J. Am. Chem. Soc.* **2003**, *125*, 13219-13224. (c) Abu-Hasanayn, F.; Goldman, A. S.; Krogh-Jespersen, K. *J. Phys. Chem.* **1993**, *97*, 5890-5896. (d) Abu-Hasanayn, F.; Krogh-Jespersen, K.; Goldman, A. S. *J. Am. Chem. Soc.* **1993**, *115*, 8019-8023.

Computational Details

All electronic structure calculations employed the DFT method¹ and the M06-L² functional. The electronic environment was modeled using the following scheme: for Ir, we applied the SDD relativistic effective (small) core potential and the associated (6s5p3d) valence basis set,³ augmented with an f-type function and a complete set of diffuse spdf functions;⁴ all-electron 6-311G(d,p) basis sets were applied to all other atoms.⁵ Reactant, transition state and product geometries were fully optimized and characterized by normal mode analysis. Expanded integration grid sizes (pruned (99,590) atomic grids invoked using the integral=ultrafine keyword) were applied to increase numerical accuracy and stability in both geometry optimizations and normal mode analysis.⁶ The (unscaled) vibrational frequencies formed the basis for the calculation of vibrational zero-point energy (ZPE) corrections; standard thermodynamic corrections (based on the harmonic oscillator/rigid rotor approximations and ideal gas behavior) were made to convert from purely electronic energies (E) to (standard) enthalpies (H°) and Gibbs free energies (G°; P = 1 atm, T = 298 K).⁷ All calculations were executed using the GAUSSIAN 09 series of computer programs.⁸

Tables of Energetic Quantities

Table S1. Relative potential energies (ΔE), enthalpies (ΔH), entropies (ΔS), and free energies (ΔG) for the proposed ethylene insertion of (Phebox)Ir under 1 atm ethylene, Scheme 6 in Manuscript. Units are kcal/mol for ΔE , ΔH , and ΔG ; units are cal/(deg•mol) for ΔS . The standard state for concentrations is 1 atm for each species participating in the reaction; T = 298 K. The sequence of species in the Table is arranged to match Scheme 6 as closely as possible.

Species	ΔE	ΔH	ΔG	ΔS
2-H	0.0	0.0	0.0	0.0
Ir(C₂H₄)H(AcO)	3.2	4.2	17.5	-44.5
IrH(C₂H₄)(AcO)	-3.1	-2.2	12.2	-48.3
TS-2-H/Et	7.9	8.0	21.0	-43.8
2-Et	-26.8	-23.5	-12.8	-36.0

Species	ΔE	ΔH	ΔG	ΔS
2-H•Na	0.0	0.0	0.0	0.0
2-H•Na	1.5	2.0	1.7	1.1
Ir(C₂H₄)H(AcO)•Na	-9.0	-7.2	5.0	-40.9
Ir(C₂H₄)H(AcO)•Na	-4.6	-2.5	10.7	-44.2
TS-2-H/Et•Na	-2.7	-2.3	13.1	-51.7
2-Et•Na	-28.2	-24.3	-12.5	-39.8

Table S2. Relative potential energies (ΔE), enthalpies (ΔH), entropies (ΔS), and free energies (ΔG) for the proposed hydrogenolysis of (Phebox)IrMe via CMD mechanism under 1 atm H_2 , Scheme 7 in Manuscript. Units are kcal/mol for ΔE , ΔH , and ΔG ; units are cal/(deg•mol) for ΔS . The standard state for concentrations is 1 atm for each species participating in the reaction; T = 298 K. The sequence of species in the Table is arranged to match Scheme 7 as closely as possible.

Species	ΔE	ΔH	ΔG	ΔS
2-Me	0.0	0.0	0.0	0.0
4a	-0.4	1.4	10.2	-29.6
TS-4a/5a-syn	4.6	5.2	13.4	-27.6
5a-syn	3.3	6.3	13.2	-23.4
4b	1.3	3.8	10.7	-23.1
TS-4b/5c	6.6	7.4	15.3	-26.6
5c	6.1	9.1	16.5	-24.9
6	31.8	34.4	29.5	16.6
5a-anti	11.6	15.5	22.4	-23.1
TS-5a-anti/2-H	14.4	15.2	23.0	-26.2
5b	12.0	16.0	21.5	-18.2
TS-5b/2-H	14.5	15.8	21.7	-20.1
2-H	-18.7	-15.3	-17.1	6.1

Table S3. Relative potential energies (ΔE), enthalpies (ΔH), entropies (ΔS), and free energies (ΔG) for the proposed hydrogenolysis of (Phebox)IrMe via H₂ adducts under 1 atm H₂, Scheme 8 in Manuscript. Units are kcal/mol for ΔE , ΔH , and ΔG ; units are cal/(deg•mol) for ΔS . The standard state for concentrations is 1 atm for each species participating in the reaction; T = 298 K. The sequence of species in the Table is arranged to match Scheme 8 as closely as possible.

Species	ΔE	ΔH	ΔG	ΔS
2-Me	0.0	0.0	0.0	0.0
4c	22.3	24.6	32.2	-25.4
TS-4c/Ir(V)	22.5	23.0	31.0	-26.7
Ir(V)	21.5	23.3	31.3	-26.8
TS-Ir(V)/Ir(H)(CH₄)(AcO)	21.7	22.9	31.2	-27.9
Ir(H)(CH₄)(AcO)	-9.3	-4.9	0.9	-19.6
2-H	-18.7	-15.3	-17.1	6.1
4b	1.3	3.8	10.7	-23.1
OHM	28.2	28.7	36.3	-25.4
Ir(CH₄)(H)(AcO)	22.6	25.9	32.4	-22.0

Table S4. Relative potential energies (ΔE), enthalpies (ΔH), entropies (ΔS), and free energies (ΔG) for the proposed hydrogenolysis of (Phebox)IrMe assisted by Na^+ under one atm H_2 , Scheme 9 in Manuscript. Units are kcal/mol for ΔE , ΔH , and ΔG ; units are cal/(deg•mol) for ΔS . The standard state for concentrations is 1 atm for each species participating in the reaction; $T = 298 \text{ K}$. The sequence of species in the Table is arranged to match Scheme 9 as closely as possible.

Species	ΔE	ΔH	ΔG	ΔS
2-Me Na^+	0.0	0.0	0.0	0.0
4c Na^+	15.2	18.0	26.5	-28.6
TS- 4c/Ir(H)(CH4)(AcO) Na^+	15.7	16.5	24.2	-25.9
Ir(H)(CH4)(AcO) Na^+	-22.2	-17.4	-11.8	-19.1
2-H Na^+	-18.6	-15.8	-17.4	5.1
4b Na^+	-8.8	-5.8	2.1	-26.4
OHM Na^+	17.3	17.9	24.5	-22.5
Ir(CH4)(H)(AcO) Na^+	14.3	17.6	24.3	-22.2

Computational Section References

- (1) Koch, W.; Holthausen, M. C. *A Chemist's Guide to Density Functional Theory*; Wiley: New York, 2001.
- (2) Zhao, Y.; Truhlar, D. G. *J. Chem. Phys.* **2006**, *125*:194101.
- (3) Andrae, D.; Haeussermann, U.; Dolg, M.; Stoll, H.; Preuss, H. *Theor. Chim. Acta* **1990**, *77*, 123-141..
- (4) Iron, M. A.; Lucassen, A. C. B.; Cohen, H.; van der Boom, M. E.; Martin, J. M. L. *J. Am. Chem. Soc.* **2004**, *126*, 11699-11710.
- (5) (a) Ditchfield, R.; Hehre, W. J.; Pople, J. A. *J. Chem. Phys.* **1971**, *54*, 724-728. (b) Hariharan, P. C.; Pople, J. A. *Molecular Physics* **1974**, *27*, 209-214. (c) Raghavachari, K.; Binkley, J. S.; Seeger, R.; Pople, J. A. *J. Chem. Phys.* **1980**, *72*, 650-654. (d) McLean, A. D.; Chandler, G. S. *J. Chem. Phys.* **1980**, *72*, 5639-5648.
- (6) Frisch, Æ.; Frisch, M. J.; Clemente, F. R.; G. W. Trucks *Gaussian 09 User's Reference*, 147.
- (7) McQuarrie, D. A. *Statistical Thermodynamics*; Harper and Row: New York, 1973.
- (8) Gaussian 09, Revision D.01, Frisch, M. J.; Trucks, G. W.; Schlegel, H. B.; Scuseria, G. E.; Robb, M. A.; Cheeseman, J. R.; Scalmani, G.; Barone, V.; Mennucci, B.; Petersson, G. A.; Nakatsuji, H.; Caricato, M.; Li, X.; Hratchian, H. P.; Izmaylov, A. F.; Bloino, J.; Zheng, G.; Sonnenberg, J. L.; Hada, M.; Ehara, M.; Toyota, K.; Fukuda, R.; Hasegawa, J.; Ishida, M.; Nakajima, T.; Honda, Y.; Kitao, O.; Nakai, H.; Vreven, T.; Montgomery, J. A., Jr.; Peralta, J. E.; Ogliaro, F.; Bearpark, M.; Heyd, J. J.; Brothers, E.; Kudin, K. N.; Staroverov, V. N.; Kobayashi, R.; Normand, J.; Raghavachari, K.; Rendell, A.; Burant, J. C.; Iyengar, S. S.; Tomasi, J.; Cossi, M.; Rega, N.; Millam, J. M.; Klene, M.; Knox, J. E.; Cross, J. B.; Bakken, V.; Adamo, C.; Jaramillo, J.; Gomperts, R.; Stratmann, R. E.; Yazyev, O.; Austin, A. J.; Cammi, R.; Pomelli, C.; Ochterski, J. W.; Martin, R. L.; Morokuma, K.; Zakrzewski, V. G.; Voth, G. A.; Salvador, P.; Dannenberg, J. J.; Dapprich, S.; Daniels, A. D.; Farkas, Ö.; Foresman, J. B.; Ortiz, J. V.; Cioslowski, J.; Fox, D. J. Gaussian, Inc., Wallingford CT, 2009.

Chapter 6
Computational Study of Biphenylene C-C Bond
Addition to Pincer-Iridium Complexes

Majority of this chapter is reproduced with permission from

**Addition of C–C and C–H bonds by pincer-iridium complexes:
a combined experimental and computational study**

David A. Laviska, Changjian Guan, Thomas J. Emge,
Miles Wilklow-Marnell, William W. Brennessel, William D. Jones,
Karsten Krogh-Jespersen and Alan S. Goldman

Dalton Trans., 2014, **43**, 16354–16365

© The Royal Society of Chemistry 2014

Introduction

The cleavage of hydrocarbon C-C bonds by oxidative addition has been a reaction of great interest to inorganic/organometallic chemists for many years.¹⁻²⁷ The microscopic reverse, reductive elimination of C-C bonds, is a key step in palladium-catalyzed cross-coupling reactions, which clearly represent one of the most important developments in modern synthetic chemistry.

Several years ago, we reported a study of C-C bond elimination from complexes $(^{\text{tBu}}\text{PCP})\text{IrR}^1\text{R}^2$ ($^{\text{R}}\text{PCP} = \kappa^3\text{-1,3-C}_6\text{H}_3(\text{CH}_2\text{PR}_2)_2$).²⁸ These eliminations were generally quite slow. Especially notable was the contrast with the rapid kinetics of elimination from $\text{L}_2\text{PdRR}'$, particularly in the case where at least one of the R or R' groups is sp^2 -carbon bound. We demonstrated that this difference is not due to intrinsic electronic properties of $(^{\text{R}}\text{PCP})\text{Ir}$ or three-coordinate d^8 fragments more generally but, surprisingly, that it was due to steric effects. Reduction with an sp^2 -carbon bound hydrocarbyl group (e.g., phenyl) was found to be very facile if that fragment was allowed to rotate so that it would face its coupling partner (e.g., methyl). In other words, the incipient carbon-carbon bond was formed approximately perpendicular to the plane of the sp^2 -C-bound hydrocarbyl, even though, in both the reactant complex and the fully formed product (toluene in this case) the coupling partner is in the plane of the sp^2 -bound group. However, the bulky t-Bu groups of the $^{\text{tBu}}\text{PCP}$ ligand strongly disfavor such a rotation for steric reasons; this factor was found to be ultimately responsible for the high barrier to C-C coupling. We also showed that rotation of the sp^2 -C-bound group was required only to avoid steric interactions between the H atoms of the two coupling groups, and between the H atoms

of the sp^2 -C-bound group and the iridium center; there was no evidence for any electronic effects such as interaction with C-C π -orbitals (see Figure 1).

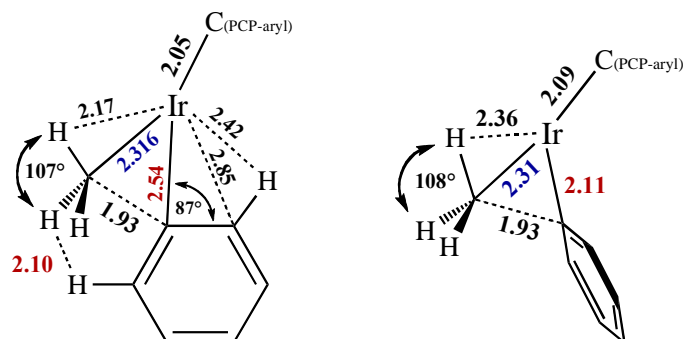
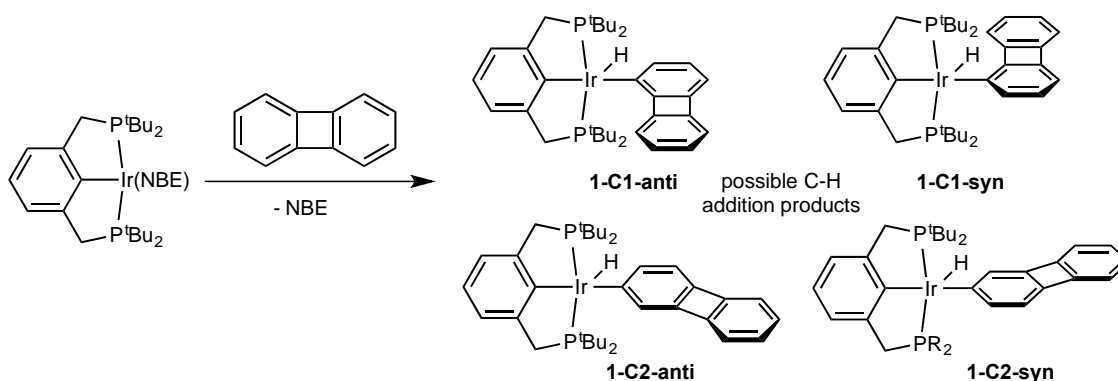


Figure 1. Schematic diagrams of Ir-C-C planes in a planar-constrained, approximate calculated TS for Ph-Me elimination from $(^{t\text{Bu}}\text{PCP})\text{Ir}(\text{Ph})(\text{Me})$ and the actual calculated TS in which the phenyl ring is allowed to rotate out of the Ir-C-C plane (in spite of severe steric crowding due to the phosphino-*t*-butyl groups) with bond distances shown (Å).

Here we report examples of the reverse reaction, addition of a C-C bond of biphenylene, to complexes $(^{\text{R}}\text{PCP})\text{Ir}$, and a computational study based on this reaction. The same factors appear relevant as in the case of the C-C eliminations, but the geometric constraints of biphenylene introduce additional consideration. Most importantly, the highly strained biphenylene C-C bond greatly favors the thermodynamics of addition and this is strongly reflected in the kinetics as well. We also report on the C-H activation chemistry of biphenylene.

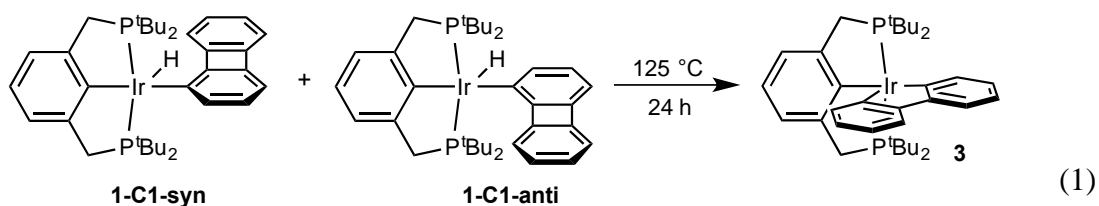
The reaction between $(^{t\text{Bu}}\text{PCP})\text{IrH}_2$ with norbornene (NBE) is known to generate $(^{t\text{Bu}}\text{PCP})\text{Ir}(\text{NBE})$ which is a precursor of the reactive fragment “ $(^{t\text{Bu}}\text{PCP})\text{Ir}$ ”, which easily adds C-H bond of biphenylene. Biphenylene has two inequivalent C-H bonds. Rotation

around the Ir-C bond is presumably slow and thus addition could afford two rotamers of each isomer (Scheme 1). As a matter of fact, only two rotamers whose Ir-C bond is formed with the alpha C atom from biphenylene are observed, i.e., **1-C1-syn** and **1-C1-anti**.



Scheme 1

Heating a solution of **1** at 125 °C for 24 h resulted in complete conversion to a product (**3**) (eq 1). Complex **3** has been independently generated by the reaction of (^tBuPCP)Ir(NBE) with biphenyl (eq 2) and was crystallographically characterized (cf. Figure 2);^{31,32} in reaction 1, complex **3** may be viewed as the product of C-H elimination and C-C addition. Similar to (^tBuPCP)Ir, the less crowded pincer complex (ⁱPrPCP)Ir was found to undergo biphenylene C-C addition much more rapidly than (^tBuPCP)Ir.



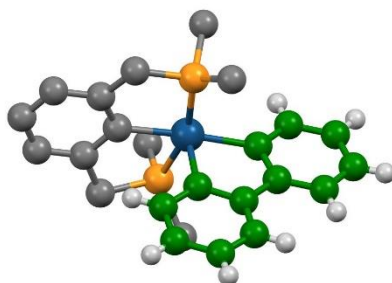
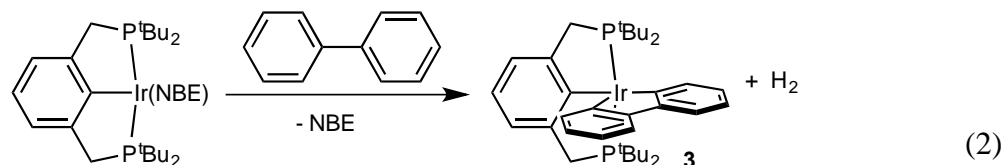


Figure 2. Crystallographically determined molecular structure of **3** (t-butyl methyl groups and all non-biphenyl H's omitted for clarity)^{31,32}

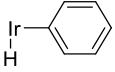
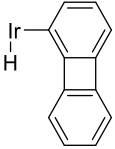
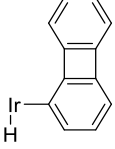
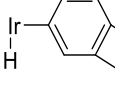
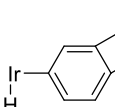
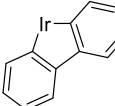
The chemistry of addition of strained C-C bonds, including that of biphenylene,^{3,5,7-9,12-16,24-27} has been the subject of great interest. In view of our aforementioned interest in C-C bond addition/elimination with pincer-iridium fragments we have conducted a computational study of this reaction.

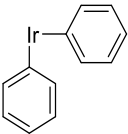
Results and Discussion

C-H bond addition. Our computational study began with calculations of the C-H addition products, **1**. The broadening of the (^tBuPCP)Ir(aryl)H hydride signals in the ¹H NMR spectrum indicates that aryl C-H elimination is kinetically very facile (the addition must be even faster than the elimination, since the elimination/addition equilibrium lies far to the addition side). Calculations indicate that the energies of the TS's for addition to give all four species are lower in energy than the free species, and ca. 6-13 kcal/mol above the corresponding C-H σ -complex energy minima. The distribution of observed

products is thus determined by their relative thermodynamics. As shown in Table 1, of the four possible C-H addition products, **1-C2-anti** has the highest enthalpy (-11.7 kcal/mol relative to free (^tBuPCP)Ir and biphenylene). This is similar to the enthalpy of benzene C-H addition (-11.2 kcal/mol) while **1-C2-syn**, **1-C1-anti** and **1-C1-syn** are 0.2 kcal/mol, 3.7 kcal/mol and 5.1 kcal/mol lower, respectively. These values are consistent with the observation of only **1-C1-anti** and **1-C1-syn** in solution, as indicated by the X-ray crystal structures of the corresponding CO adducts.

Table 1. Energy (E), enthalpy (H) and Gibbs Free Energy (relative to free arene and free (^tBuPCP)Ir) of products of biphenylene C-H and C-C addition to (^tBuPCP)Ir, and corresponding transition states and σ -C-H or σ -C-C intermediates.

Species	E			H			G		
	σ -complex	TS	product	σ -complex	TS	product	σ -complex	TS	product
Ir = (^t BuPCP)Ir									
	-8.5	3.6	-10.6	-9.1	3.0	-11.2	1.8	16.4	2.6
 1-C1-syn	-9.8	-3.3	-16.2	-10.4	-3.9	-16.8	2.3	10.9	-2.8
 1-C1-anti	-13.9	-2.6	-14.8	-14.5	-3.2	-15.4	-1.4	11.0	-1.7
 1-C2-syn	-12.9	0.5	-11.3	-13.5	-0.1	-11.9	-0.9	14.8	2.0
 1-C2-anti	-13.1	0.1	-11.1	-13.7	-0.5	-11.7	-0.9	14.1	2.4
	-13.8	4.7	-57.2	-14.4	4.1	-57.8	-0.3	20.5	-41.9

					31. 7	4.2			
---	--	--	--	--	----------	-----	--	--	--

We considered that the markedly more favorable addition at C1 could be attributable to Ir-C pi-pi interactions (donation or withdrawal) particularly in view of the unusual 12-electron π -system of biphenylene. We therefore compared the relative energetics of formation of the iridium-carbon bonds, with formation of the corresponding lithium carbon bonds. Lithiation at C1 is calculated to be 3.2 kcal/mol more favorable than at C2, and 4.3 kcal/mol more favorable than at benzene, in good agreement with closely related calculations by Streitwieser.³⁴ These values are essentially equal to the differences calculated for C-H addition to give **1-C1-anti** vs. **1-C2-syn** and vs. benzene (3.5 kcal/mol and 4.2 kcal/mol more exothermic, respectively). Although **1-C1-syn** is slightly lower in enthalpy than **1-C1-anti**, it seems unlikely that this difference is due to pi-effects but is instead likely due to more favorable van der Waals interactions. Accordingly, for the (^{Me}PCP)Ir analogues, the C1-bound adducts are on average ca. 4 kcal/mol more stable than C2-bound and 4.7 kcal/mol more stable than the benzene C-H addition product, values very similar to those for (^{tBu}PCP)Ir; however, the anti-rotamer, **1-PMe2-C1-anti**, is *more* stable than **1-PMe2-C1-syn**. Thus, we tentatively attribute the high stability of the C1-H iridium addition products to the same factor or factors responsible for the greater stability of the C1-lithiated biphenylene, which presumably reflect greater electronegativity or acidity at the C1 position.

C-C bond addition. The calculated structure of the C-C addition product **3** (Figure 3) is in good agreement with the structure determined crystallographically.^{32,33} The

biphenyl unit is perpendicular to the approximate plane of the (^tBuPCP)Ir fragment and the P-Ir-P axis; we will refer to this plane as equatorial. The coordination geometry is nearly ideally square pyramidal (cf. Figure 3).

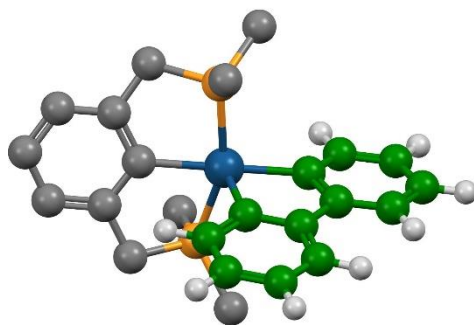


Figure 3. Calculated molecular structure of **3** (t-butyl methyl groups and all non-biphenyl H's omitted for clarity)

Reflecting the very substantial ring strain in biphenylene, the C-C addition reaction is calculated to be extremely exothermic: $\Delta H^\circ = -57.8$ kcal/mol relative to free (^tBuPCP)Ir and biphenylene (each at P = 1 atm). Perhaps more meaningfully, $\Delta H^\circ = -51.0$ kcal/mol for conversion from the lowest energy C-H addition product, **1-C1-syn**. The TS for C-C addition is 6-10 kcal/mol higher in free energy than for the TS's for C-H addition, consistent with the observation that only the C-H addition products (**1**) are initially observed.

It might be anticipated that the biphenylene molecule would remain in the equatorial plane throughout the C-C addition reaction coordinate. The presence of the bulky t-butyl groups, in particular, would favor a path in which the biphenylene would slip into the cleft in this plane defined by the t-butyl groups. However, in the TS

calculated for C-C addition, the biphenylene unit is severely tilted from this plane; the core cyclobutadiene plane and the Ir-C-C bond cleavage plane intersect at an angle of 50.0° (Figures 4 and 5). This results in significantly close contacts between the biphenylene and the ^tBuPCP ligand including H-H distances of 1.85 Å and 1.74 Å, and H(t-Bu)-C(biphenylene) distances of 2.45 Å and 2.48 Å. (For reference, the van der Waals radii of hydrogen and carbon are 1.10 Å and 1.70 Å, respectively; the calculated distances are therefore as much as 0.46 Å and 0.35 Å below the sum of the respective van der Waals radii.)

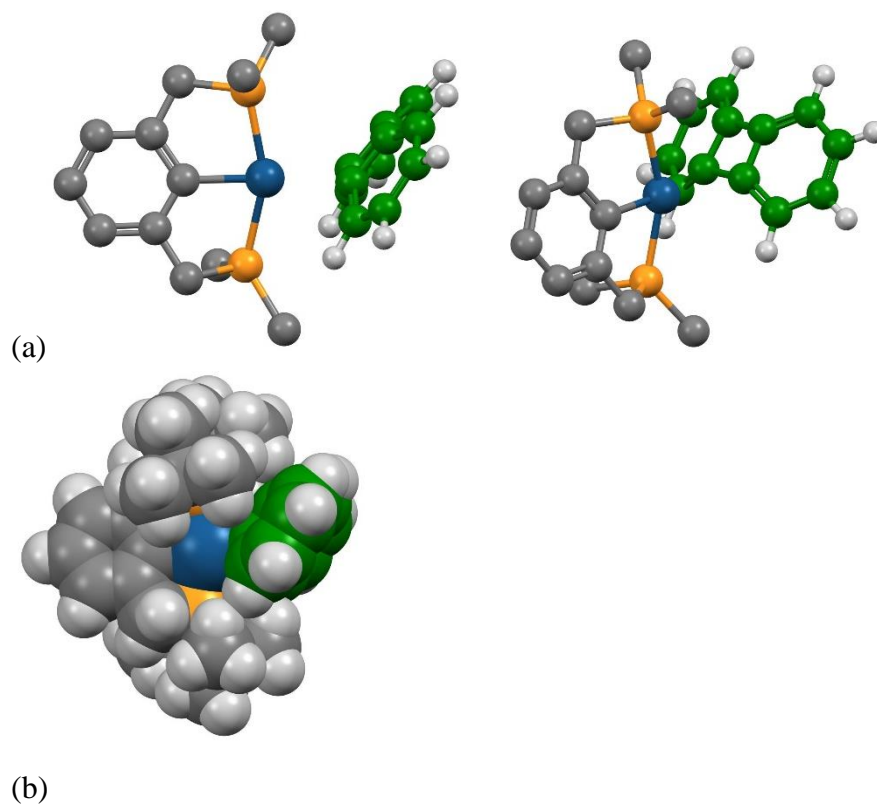


Figure 4. Calculated TS for biphenylene C-C addition to (^tBuPCP)Ir to yield **3**. (a) Two perspectives, ball-and-stick model (t-butyl methyl groups and all non-biphenyl H's omitted for clarity) (b) Space-filling model, 85% van der Waals radii (no atoms omitted)

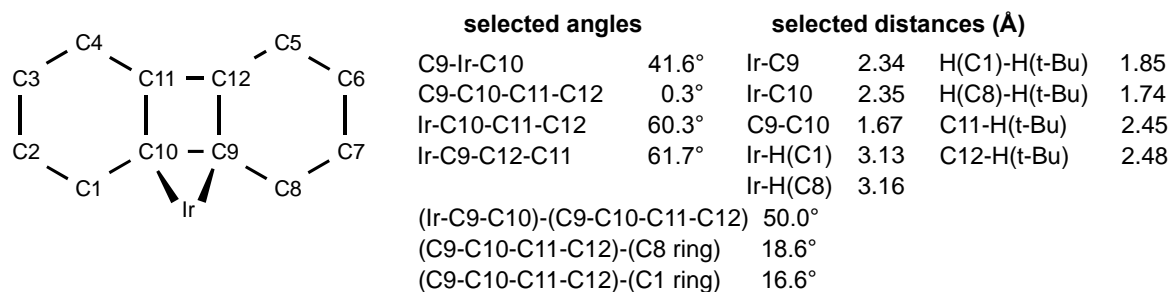


Figure 5. Selected angles (simple, torsional, and intersecting mean planes) and selected distances for **TS-3-PtBu2**, the calculated TS for C-C addition to yield **3**.

Although **3**, the product of the C-C addition reaction, is not particularly crowded, the calculated TS (**TS-3-PtBu2**) would appear to be much more disfavored than **3** by the bulky t-butyl groups. We computationally investigated the reactions of biphenylene with the much less sterically demanding (^{Me}PCP)Ir fragment. Geometrically, the TS for C-C addition to (^{Me}PCP)Ir (**TS-3-PMe2**) is remarkably similar to **TS-3-PtBu2**; the Ir-C9-C10 units have nearly identical metric parameters and the 6-membered rings of the biphenylene unit are bent back from co-planarity with the cyclobutadiene ring approximately 17 ° in both complexes (Figures 6 and 7). The only significant geometric difference between **TS-3-PMe2** and **TS-3-PtBu2** is that the tilt is somewhat greater in the former (60.1 ° vs. 50.0 °). In spite of the greater tilt, however, there are no close contacts between the biphenylene unit and the much less sterically demanding ^{Me}PCP ligand. Additional calculations on biphenylene C-C addition to (^HPCP)Ir reveal a tilt (60.0 °) equal to that found for (^{Me}PCP)Ir; this indicates that ca. 60 ° is the electronically optimal tilt angle and thus supports the conclusion that there are no significant steric interactions between the ^{Me}PCP ligand and the biphenylene unit in **TS-3-PMe2**.

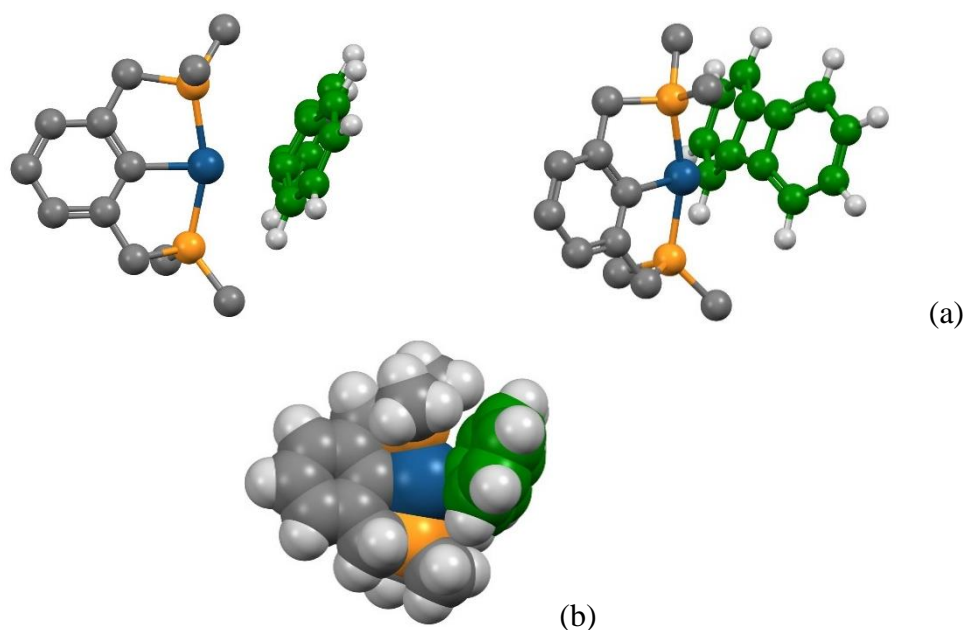


Figure 6. Calculated TS (**TS-3-PMe2**) for biphenylene C-C addition to (^{Me}PCP)Ir to yield **3-PMe2**. (a) Two perspectives, ball-and-stick model (all non-biphenyl H's omitted for clarity) (b) Space-filling model, 85% van der Waals radii (no atoms omitted).

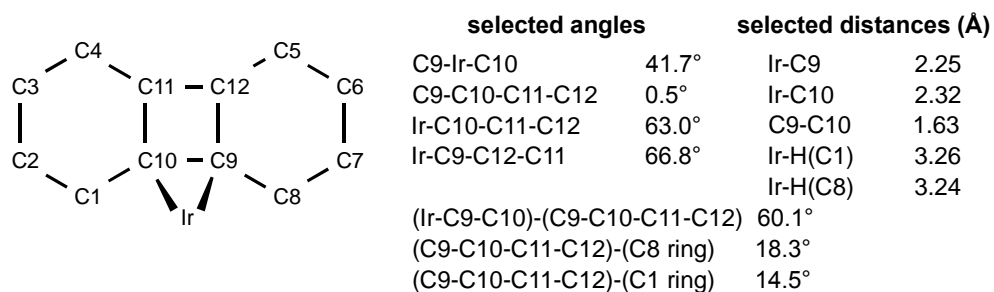
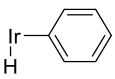
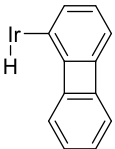
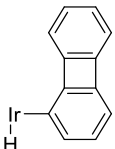
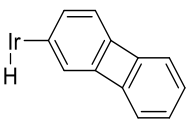
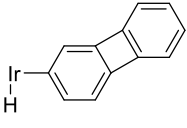
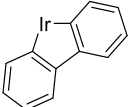
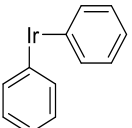


Figure 7. Selected angles (simple, torsional, and intersecting mean planes) and selected distances for **TS-3-PMe2**, the calculated TS for C-C addition to yield **3-PMe2**.

The thermodynamics of addition to (^{Me}PCP)Ir are very similar to those for addition to (^{tBu}PCP)Ir: $\Delta H = -59.4$ kcal/mol and -57.8 kcal/mol, respectively (Table 2), indicating that there is no significant crowding in the ^{tBu}PCP complex, **3**. The difference in the C-C cleavage *transition state* enthalpies, however, is quite substantial: -10.3 kcal/mol vs. 4.1 kcal/mol (relative to free biphenylene and the respective free pincer-iridium fragment). Most remarkably, *the enthalpy of the TS calculated for C-C addition to (^{Me}PCP)Ir is even lower than that for C-H addition.*

Table 2. Energy (E), enthalpy (H) and Gibbs Free Energy (relative to free arene and free (^{Me}PCP)Ir) of products of biphenylene C-H and C-C addition to (^{Me}PCP)Ir, and corresponding transition states.

Species	E		H		G	
	TS	product	TS	product	TS	product
	-5.8	-8.6	-6.4	-9.2	6.1	3.0
 1-C1-syn	-9.1	-12.8	-9.7	-13.4	3.4	-1.4
 1-C1-anti	-5.6	-13.7	-6.2	-14.3	6.8	-2.8
 1-C2-syn	-6.5	-9.7	-7.1	-10.3	5.6	1.8
 1-C2-anti	-6.7	-9.5	-7.3	-10.1	5.1	2.1
	-9.7	-58.8	-10.3	-59.4	3.4	-46.2
	9.4	-3.1	8.8	-3.7	24.0	8.6

These results predict that C-C addition, absent substantial steric crowding, is a kinetically very facile process. In the case of (^{Me}PCP)Ir and biphenylene, it seems highly probable that the reaction to give the C-C addition product would be much faster than generation of the reactive fragment (e.g. loss of olefin from a precursor (^{Me}PCP)Ir(olefin) complex). These conclusions are strongly supported by the C-C bond cleavage of biphenylene by (^{iPr}PCP)Ir being far more facile than the reaction of (^{tBu}PCP)Ir. (We did not conduct calculations on the (^{iPr}PCP)Ir analogues as such calculations are greatly complicated by the many conformational possibilities presented by four *i*-Pr groups.³⁵ Instead, we believe that calculations on (^{Me}PCP)Ir and (^{tBu}PCP)Ir more reliably capture the effect of varying steric demands of the PCP ligand.) The barrier to C-C addition to (^{tBu}PCP)Ir is thus predominantly due to steric crowding, which results from the pronounced “tilting” of the biphenylene in the TS.

The above conclusion obviously raises the question of why the tilting of the biphenylene is so energetically important. There are no apparent orbital- or electronics-based factors that would appear to require this tilting. Thus, given that the biphenyl unit in the addition product is not tilted (all torsional angles within the five-membered iridacyclic ring are less than 5 °, and none of the atoms are more than 0.03 Å out of the least-squares calculated plane), an in-plane reaction coordinate might be expected to be much smoother. However, consideration of the geometry of such an approach immediately indicates that severe steric interactions would arise, not involving the phosphino-alkyl groups, but between the iridium and the C1- and C8-bound hydrogen atoms.

The H(C1)-H(C8) distance in free biphenylene is calculated to be 3.85 Å. In the hypothetical limiting case with no distortion of the biphenylene moiety, if the iridium were to approach the C-C bond in the biphenylene plane the Ir-H distances would decrease to as little as 1.93 Å (Figure 8). Of course, elongation of the C-C bond would obviate this somewhat. However, even at an Ir-C distance of 3.0 Å, which is presumably too far to assist in the C-C bond elongation, the Ir-H distances would be only 2.21 Å. The van der Waals radii of Ir and H are 2.02 Å and 1.10 Å, respectively, thus an Ir-H distance of 2.21 Å would be far more crowded than even the above-noted severe crowding (involving the t-butyl groups) found in the actual calculated tilted transition state, **TS-3-PtBu2**.

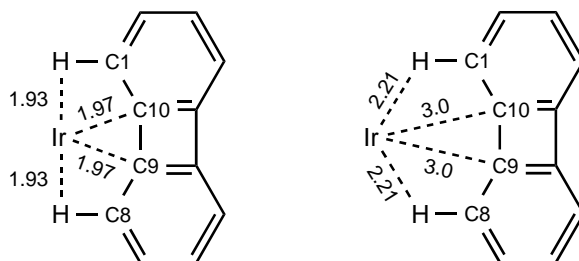


Figure 8. Selected non-bonding distances calculated for a hypothetical approach of an iridium atom in the plane of an undistorted biphenylene molecule. “Tilting” (or rotation of the biphenylene around the C9-C10 bond) while maintaining a given Ir-C9 and Ir-C10 distance increases the Ir-H distance and thus presumably reduces steric repulsion.

In **TS-3-PMe2** (tilt = 60.1 °) the Ir-H(C1) and Ir-H(C8) distances are 3.24 Å and 3.26 Å; this is greater than the sum of the van der Waals radii. In **TS-3-PtBu2** the tilt (50.0 °) is limited by interactions with the t-Bu groups and as a result, the Ir-H distances

are slightly less at 3.13 and 3.16 Å, essentially equal to the sum of the van der Waals radii (indicating the possibility of some repulsive interactions). Thus it appears that if the biphenylene unit were tilted even less than the calculated 50 °, steric interactions (Ir-H(C1) and Ir-H(C8)) would become significant. This appears to explain the origin of the tilt and ultimately the large difference between the calculated activation barriers for C-C addition to (^tBuPCP)Ir vs. (^{Me}PCP)Ir or (ⁱPrPCP)Ir.

Addition of the phenyl-phenyl bond of biphenyl. The transition states for the biphenylene additions offer an interesting perspective into addition/elimination of a simple C-C bond such as the phenyl-phenyl bond of biphenyl. The TS for this reaction has been calculated for (^tBuPCP)Ir (Figure 9), and it is found to bear a surprising resemblance to **TS-3-PtBu2** or **TS-3-PMe2**.

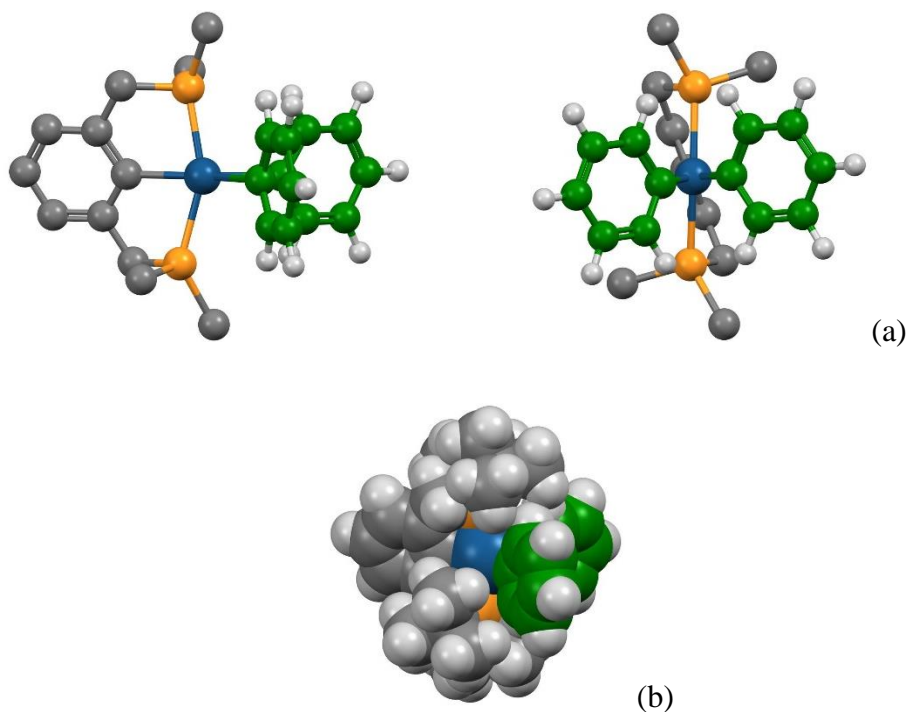


Figure 9. Calculated TS for biphenyl C-C addition to (^tBuPCP)Ir. (a) Two perspectives, ball-and-stick model (t-butyl methyl groups and all non-biphenyl H's omitted for clarity) (b) Space-filling model, 85% van der Waals radii (no atoms omitted)

	selected angles	selected distances (Å)				
	C9-Ir-C10	53.2°	Ir-C9	2.13	Ir-H(C11)	3.22
	C9-C10-C11-C12	0.5°	Ir-C10	2.13	Ir-H(C12)	3.18
	(Ir-C9-C10)-(C1-ring)	89.4°	C9-C10	1.91	H(C1)-H(t-Bu)	1.80
	(Ir-C9-C10)-(C8-ring)	89.4°	Ir-H(C1)	3.18	H(C8)-H(t-Bu)	2.08
			Ir-H(C8)	3.22	C11-H(t-Bu)	1.80
					C12-H(t-Bu)	2.08

Figure 10. Selected angles (simple, torsional, and intersecting mean planes) and selected distances for the calculated TS for biphenyl C-C addition to yield (^tBuPCP)Ir(Ph)₂

Addition in the plane of the molecule in the case of biphenyl (in its planar conformation) would be much more unfavorable than in the case of biphenylene, since

the flanking hydrogens are oriented so as to much more severely restrict access to the C-C bond via the plane of the molecule (the H(C1)-H(C8) distance is only 2.26 Å in the planar conformation). Even if the rings are not co-planar, each ortho C-H bond blocks the C-C linkage. Ir-H(C1 or C8) interactions would be minimized by a pathway in which the iridium center approaches the C-C bond perpendicularly to the plane of the molecule (with the rings in a co-planar conformation). Indeed, in the TS calculated for the reaction of biphenyl with (^tBuPCP)Ir both phenyl rings are perpendicular to the C-Ir-C bond cleavage plane, i.e. the “tilt” is approximately a full 90 ° (Figures 9 and 10). This however results in severe crowding with the t-Bu groups, manifest in particular with two very short H(biphenyl)-H(t-Butyl) distances of 1.80 Å. For addition to (^{Me}PCP)Ir the TS (Figures 11 and 12) is virtually identical to that for (^tBuPCP)Ir with respect to the iridium center cf. (Figs. 9 and 10 above) but the crowding is much less severe. Accordingly, the TS for addition to this fragment is 22.9 kcal/mol lower than for (^tBuPCP)Ir.

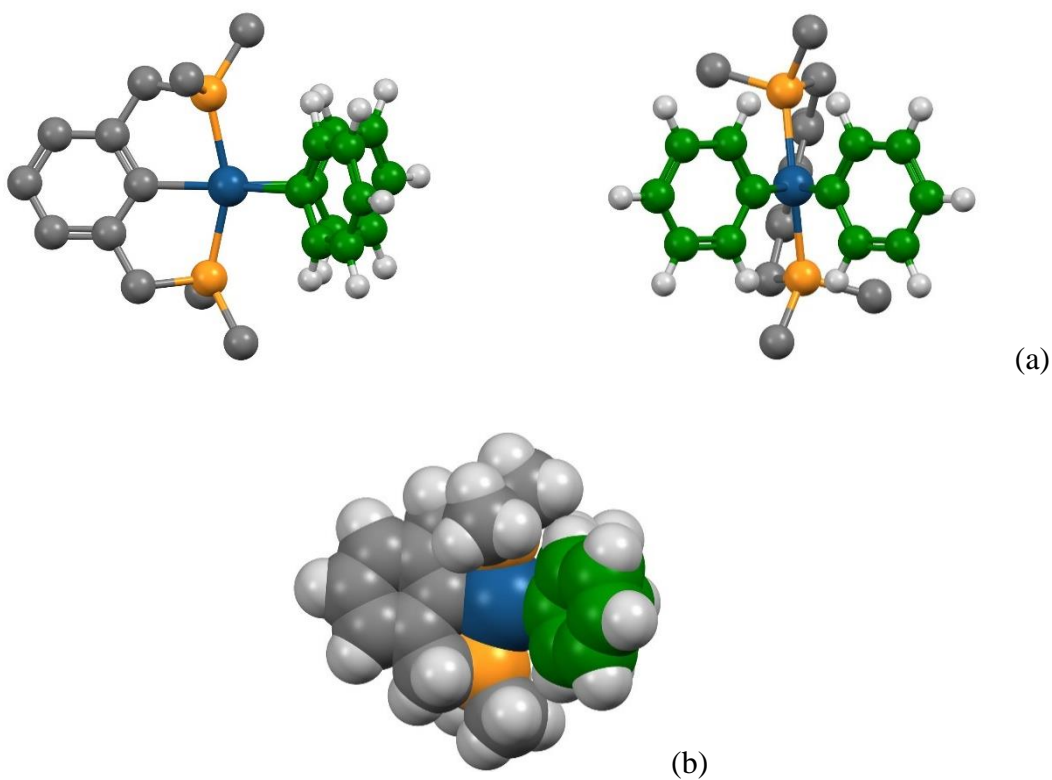


Figure 11. Calculated TS for biphenyl C-C addition to (^{Me}PCP)Ir. (a) Two perspectives, ball-and-stick model (all non-biphenyl H's omitted for clarity) (b) Space-filling model, 85% van der Waals radii (no atoms omitted).

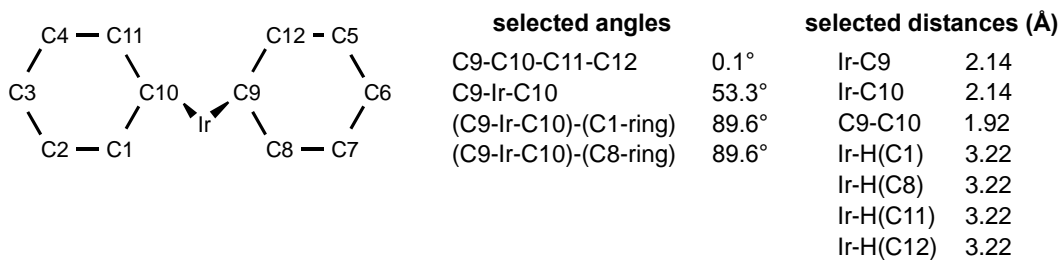


Figure 12. Selected angles and distances for calculated TS for C-C addition of biphenyl to yield (^{Me}PCP)Ir(Ph)₂

The difference between TS enthalpies for addition to (^tBuPCP)Ir vs. (^{Me}PCP)Ir is thus even more pronounced for biphenyl (22.9 kcal/mol) than for biphenylene (14.4 kcal/mol). This may be attributable to the greater “tilt” that is required due to the orientation of the flanking C-H units. It should be noted that this is of course the TS for C-C reductive elimination as well. The thermodynamic enthalpy of biphenyl addition is 7.9 kcal/mol more favorable for (^{Me}PCP)Ir than for (^tBuPCP)Ir. This contrasts with biphenylene for which the difference is only 1.6 kcal/mol; presumably this is due to the fact that the biphenylene unit must remain planar after addition, mitigating steric interactions, whereas the two phenyl ligands cannot adopt a co-planar configuration when bound to iridium. Nevertheless, the kinetics of C-C elimination from the more thermodynamically stable (^{Me}PCP)IrPh₂ are much more facile ($\Delta H^\ddagger = 12.5$ kcal/mol) than from the much more crowded (^tBuPCP)IrPh₂ ($\Delta H^\ddagger = 27.5$ kcal/mol).

Conclusions

(^tBuPCP)Ir undergoes oxidative addition of the C(1)-H bond of biphenylene to give an adduct much more stable than either the C(2)-H addition product or the previously reported phenyl hydride. Although C-H activation is the kinetically preferred reaction, eventually addition of the strained C-C bond occurs, at 125 °C in this case, to give a very stable iridacycle (calculated ΔH° for conversion of the C-H adduct to the C-C adduct is -41 kcal/mol).

DFT calculations indicate that the geometry of the TS for biphenylene C-C addition is severely tilted, i.e. the plane of the cyclobutadiene core of biphenylene deviates by 50 ° from the C-Ir-C bond cleavage plane. This tilt is attributed to the

presence of the C-H groups flanking the C-C bond, which do not allow the iridium center to approach the C-C bond in or near the biphenylene plane. In turn, the tilt results in significant interactions with the ^tBuPCP t-Bu groups. Accordingly, with (^{Me}PCP)Ir, the tilt is calculated to be somewhat greater (60 °), and the TS is calculated to be 14.4 kcal/mol lower in enthalpy than in the case of (^tBuPCP)Ir, relative to the respective free pincer-Ir fragments. The TS for biphenylene C-C bond addition to (^{Me}PCP)Ir is even lower than that for C-H addition to the same fragment, while the reaction is ca. 45 kcal/mol more exothermic. Supporting the conclusion that steric factors contribute strongly to the barrier to C-C addition, (ⁱPrPCP)Ir is found to undergo C-C addition readily at room temperature, as compared with ca. 24 h at 125 °C for (^tBuPCP)Ir.

The factors calculated for biphenyl C-C addition (or Ph-Ph elimination) are closely related to those for biphenylene C-C addition. In the case of biphenyl, the flanking C-H bonds even more strongly inhibit an approach to the C-C bond by the iridium in the plane of the aryl groups. Accordingly the tilting is essentially complete, i.e., the plane of each phenyl group is calculated to be perpendicular to the C-Ir-C bond cleavage plane. This results in strong steric interactions with the ^tBuPCP t-Bu groups and a TS that is ca. 44 kcal/mol above the C-H activation products. By contrast, biphenyl C-C addition to (^{Me}PCP)Ir has a TS with an enthalpy only ca. 18 kcal/mol above the C-H activation products. The product of biphenyl C-C addition is calculated to be about 5.5 kcal/mol above the C-H activation products; however, the low kinetic barrier to C-C addition, and the only slight thermodynamic unfavorability, leads us to consider that relatively small modifications of the complex and/or the substrate could lead to the discovery of systems capable of oxidative addition of unstrained aryl-aryl bonds.

References

- (1) Crabtree, R. H.; Dion, R. P.; Gibboni, D. J.; McGrath, D. V.; Holt, E. M. *J. Am. Chem. Soc.* **1986**, *108*, 7222-7227.
- (2) Periana, R. A.; Bergman, R. G. *J. Am. Chem. Soc.* **1986**, *108*, 7346-7355.
- (3) Perthuisot, C.; Jones, W. D. *J. Am. Chem. Soc.* **1994**, *116*, 3647-3648.
- (4) Murakami, M.; Amii, H.; Shigeto, K.; Ito, Y. *J. Am. Chem. Soc.* **1996**, *118*, 8285-8290.
- (5) Perthuisot, C.; Edelbach, B. L.; Zubris, D. L.; Jones, W. D. *Organometallics* **1997**, *16*, 2016-2023.
- (6) Wick, D. D.; Northcutt, T. O.; Lachicotte, R. J.; Jones, W. D. *Organometallics* **1998**, *17*, 4484-4492.
- (7) Edelbach, B. L.; Lachicotte, R. J.; Jones, W. D. *J. Am. Chem. Soc.* **1998**, *120*, 2843-2853.
- (8) Edelbach, B. L.; Vicic, D. A.; Lachicotte, R. J.; Jones, W. D. *Organometallics* **1998**, *17*, 4784-4794.
- (9) Edelbach, B. L.; Lachicotte, R. J.; Jones, W. D. *Organometallics* **1999**, *18*, 4040-4049.
- (10) Rybtchinski, B.; Milstein, D. *Angew. Chem., Intl. Ed.* **1999**, *38*, 871-883.
- (11) Mueller, C.; Iverson, C. N.; Lachicotte, R. J.; Jones, W. D. *J. Am. Chem. Soc.* **2001**, *123*, 9718-9719.
- (12) Iverson, C. N.; Jones, W. D. *Organometallics* **2001**, *20*, 5745-5750.
- (13) Satoh, T.; Jones, W. D. *Organometallics* **2001**, *20*, 2916-2919.
- (14) Mueller, C.; Lachicotte, R. J.; Jones, W. D. *Organometallics* **2002**, *21*, 1975-1981.
- (15) Perthuisot, C.; Edelbach, B. L.; Zubris, D. L.; Simhai, N.; Iverson, C. N.; Muller, C.; Satoh, T.; Jones, W. D. *J. Mol. Catal. A: Chem.* **2002**, *189*, 157-168.
- (16) Oh, M.; Yu, K. Q.; Li, H. Z.; Watson, E. J.; Carpenter, G. B.; Sweigart, D. A. *Adv. Synth. Catal.* **2003**, *345*, 1053-1060.
- (17) Bart, S. C.; Chirik, P. J. *J. Am. Chem. Soc.* **2003**, *125*, 886-887.
- (18) Itazaki, M.; Yoda, C.; Nishihara, Y.; Osakada, K. *Organometallics* **2004**, *23*, 5402-5409.
- (19) Jun, C.-H. *Chem. Soc. Rev.* **2004**, *33*, 610-618 and references therein.

- (20) Rybtchinski, B.; Milstein, D. In *Activation and Functionalization of C-H Bonds* 2004; Vol. ACS Symposium Series 885, p 70-85.
- (21) De Jong, G. T.; Geerke, D. P.; Diefenbach, A.; Sola, M.; Bickelhaupt, F. M. *J. Computational Chem.* **2005**, *26*, 1006-1020.
- (22) Anstey, M. R.; Yung, C. M.; Du, J.; Bergman, R. G. *J. Am. Chem. Soc.* **2007**, *129*, 776-777.
- (23) Gunay, A.; Jones, W. D. *J. Am. Chem. Soc.* **2007**, *129*, 8729-8735.
- (24) Wick, D. D.; Jones, W. D. *Inorg. Chim. Acta* **2009**, *362*, 4416-4421.
- (25) Chaplin, A. B.; Tonner, R.; Weller, A. S. *Organometallics* **2010**, *29*, 2710-2714.
- (26) Matsuda, T.; Kirikae, H. *Organometallics* **2011**, *30*, 3923-3925.
- (27) Korotvicka, A.; Cisarova, I.; Roithova, J.; Katora, M. *Chem.-Eur. J.* **2012**, *18*, 4200-4207.
- (28) Ghosh, R.; Emge, T. J.; Krogh-Jespersen, K.; Goldman, A. S. *J. Am. Chem. Soc.* **2008**, *130*, 11317-11327.
- (29) Kanzelberger, M.; Singh, B.; Czerw, M.; Krogh-Jespersen, K.; Goldman, A. S. *J. Am. Chem. Soc.* **2000**, *122*, 11017-11018.
- (30) Krogh-Jespersen, K.; Czerw, M.; Zhu, K.; Singh, B.; Kanzelberger, M.; Darji, N.; Achord, P. D.; Renkema, K. B.; Goldman, A. S. *J. Am. Chem. Soc.* **2002**, *124*, 10797-10809.
- (31) Laviska, D. A. Ph.D. thesis, Rutgers University, 2013.
- (32) Laviska, D. A.; Zhou, T.; Emge, T. J.; Krogh-Jespersen, K.; Goldman, A. S., manuscript in preparation.
- (33) Liu, F.; Goldman, A. S. *Chem. Commun.* **1999**, 655-656.
- (34) Streitwieser, A.; Shah, K.; Reyes, J. R.; Zhang, X.; Davis, N. R.; Wu, E. C. *J. Phys. Chem. A* **2010**, *114*, 8793-8797.
- (35) Haibach, M. C.; Guan, C.; Wang, D. Y.; Li, B.; Lease, N.; Steffens, A. M.; Krogh-Jespersen, K.; Goldman, A. S. *J. Am. Chem. Soc.* **2013**, *135*, 15062-15070.

Computational Details

DFT calculations¹ employed the M06-L exchange-correlation functional.² The electronic environment was modeled using the following scheme: for Ir, we applied the SDD relativistic effective (small) core potential and the associated (6s5p3d) valence basis set;³ all other atoms (P, C and H) were assigned 6-311G(d,p) basis sets.⁴ Expanded integration grids (integral=ultrafine) were used throughout. Standard optimization procedures were employed to obtain the geometries and electronic energies for stationary points. Normal mode analysis was performed for each species, and the resulting set of vibrational frequencies was employed (without scaling) to determine zero-point energy corrections. Enthalpies (H) and Gibbs' free energies (G; T = 298.15 K, P = 1 atm) were obtained from the electronic energies (E) using standard statistical mechanical expressions. All calculations have been performed using the Gaussian 09 collection of electronic structure computer programs.⁵

Computational Section References

1. Parr, R. G.; Yang, W. *Density-Functional Theory of Atoms and Molecules* (University Press: Oxford, 1989).
2. Zhao, Y.; Truhlar, D. G. *Theo. Chem. Acc.* **2008**, *120*, 215-241. 650-654.
3. Andrae, D.; Haeussermann, U.; Dolg, M.; Stoll, H.; Preuss, H. *Theor. Chim. Acta* **1990**, *77*, 123-141.
4. (a) Raghavachari, K.; Binkley, J. S.; Seeger, R.; Pople, J. A. *Chem. Phys.* **1980**, *72*, 650-654 *J. Chem. Phys.* **72**, 650-654 (1980). (b) McLean, A. D; Chandler, G. S. *J. Chem. Phys.* **1980**, *72*, 5639-5648.
5. Gaussian 09, Revision C.01, Frisch, M. J.; Trucks, G. W.; Schlegel, H. B.; Scuseria, G. E.; Robb, M. A.; Cheeseman, J. R.; Scalmani, G.; Barone, V.; Mennucci, B.; Petersson, G. A.; Nakatsuji, H.; Caricato, M.; Li, X.; Hratchian, H. P.; Izmaylov, A. F.; Bloino, J.; Zheng, G.; Sonnenberg, J. L.; Hada, M.; Ehara, M.; Toyota, K.; Fukuda, R.; Hasegawa, J.; Ishida, M.; Nakajima, T.; Honda, Y.; Kitao, O.; Nakai, H.; Vreven, T.; Montgomery, Jr., J. A.; Peralta, J. E.; Ogliaro, F.; Bearpark, M.; Heyd, J. J.; Brothers, E.; Kudin, K. N.; Staroverov, V. N.; Kobayashi, R.; Normand, J.; Raghavachari, K.; Rendell, A.; Burant, J. C.; Iyengar, S. S.; Tomasi, J.; Cossi, M.; Rega, N.; Millam, J. M.; Klene, M.; Knox, J. E.; Cross, J. B.; Bakken, V.; Adamo, C.; Jaramillo, J.; Gomperts, R.; Stratmann, R. E.; Yazyev, O.; Austin, A. J.; Cammi, R.; Pomelli, C.; Ochterski, J. W.; Martin, R. L.; Morokuma, K.; Zakrzewski, V. G.; Voth, G. A.; Salvador, P.; Dannenberg, J. J.; Dapprich, S.; Daniels, A. D.; Farkas, O.; Foresman, J. B.; Ortiz, J. V.; Cioslowski, J.; and Fox, D. J., Gaussian, Inc., Wallingford CT, 2009.